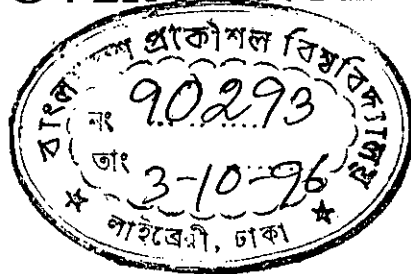


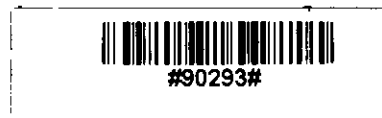
NUMERICAL STUDY OF LAMINAR FLOW SEPARATION OVER ANNULAR BACKSTEPS



By

MOHAMMAD MUSTAFIZUR RAHMAN

Thesis submitted to the
DEPARTMENT OF MECHANICAL ENGINEERING
In partial fulfillment of the requirements for the award of the degree of
MASTER OF SCIENCE
in
MECHANICAL ENGINEERING



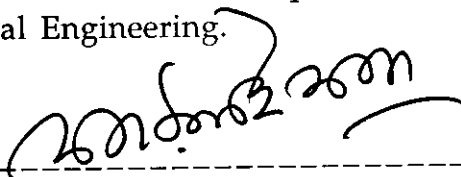
BANGLADESH UNIVERSITY OF ENGINEERING AND TECHNOLOGY
DHAKA-1000, BANGLADESH.

SEPTEMBER, 1996.

RECOMMENDATION OF THE BOARD OF EXAMINERS

The board of examiners hereby recommends to the Department of Mechanical Engineering, Bangladesh University of Engineering and Technology (BUET), Dhaka- 1000, Bangladesh, the acceptance of the thesis "*NUMERICAL STUDY OF LAMINAR FLOW SEPARATION OVER ANNULAR BACKSTEPS*" submitted by *Mohammad Mustafizur Rahman* , Roll No: 921464F, Session: 1990-91-92 in partial fulfillment of the requirements for the degree of Master of Science in Mechanical Engineering.

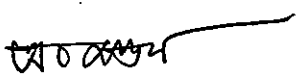
1.



Dr. A. K. M. Sadrul Islam
Professor
Mechanical Engineering Department
BUET, Dhaka-1000

Chairman
(Supervisor)

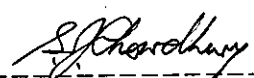
2.



Dr. Amallesh Chandra Mandal
Professor and Head
Mechanical Engineering Department
BUET, Dhaka-1000

Member
(Ex-Officio)

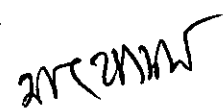
3.



Dr. Showkat Jahan Chowdhury
Professor
Mechanical Engineering Department
BUET, Dhaka-1000

Member

4.



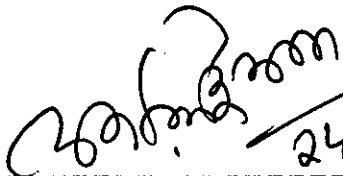
Dr. Md. Akram Hossain
Sr. Principal Engineer
Pilot Plant and Process Dev. Centre
BCSIR, Mirpur Road
Dhanmondi, Dhaka.

Member
(External)


SEPTEMBER 24, 1996.

CERTIFICATE OF RESEARCH

This is to certify that the work presented in this dissertation is the outcome of the investigation carried out by the candidate under the supervision of Dr. A. K. M. Sadrul Islam, Professor, Department of Mechanical Engineering of Bangladesh University of Engineering & Technology(BUET), Dhaka- 1000, Bangladesh and it has not been submitted elsewhere for the award of any degree or diploma or for publication.


24.9.96

Supervisor


24.09.96

Candidate

ACKNOWLEDGEMENTS

It gives me great pleasure to express my gratitude to all those who provided help and support during the period of my M.Sc. thesis.

√ The work was carried out under the guidance and supervision of Dr. A. K. M. Sadrul Islam, Professor, Department of Mechanical Engineering, BUET, Dhaka. It is a pleasure working with him and learning the different facets of research. I would like to take this opportunity to thank him for his cordial support, valuable suggestions, continuous encouragement and constructive criticism throughout this work.

I would like to thank Dr. Amallesh Chandra Mandal, Dr. Showkat Jahan Chowdhury, and Dr. Md. Akram Hossain, for their comments and suggestions have certainly improved the quality of this work. I am indebted to the other faculty members of the Mechanical Engineering Department for providing me with all necessary facilities.

I am also indebted to Md. Mamdud Hossain, Lecturer, Department of Mechanical Engineering, BUET, Dhaka for his constructive assistance and advise that inspired me to achieve my goals.

I would like to acknowledge the assistance of Mr. Md. Fakhrul Hazra, Accounts-cum-typist of Mechanical Engineering Department for typing a major part of this thesis.

Finally, I am grateful to my parents for their encouragement, understanding during the course of this study.

ABSTRACT

This thesis deals with the numerical study of laminar flow separation over annular backsteps. Both inner- and outer-radius annular backsteps are considered. The governing differential equations are solved by a control-volume based iterative finite difference technique. A non uniform staggered grid with finer spacing near the step and the walls is used. The differential equations are integrated over their appropriate staggered control volumes and discretised using a hybrid difference scheme. The discretised equations with boundary condition modifications are solved utilizing the SIMPLE with TDMA algorithms. The capability of the computational code for predicting recirculation flows is first tested by comparing the results with the available predicted and experimental data. It is found that the present numerical predictions have good matching with the available predicted and experimental data. The computational model is then used to analyze the flow separation over annular backsteps. Computations are done for different annular radius ratio and different Reynolds number for both cases. Constant streamline contours, constant vorticity contours and vorticity distribution along the walls for both cases are presented. The Reynolds number is based on the average velocity at the inlet and the step height.

It is observed that the length of the primary vortex attached to the step increases with Reynolds number in both the cases, but this increment is much higher in case of outer radius annular backstep. The length of the primary vortex increases with annular radius ratio in case of inner-radius annular backstep but decreases with annular radius ratio in outer-radius annular backstep. Secondary vortex forms on the opposite wall at higher Reynolds number and at larger annular radius ratio. The effect of Reynolds number and annular radius ratio on the flow field is also examined. The previous research work in this field was limited to lower Reynolds number (25 ~100) and single annular radius ratio ($\alpha = 0.2$) for inner- radius annular backstep geometry but the present research is extended to a wider range of Reynolds number (50 ~ 500) and different annular radius ratio (0.1 ~ 1.0) for inner- radius annular backstep. The work reveals its own identity with its application on the outer- radius annular backstep geometry.

CONTENTS

	PAGE
TITLE	i
CERTIFICATE OF APPROVAL	ii
CERTIFICATE OF RESEARCH	iii
DECLARATION	iv
ACKNOWLEDGEMENTS	v
ABSTRACT	vi
CONTENTS	vii
LIST OF FIGURES	ix
LIST OF TABLES	xii
NOMENCLATURE	xiii

CHAPTER 1 INTRODUCTION

1.1	Background	1
1.1.1	Characteristic Physical Features of Flow	2
1.1.2	Mechanics of Flow Separation	3
1.1.3	Classical Concept of Onset of Flow Separation	3
1.2	Annulus and Its Application	4
1.3	Motivation of the Present Investigation	4
1.4	Objectives of the Present Research	5
1.5	Outlines of the Thesis.	6

CHAPTER 2 LITERATURE REVIEW

2.1	Scope	7
2.2	Previous Work	7

CHAPTER	3	METHODOLOGY OF SOLUTION	Page No.
	3.1	Scope	11
	3.2	Governing Equations	11
	3.3	Boundary Conditions	12
	3.4	The Governing Equations in General Forms	13
	3.5	Numerical Solution of Differential Equations	14
	3.5.1	The Finite Difference Equations - General Remarks	15
	3.5.2	The Discretization Scheme	15
	3.5.3	Solution Algorithm	16
	3.6	Closure	17
CHAPTER	4	RESULTS AND DISCUSSIONS	
	4.1	Scope	18
	4.2	Problem Statement	18
	4.3	Validation of the Numerical Model	19
	4.4	Comparison with Available Data	19
	4.5	Effect of Reynolds Numbers	21
	4.6	Effect of Annular Radius Ratio (α)	23
	4.7	Vorticity Distribution Along the Walls	24
	4.8	Closure	26
CHAPTER	5	CONCLUSIONS AND RECOMMENDATIONS	
	5.1	Scope	27
	5.2	Conclusions	27
	5.3	Recommendations for Future Works	28
REFERENCES			29
FIGURES			35
APPENDIX A		Computer Program Flow Chart.	84

LIST OF FIGURES

	Page No.	
Fig : 3.1	Control volumes for 2-D co-ordinate system	35
Fig : 3.2	Cell face value interpolation (for uniform grid spacings) with different discretisation schemes.	36
Fig : 4.1	Flow configuration and computational domain.	37
Fig : 4.2	Grid dependancy test for $\alpha = 0.2$	38
Fig : 4.3	Comparison between Mohamed et. al. [15] and present prediction.	38
Fig : 4.4	Length of primary vortex for inner-radius annular backstep.	39
Fig : 4.5	Length of primary vortex for outer-radius annular backstep.	39
Fig : 4.6	Lengths of secondary vortex for inner-radius annular backstep.	40
Fig : 4.7	Lengths of secondary vortex for outer-radius annular backstep.	40
Fig : 4.8	Constant streamline contours for inner-radius annular backstep at $\alpha = 0.1$ [Note that the axial distance compressed by 5 times].	41
Fig : 4.9	Constant streamline contours for outer-radius annular backstep at $\alpha = 0.1$ [Note that the axial distance compressed by 5 times].	42
Fig : 4.10	Constant streamline contours for inner-radius annular backstep at $\alpha = 0.2$ [Note that the axial distance compressed by 5 times].	43
Fig : 4.11	Constant streamline contours for outer-radius annular backstep at $\alpha = 0.2$ [Note that the axial distance compressed by 5 times].	44
Fig : 4.12	Constant streamline contours for inner-radius annular backstep at $\alpha = 0.5$ [Note that the axial distance compressed by 5 times].	45

Fig : 4.13	Constant streamline contours for outer-radius annular backstep at $\alpha = 0.5$ [Note that the axial distance compressed by 5 times].	46
Fig : 4.14	Constant streamline contours for inner-radius annular backstep at $\alpha = 0.75$ [Note that the axial distance compressed by 5 times].	47
Fig : 4.15	Constant streamline contours for outer-radius annular backstep at $\alpha = 0.75$ [Note that the axial distance compressed by 5 times].	48
Fig : 4.16	Constant streamline contours for inner-radius annular backstep at $\alpha = 1.0$ [Note that the axial distance compressed by 5 times].	49
Fig : 4.17	Constant vorticity contours for inner-radius annular backstep at $\alpha = 0.1$ [Note that the axial distance compressed by 5 times].	50
Fig : 4.18	Constant vorticity contours for inner-radius annular backstep at $\alpha = 0.2$ [Note that the axial distance compressed by 5 times].	51
Fig : 4.19	Constant vorticity contours for inner-radius annular backstep at $\alpha = 0.5$ [Note that the axial distance compressed by 5 times].	52
Fig : 4.20	Constant vorticity contours for inner-radius annular backstep at $\alpha = 0.75$ [Note that the axial distance compressed by 5 times].	53
Fig : 4.21	Constant vorticity contours for inner-radius annular backstep at $\alpha = 1.0$ [Note that the axial distance compressed by 5 times].	54
Fig : 4.22	Constant vorticity contours for outer-radius annular backstep at $\alpha = 0.1$ [Note that the axial distance compressed by 5 times].	55
Fig : 4.23	Constant vorticity contours for outer-radius annular backstep at $\alpha = 0.2$ [Note that the axial distance compressed by 5 times].	56
Fig : 4.24	Constant vorticity contours for outer-radius annular backstep at $\alpha = 0.5$ [Note that the axial distance compressed by 5 times].	57
Fig : 4.25	Constant vorticity contours for outer-radius annular backstep at $\alpha = 0.75$ [Note that the axial distance compressed by 5 times].	58
Fig : 4.26	Constant streamline contours for inner-radius annular backstep at $Re_S = 100$ [Note that the axial distance compressed by 5 times].	59

Fig : 4.27	Constant streamline contours for outer-radius annular backstep at $Re_S = 100$ [Note that the axial distance compressed by 5 times].	60
Fig : 4.28	Constant streamline contours for inner-radius annular backstep at $Re_S = 200$ [Note that the axial distance compressed by 5 times].	61
Fig : 4.29	Constant streamline contours for outer-radius annular backstep at $Re_S = 200$ [Note that the axial distance compressed by 5 times].	62
Fig : 4.30	Constant streamline contours for inner-radius annular backstep at $Re_S = 300$ [Note that the axial distance compressed by 5 times].	63
Fig : 4.31	Constant streamline contours for outer-radius annular backstep at $Re_S = 300$ [Note that the axial distance compressed by 5 times].	64
Fig : 4.32	Constant streamline contours for inner-radius annular backstep at $Re_S = 500$ [Note that the axial distance compressed by 5 times].	65
Fig : 4.33	Constant streamline contours for outer-radius annular backstep at $Re_S = 500$ [Note that the axial distance compressed by 5 times].	66
Fig : 4.34	Vorticity distribution along the walls for an inner- radius annular backsteps at an annular radius ratio (α) = 0.1	67
Fig : 4.35	Vorticity distribution along the walls for an outer- radius annular backsteps at an annular radius ratio (α) = 0.1	70
Fig : 4.36	Vorticity distribution along the stepside wall of an inner- radius annular backstep.	73
Fig : 4.37	Vorticity distribution along the opposite wall of an inner- radius annular backstep.	76
Fig : 4.38	Vorticity distribution along the stepside wall of an outer- radius annular backstep.	79
Fig : 4.39	Vorticity distribution along the opposite wall of an outer- radius annular backstep.	82

LIST OF TABLES

Table 3.1 Source terms for general equation.

NOMENCLATURE

SYMBOL	MEANING
a_i	Discretisation coefficients
c_f	Skin friction co-efficient
h	Inlet annular depth
H	Depth of larger cylinder after expansion
n	Normal to the wall into the flow region
p	Pressure
r	Radial distance
Re_s	Reynolds number, $\frac{U_o s}{\nu}$
r_1	Radius of inner cylinder after expansion
r_2	Radius of inlet cylinder before expansion
r_3	Radius of outer cylinder expansion
s	Step height
S_ϕ	Source terms for variable ϕ

u	Mean axial velocity
U	Characteristic velocity
U_0	Average velocity
v	Mean radial velocity
x	Axial distance
x_1	Reattachment length (length of the primary vortex)
x_2	Starting length of secondary on- axis recirculation
x_3	Finishing length of secondary on- axis recirculation

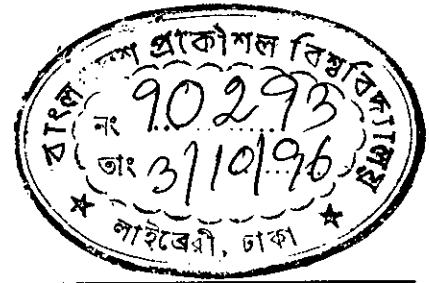
GREEK LETTERS:

SYMBOL	MEANING
α	Annular radius ratio
ϕ	General Source term
ψ	Stream function
δ	Displacement thickness
Ω	Vorticity
μ	Viscosity

ν	Kinematic viscosity
ε	Energy dissipation rate
ρ	Density
θ	General dependent variable
τ_w	The shear stress along the wall

CHAPTER - 1

CHAPTER - 1



INTRODUCTION

1.1 BACKGROUND

The subject of fluid flow separation is one of the many aspects of viscous flow, which is very important but complicated. Because of flow separation, energy is lost. In case of external flow at subsonic speeds such as in air borne vehicles, the stream lines deviate, the drag increases, the lift decreases and reverse flow and stalling occur. In the transonic speed range, control and structure problems are created by flow separations. For cases of internal flow, separation can cause reduction in efficiencies. The optimum performance of fluids handling devices such as fans, turbines, pumps, compressors, etc., can only be predicted with accurate understanding of flow separation, because the separation occurs just prior to or at maximum loading. Separation is a phenomenon that can occur under widely varying conditions. For several reasons at high Reynolds number i.e. boundary layer separation, has received far more attention than low Reynolds number separation. Firstly, high Reynolds flows are encountered much more widely. Secondly, there are some flow configurations for which separation occurs at high Reynolds but not at low whereas the converse is probably not true.

Among the many flow geometries employed to carry out basic studies of separated flows, backward facing step has gained particular attention due to its geometrical simplicity. Flow separation over a backstep has been studied in considerable details. The separated flows are of considerable interest to the designs of fluids engineering devices [1]. The separation of the shear layer adjacent to a wall may occur if the adverse pressure gradient in the direction of motion is sufficiently large or if there is a sufficiently abrupt change in the guiding wall geometry. The flow over a backstep is a problem in which the guiding wall has a step change in its geometry that is perpendicular to the direction of the flow approaching the step. The guiding wall is assumed to be planar upstream and downstream of the step. In this problem the separation

point is fixed and the flow leaves the boundary at zero angle of separation. It is the simplest problem that contains the essential features of a separated flow.

1.1.1 CHARACTERISTIC PHYSICAL FEATURES OF FLOW

There are certain characteristic physical features of the flow of a viscous fluid. A study of the characteristics phenomena is very useful in gaining a general understanding of flow. Basic to an understanding of the flow of fluids is the observation first recorded by Osborne Reynolds [29] of distinct types of flow. The list of these characteristics as: Laminar flow; turbulent flow; transition between Laminar and turbulent flow ; formation of boundary layers; and separation.

Laminar flow is also called viscous or streamline flow. In laminar flow the fluid flows in layer or laminae; there is no mixing of minute particles of fluid on a macroscopic scale. The only mixing which occurs is on a molecular level. In laminar flow the velocity at any point is either constant or varies with time in some non random manner. Separation is found that the fluid breaks away from the surface; there may be an eddying wake [33].

A **streamline** is a line in a fluid flow which, at every point along the line has the direction on the local velocity of the fluid at some instant of time. The streamline form the flow pattern at any instant of time. If the flow is steady, then the streamlines describe the motion of individual fluid particles. For steady flow, a streamline by definition is a line across which no fluid flows.

Pathline: The motion of individual particle over a finite time interval is called its pathline. In steady flow the streamlines and pathlines are identical.

Streakline : A streakline in the current location of fluid particles, all of which passed through a fixed point in the fluid at some previous time. They are identical to streamlines for steady flow.

1.1.2 MECHANICS OF FLOW SEPARATION

The problem of the flow separation is perhaps, one of the most important hydrodynamics problems to be investigated intensively in order to find its solution satisfactorily. Because of the complexity of the problem, a rigorous definition of flow separation and stall should be made. The classical concept of flow separation is due to viscosity. In addition a necessary condition for flow separation is the adverse pressure gradient.

In a general sense according to Maskell's concept of separation, flow separation is inevitable for flow over the finite dimension. Flow will separate from the solid body surface at the trailing edge and also upstream of it if the required conditions are met there. The flow separation is not only caused by a gradual process, which is the case of flow over a smooth surface, but also by severe discontinuity of the tangent to the surface.

1.1.3 CLASSICAL CONCEPT OF ONSET OF FLOW SEPARATION

As a young engineer at the Maschinen Fabrik Augsburg- Nurnberg (MAN), Prandtl found that the computed pressure recovery could not be achieved in actual diffusers. He was occupied for 3 years in figuring out why and how the flow separations and pressure losses were caused. This problem was solved finally by his theoretical concept of the boundary layer [47]. His concept may be referred to as classical in comparison to the modern development of separation of flow theory.

The classical concept of flow separation is found for two-dimensional and axisymmetric steady flow. Prandtl [47] states clearly that the necessary condition for flow separation from the wall is the increasing pressure in the streamwise direction i.e. positive (or adverse) pressure gradient along the flow path. This statement holds for compressible as well as incompressible flow. Therefore it may be said that, in general, flow separation occurs under adverse pressure gradient and with laminar or turbulent viscosity effects. If one of these two factors is missing, then the flow does not separate.

1.2 ANNULUS AND ITS APPLICATION

An annulus is formed by introducing a core through a circular tube. The ratio of the inner and outer radii (annular radius ratio, α) is an important parameter in addition to other variables that determines the nature of the flow in the annuli. A pipe ($\alpha = 0$) and a parallel plate channel ($\alpha = 1$) are the two limiting cases of an annulus.

Laminar flows are not just of academic interest. Flow separations are of considerable practical importance to the designers of forced convection heating and cooling devices used in the electronics, bio-mechanics and aerospace industries, among others [2]. There has been a continued interest within the fluid mechanics community in the prediction of laminar flow separation over backsteps.

In Industrial heat exchangers, bio-mechanics, aerospace industries, nuclear reactors etc there are many cases where heat transfer begins immediately at the entrance of the annulus and therefore the calculation of heat transfer coefficients for these cases requires a detailed knowledge of the velocity field in the entrance region of the annular passage.

1.3 MOTIVATION OF THE PRESENT INVESTIGATION

In recent years laminar flow separation over annular backsteps have been studied in considerable detail due to their relevance to the problems of heating and cooling heat exchanger.

A literature review indicates that until now there seems to be no sufficient data available on annular backsteps. In many engineering applications flow separation and reattachments occur and hence they have been the subject of study for many years. Laminar flows are of considerable practical importance to the designers of fluids engineering devices, forced convection heating and cooling devices used in the electronics, bio-mechanics equipments, combustors, heat exchanger, micro-electronics equipment and aerospace industries etc.

The sudden expansion geometry produces recirculating region downstream of the expansion that are substantially higher than those that would be obtained at the same Reynolds number in the entrance region of a annular passage.

Hence detail knowledge of the flow properties are required before manufacturing the equipment's encountering investigations are quite expensive. This thesis, therefore, suggests numerical studies to investigate the effect of different flow parameters and also to generate information which would be helpful for production purpose in the lost effective way.

1.4 OBJECTIVES OF THE PRESENT RESEARCH

The objective of this study is to investigate numerically some important flow characteristics, valuable for greater understanding of the behavior of the inner-radius annular and outer-radius annular backstep. A modified version of the PACE Computer program was done by Jones, W. P. [39], will be used for the present study. This version offers fast and reliable computer program for solving the governing finite difference equations at given boundary conditions.

The specific objectives of this research are:

- i. To test the capability of the model in predicting complex recirculating flow.
- ii. To study the effect of Reynolds number on the primary and secondary vortices for both cases.
- iii. To analyze the effect of annular radius ratio on the primary and secondary vortices for both inner and outer radius annular backsteps.
- iv. To compared with the available experimental and computational results.

- v. To observe the vorticity distribution along the walls for both inner and outer radius annular backsteps.
- vi. To also observe the effect of annular radius ratio on the variation of vorticity along the stepside and opposite walls for both cases.

1.5 SCOPE OF THE THESIS

The main purpose of this thesis is to analyze numerically the flow of laminar separation over an inner-and outer- radius annular backsteps. The remaining part of this thesis is divided into four chapters. The general necessity of research in the field of laminar flow separation over annular backsteps and the objectives of this research work is described in chapter-1. A comprehensive review of the literature is described in chapter - 2. The mathematical model used and the numerical algorithm for the prediction method, boundary conditions are briefly described in chapter-3.

Chapter-4 contains the results and discussion. In this chapter, the present predicted results are first compared with the experimental data and available predicted results to prove the capability of the program. Then the effect of Reynolds number, annular radius ratio, vorticity distribution along the walls on an inner- and outer -radius annular backsteps are carefully investigated.

The summary of the achievements obtained in this study and suggestion for the possible future work are presented in chapter-5.

References and figures are given at the end of this research work.

CHAPTER - 2

CHAPTER - 2

LITERATURE REVIEW

2.1 SCOPE

In many engineering applications flow separation and reattachment occur and hence they have been the subject of study for many years. Two dimensional annular backstep is one of such geometries where the separation and reattachment occur and this has gained particular interest for its simple geometry. The majority of reported studies for this configuration deals with turbulent flow, however in the aforementioned applications, the fluid velocities and/ or channel dimensions are small and hence laminar flow prevails, following is a brief outline of some of the important work.

2.2 PREVIOUS WORK

Recent studies of laminar flow over planar backsteps Goldstein et al. [10] carried out Results of an experimental investigation of the laminar flow of air over a downstream facing step. The experiments include visual observations of smoke filaments (in the viscous layer), qualitative velocity fluctuation measurements and mean velocity profiles. Results are reported over a range of 0.36 ~ 1.02 cm in step height, 0.61 ~ 2.44 m/sec in free stream velocity at the step and 0.16 ~ 0.51 cm in boundary layer displacement thickness at the step. Laminar flow to reattachment of a free shear layer is observed for subsonic flow and two criteria for which transition to turbulence at reattachment exists are presented. The laminar reattachment length is not a constant number of step heights as for turbulent flow but varies with Reynolds number and boundary layer thickness at the step.

Cramer [9] postulates a rather idealized model to obtain analytically a correlation for laminar separation bubbles. He assumes incompressible flow over a stepped flat plate and that "The usual laminar boundary layer

assumptions are applicable". He further assumes that for a small step height, the air in the bubbles is stagnant and the flow downstream of the step before reattachment grows toward the wall in the manner of a spreading laminar jet.

Chapman et al. [12] reported laminar separations that are steady in the supersonic stream and depends only to a relatively small extent on Reynolds number. They also note that the stability of a separated laminar mixing layer increases markedly with much number. Laminar reattachment lengths of about 18 step heights and turbulent reattachment lengths of about 6 step heights are reported for a down stream facing step in a along the separation streamline. At Reynolds numbers above this the vortices began to lose definition and to form eddies of a more random nature as the flow became turbulent.

Macagno and Hung [2] carried out both an experimental and a numerical investigation of laminar flow in a step expansion geometry. They chose $H/h = 2$ and $0 < Re \leq 200$. For $Re \leq 70$ their ψ and ω calculation used a time-independent central difference scheme. Since this was unstable for higher Reynolds number. They used an unsteady approach to obtain results upto $Re = 200$. Their experimental work gave measurements of the reattachment length and eddy centre for $Re < 135$ and these results were in authenticatul their computations. The streamlines and vorticity contours are presented as function of the Reynolds number of the flow. The dynamic interaction between the main flow and the captive eddy between it and the walls is analyzed.

Hung and Macagno [20], examined the laminar flow separation over a circular backstep produced by a sudden pipe expansion and Reynolds number range from 36 ~ 4500. The results revealed that, at a Reynolds number 36, clear cellular eddies could be observed behind the sudden expansion and appeared to be symmetry in form. The flow sustained its symmetry at higher Reynolds number by the trapped eddy became progressively longer and less pronounced.

Durst, et al. [19] studied the low Reynolds number flow over a 2:1 double expansion located in a channel of aspect ratio 3.75:1 in this geometry it was

found that the flow was not sensibly two-dimensional in the vicinity of the duct centre-line.

Durst et al. [44] found that complex three-dimensional flow patterns occurred in a 3:1 planar expansion with an aspect ratio of 9 to 1 at Reynolds number as low as 114. At Reynolds numbers above 250, strong periodic fluctuations in velocities were observed. In an experimental investigation of a two-dimensional step, Armaly et al. [5] found that the flow was not two-dimensional at Reynolds number above 400. At even higher Reynolds number it was noticed that additional regions of flow separation occurred with each having their own characteristic parameters. It is not known at what Reynolds number each of these factors will arise for the boundary conditions and geometries considered in the present study.

Scott et al. [41] laminar flow of a Newtonian fluid in planar and axisymmetric abrupt expansions is studied the Navier-stokes equations using the finite element method.

Denham [13] and Atkins [14] have both carried out visualization studies for laminar flow over a backward facing step and observed that as the Reynolds number increased above a certain value, the flow became progressively unsteady. Large eddies were observed to be shed off the step edge and the occurrence of this phenomena was seen to correspond with a reduction in the recirculation zone length.

Back and Roschke [61] carried out an investigation into the hydrodynamic behavior of flow through an axisymmetric sudden expansion of a circular pipe for a Reynolds number range of 20 ~ 4200. Their investigation was for an expansion ratio of 2.6 and a nearly flat inlet velocity profile. The reattachment length reached a peak at a Reynolds number of approximately 250 and then decreased until the flow became turbulent at a Reynolds number of about 1000, when the reattachment length began to increase slowly. Visual observations showed that for Reynolds number in the range 200-400 there was a "vortex street-like" region.

Abbott and Kline [21] studied the effect of the expansion ratio in turbulent flow and observed that the main effect was a lengthening of the separation zones with increasing step heights, the longer zone growing proportionally a

little faster than the smaller zone, but there was no evidence of a third separation region.

Recent also studies of the laminar flow over planar backsteps include the works of Goldstein et al. [10], Denham and Patrick [13], Sinha et al. [42], Leal and Acrivos [22], Durst et al. [44] and Armaly et al. [5]. Macagno and Hung [2] presented numerical predictions of laminar separation in a 2-D conduit expansion. Aung [45] examined the forced convection heat transfer problem associated with the flow over a planar backstep. Iribarne et al. [3], and Hung and Macagno [20] examined the laminar flow separation over a circular backstep produced by a sudden pipe expansion.

Napolitano and Cinnella [51], Lewis and Pletcher [32] and Kwon et al. [8] investigated sudden expansion flows with boundary layer equations. They compared solutions from finite difference approximations of the Navier-stokes equations with solutions. As expected, the boundary layer solutions were acceptable for sufficiently large Reynolds number only.

Valentine and Hyde [4] presented numerical predictions of the size of the recirculation region behind an annular backstep created by an abrupt change in radius of the inside cylinder in an annular flow passage. Their predictions were based on a Navier-stokes solver that implemented a nearly 2nd order finite difference method that used the ADI method complied with an artificial compressibility scheme to accelerate convergence to steady state. The present investigation examined the inner- and outer- radius annular backsteps flow problem in more detail.

CHAPTER - 3

CHAPTER - 3

METHOD OF SOLUTIONS

3.1 SCOPE

In this chapter, the method of the numerical simulation is briefly described. The governing equations are first summarized. The solution of the set of equations requires specification of boundary conditions for all the unknown variables. Certain types of boundary are common in all flows examined in this thesis and corresponding "problem independent" boundary conditions are described in section 3.3. In sections 3.4 and 3.5, important aspects of the governing equations in general forms and the numerical solution of the governing partial differential equations relevant to the problems studied are discussed respectively. The solution technique is then briefly outlined. Boundary conditions are described in short. Finally, closing remarks are also given.

3.2 GOVERNING EQUATIONS

Considering an incompressible, steady axisymmetric flow with a Newtonian constant viscosity fluid, the governing differential equations are as follows:

The continuity equation for an axisymmetric flow is

$$\frac{\partial u}{\partial x} + \frac{\partial v}{\partial r} + \frac{v}{r} = 0 \quad (3.1)$$

The Navier stokes equations for an axisymmetric incompressible flow are

x-momentum equation

$$u \frac{\partial u}{\partial x} + v \frac{\partial v}{\partial r} = -\frac{1}{\rho} \frac{\partial p}{\partial x} + \nu \left[\frac{\partial^2 u}{\partial x^2} + \frac{1}{r} \frac{\partial u}{\partial r} + \frac{\partial^2 u}{\partial r^2} \right] \quad (3.2)$$

r-momentum equation

$$u \frac{\partial v}{\partial x} + v \frac{\partial v}{\partial r} = -\frac{1}{\rho} \frac{\partial p}{\partial r} + \nu \left[\frac{\partial^2 v}{\partial x^2} + \frac{1}{r} \frac{\partial v}{\partial r} + \frac{\partial^2 v}{\partial r^2} - \frac{v}{r^2} \right] \quad (3.3)$$

where ρ is the density, ν is the kinematic viscosity and p is pressure, u and v are the velocity components in the x - and r - directions respectively, x and r are the axisymmetric cylindrical co-ordinates as shown in figure-4.1.

3.3 BOUNDARY CONDITIONS

The transport equations mentioned above are of elliptic type. The solution of elliptic partial differential equations requires information to be provided at all points on a closed boundary surrounding the solution domain. The specification of these conditions varies according to the type of boundary and the dependent variable under consideration.

i. INLET BOUNDARY:

At inlet, a fully developed velocity profile

$$\frac{U}{U_o} = 2 \frac{\left[a^2 - r^2 + \frac{a^2 - b^2}{\ln(b/a)} \ln \frac{a}{r} \right]}{\left[a^2 + b^2 + \frac{a^2 - b^2}{\ln(a/b)} \right]}$$

was used where U_o is the average velocity at the inlet. Here $a = r_3$ and $b = r_2$ for inner- radius annular backstep and $a = r_2$ and $b = r_1$ for outer- radius annular backstep.

ii. PLANE OR AXIS OF SYMMETRY

At a symmetry plane or at an axis of symmetry, the normal gradient is zero for all scalar quantities and velocity components parallel to the plane; the velocity component normal to the plane is set to zero.

iii. OUTLET CONDITION

The imposed exit boundary condition is a parallel outflow with the pressure gradient in the r-direction set equal to zero and the vertical velocity component set equal to zero as well.

iv. SOLID WALL

No-slip boundary conditions were applied to all solid walls (i.e. top, side and bottom wall).

3.4 THE GOVERNING EQUATIONS IN GENERAL FORM

The governing differential equations for steady, incompressible, two-dimensional laminar flows of Newtonian fluid in cylindrical co-ordinates in the following forms:

$$\frac{\partial}{\partial x}(\rho u \phi) + \frac{1}{r} \frac{\partial}{\partial r}(r \rho v \phi) = \frac{\partial}{\partial x} \left(\mu \frac{\partial \phi}{\partial x} \right) + \frac{1}{r} \frac{\partial}{\partial r} \left(r \mu \frac{\partial \phi}{\partial r} \right) + S_{\phi} \quad [3.4]$$

In equation 3.4 the first two terms are the convection terms, third and fourth terms are the diffusion terms and S_{ϕ} is the source terms which contains terms describing the generation (creation) and consumption (dissipation) of variable ϕ . In above equation, replacement of ϕ with value 1 gives the continuity equation, while for $\phi = u, v$ gives the two momentum equations are obtained. The forms for the source term S_{ϕ} are given in Table 3.1.

TABLE - 3.1
Source Terms for General Equation (3.4)

Value of ϕ	Name of equation	Source Term, S_ϕ
1	continuity	0
u	x- momentum	$-\frac{\partial p}{\partial x} + S^u$
v	r- momentum	$-\frac{\partial p}{\partial r} - \frac{\mu v}{r^2} + S^v$

where,

$$S^u = \frac{\partial}{\partial x} \left(\mu \frac{\partial u}{\partial x} \right) + \frac{1}{r} \frac{\partial}{\partial r} \left(r \mu \frac{\partial u}{\partial x} \right)$$

$$S^v = \frac{\partial}{\partial x} \left(\mu \frac{\partial v}{\partial x} \right) + \frac{1}{r} \frac{\partial}{\partial r} \left(r \mu \frac{\partial v}{\partial x} \right)$$

The above equations have to be solved for the pressure, p ; velocity component u, v .

3.5 NUMERICAL SOLUTION OF DIFFERENTIAL EQUATIONS

All partial differential equations have the following generalized form:

$$\frac{\partial}{\partial t} (\rho \phi) + \frac{\partial}{\partial x_i} (\rho U_i \phi) = \frac{\partial}{\partial x_i} \left(\mu \frac{\partial \phi}{\partial x_i} \right) + S_\phi \quad (3.5)$$

where ϕ is a general dependent variable and can be equated to 1 for continuity ($S_1 = 0$), U_i for momentum. These equations differ only in the form of the source term, S_ϕ and their dynamic viscosity, μ

Along with the boundary conditions, these elliptic equations are solved numerically by a standard finite volume method. The detailed derivation and formulation of this method can be found for example in Patankar [37]; here

only a brief description of the general make-up of the method is provided together with a few remarks of special practices particular to the flows considered in this thesis.

3.5.1 THE FINITE-DIFFERENCE EQUATIONS - GENERAL REMARKS

The differential equation (3.5) is reduced to a set of algebraic equations by integration over small control volumes or cells. The calculation domain is divided into a finite number of such control volumes by a computational grid which for the present problems conforms to either cartesian or cylindrical polar co-ordinate lines. Numerical values of the scalar variables and pressure are determined at the intersection of these mesh lines (grid node). The velocities are calculated at a point half way between these grid nodes. This "staggered" location for velocities makes the calculation of the pressure gradients easy which drive the velocity and necessitates the adoption of different control volumes for each of the velocity components. Figure 3.1 shows such control volumes for a 2-D case in cartesian co-ordinates.

Integration of equation 3.5 [excluding the time-dependent term] over the corresponding control volume for the variable in question together with appropriate assumptions about the way in which quantities vary between grid nodes leads to algebraic equations of the following form [37].

$$a_p \theta_p = \sum_{i=N,S,E,W} a_i \theta_i + S_{\theta,p} \quad (3.6)$$

where $a_p = \sum a_i$ and P is the central node of the control volume and N, S, E, W are neighbour nodes of the control volume (see figure 3.1). The neighbour coefficients a_i contain the influence of the convective and diffusive fluxes through the cell faces.

3.5.2 THE DISCRETIZATION SCHEME

The integration of the convection terms on the left hand side of equation (3.5) leads to the need to interpolate θ values at the cell faces from adjacent nodal

values. This interpolation practice constitutes the most problematic element of the discretization scheme (the diffusive fluxes are always discretized using second order accurate central differencing). In the present work the quadratic upstream weighted scheme proposed by Leonard [16] known as QUICK (Quadratic Upstream Interpolation for Convective Kinematics) has been used. This avoids many of the numerical stability problems associated with central differencing and the numerical or false diffusion inaccuracies related to the first order UPWIND scheme (Leonard et. al. [56], Leonard [16], Leschziner [57], Leschziner & Rodi [58]), both of which are common alternatives used often in the past. Figure 3.2 presents an illustration of the differences between these schemes for the interpolation of θ at one cell face in terms of the adjacent nodal values (uniform mesh used for simplicity).

Although the QUICK scheme improves the false diffusion aspect of the crude UPWIND scheme, the solutions it produces may not be bounded (i.e. under/overshoots may occur) and problems may be experienced due to the generation of oscillations in the dependent variables in circumstances where the flow displays a combination of high cell Peclet number and high spatial gradients [Leonard, 16]. These oscillations are mainly due to the appearance of negative values of the finite difference a_j coefficients with the QUICK scheme and may (i) produce physically unrealistic solution (e.g. negative k and e) and (ii) destroy the diagonal dominance of the coefficient matrix which eventually produces numerical divergence when a line-by-line iterative method of solution of the linearised equations is employed.

3.5.3 SOLUTION ALGORITHM

The mass conservation, momentum and the coupled scalar equations are solved simultaneously using the SIMPLE (Semi Implicit Method for Pressure-Linked Equations) algorithm proposed by Patankar & Spalding [60] to obtain the pressure field. This algorithm has been described in detail by Patankar [37].

The algebraic equations (3.6) are solved by repeated sweeps of a line-by-line application of the well known Tri-diagonal Matrix algorithm (TDMA) (See Patankar [37]). The equations solved along constant x_j lines and in so doing

the variables located along adjacent lines are kept constant. The a_j coefficients of equation (3.6) and source term, S_θ are evaluated using values of the variables at the start of the TDMA sweep and are not changed during TDMA solution.

The convergence history of all solutions was monitored by using a normalized mass source error whose value has to be less than 10^{-5} for convergence to be accepted. This mass source error was defined as:

$$\text{Error} = \sum_{i=1}^n \left| \frac{\partial}{\partial x_j} (\rho U_j) \right|_i; \quad n = \text{number of cells}$$

This was then normalized by the actual flow rate into the calculation domain.

3.6 Closure

The governing differential equations are presented in this chapter in a form which has been used in the computer program. The solution technique, finite difference formulations and boundary conditions are discussed briefly. Finally the solution procedure is also outlined.

An available computer program is used to simulate the present flow field and the results are discussed in the next chapter.

CHAPTER - 4

CHAPTER - 4

RESULTS AND DISCUSSIONS

4.1 SCOPE

This chapter is devoted to the analysis of results obtained from the numerical predictions of the laminar flow separation over an inner- and outer-radius annular backsteps, using a modified version of the PACE Computer Code of Jones [39]. The governing equations presented in the previous chapter are used for the present study. The problem is first defined, and then the validity and credibility of the computer code are verified by comparing the numerical prediction for similar problems for which experimental data are available. The effect of Reynolds number and the annular radius ratio are studied. Also the vorticity (skin friction co-efficient) distribution along the walls are investigated. Closing remarks are provided at the end of the chapter.

4.2 PROBLEM STATEMENT

The computational domain is shown in figure 4.1. Primarily, the prediction was performed using the flow geometry considered was made up of an inlet annular depth of $h = 40$ mm merging into an another annular cylinder of depth $H = (h + s) = 80$ mm yielding a depth ratio $H/h = 2.0$. The length of the computational domain was considered 30 times of the larger annular depth, H ; so that the exit boundary should be far away from the separated regions. The annular radius ratio is defined as $\alpha = r_1/r_3$ where $r_3 = r_1 + H$. Then the effect of the radius ratio was tested using $H = 80$ mm but varying the inlet annular depth, h . Present study predicts the numerical study of Mohamed et al. [15] and experimental study of Armaly et al. [5] and also predicted Islam et al. [7] for $\alpha = 1.0$ and for an expansion ratio $H/h = 1.94$. All the dimensions of the configurations are also shown in figure 4.1. The computational domain was divided with a $(70 * 50)$ grid using non-uniform line spacing. 70 grid lines in the streamwise direction and 50 grid lines in the transverse direction. Grid dependency was tested by repeating calculations for $\alpha = 0.2$ with $65 * 45$, $100 * 40$ and $70 * 50$ grids. The $70 * 50$ grid gave reasonably good predictions.

when compared to the numerical prediction of Mohammed et al. [15] (see fig 4.2). A fine grid was used in the flow separation area and solid walls and a relatively course grid used in the flow regions far from the step.

4.3 VALIDATION OF THE NUMERICAL MODEL

To validate the present methodology primarily a series of predictions are performed for Reynolds number ranging $Re_s = 50 \sim 500$. The Reynolds number, Re_s is defined as: $Re_s = \frac{U_o s}{\nu}$. The present numerical prediction is compared with available predicted results for an expansion ratio 2.0 with fully developed velocity profile at inlet in fig 4.3 (Mohamed et al. [15]). It appears that the predictions of the present methodology are in good agreement with the experimental data and available predicted data and hence it may be concluded that the present numerical model has the capability of predicting complex laminar flows with reasonable accuracy.

The computer code is then modified to incorporate calculation for the present study.

4.4 COMPARISON WITH AVAILABLE DATA

The qualitative results of the lengths of the primary and secondary vortices are presented in figs. 4.4 ~ 4.7. Figure 4.4 shows the variations of the length of the primary vortex with Reynolds number (Re_s) for different annular radius ratio (α) for the inner-radius annular backstep. The results for $\alpha = 0.2$ and $\alpha = 1.0$ (Planar backstep) are compared with the available predicted and experimental data. Note that the results of Armaly et al. [5] and Islam et al. [7] for $\alpha = 1.0$ are for an expansion ratio $H/h = 1.94$, whereas the present prediction is for $H/h = 2.0$. However, the present prediction provides an excellent agreement for this case upto $Re_s = 300$. For the Reynolds number $Re_s > 300$, the agreement to be less good for the case of the present prediction and Armaly et al. [5], but the results of Islam et al. [7] are also agreement with higher Reynolds number. This increased disagreement between experimental and present predicted results at higher Reynolds number is caused by the

occurrence of inherent three dimensional effects in the experiments that reach the centre plane of the Channel [5]. Armaly et al. [5] pointed out that the experimental values were determined from photographic records that depend on a flow visualization that used entrained air bubbles, appropriate illumination, depth of field and time of exposure. The length of the recirculation region presented by Leal and Acrivos [22] are known to be higher than the lengths presented by others for the planar backsteps; (see Islam et al. [7]). The results of Mohamed et al. [15] for $\alpha = 0.2$ and expansion ratio $H/h = 1.5$, whereas the present prediction is for $H/h = 2.0$. However the present prediction provides an good matching. The present prediction is consistent with the same conclusions drawn by Denham and Patrick [13] in their investigations of the laminar recirculation zone behind a planar, 2-D backstep in a channel. The experimental data and supporting numerical predictions for planar backstep indicate that the length of the recirculation is a strong function of Reynolds number and annular radius ratio (α), and a relatively weak function of the other parameters. The predicted fact that the change in length of the recirculation region with Re_s was also found by Macagno and Hung [20] for the pipe expansion backstep problem. It is also shown that the inner-radius annular backstep geometry produces the shortest recirculation zones.

The predicted length of the primary vortex for the outer-radius annular backstep is presented in fig. 4.5 and also compared with pipe expansion. The area expansion ratio (α) for the pipe expansion data is 0.25. For $\alpha = 0.1$ and 0.2, the length of the primary vortex increases linearly with Re_s like the pipe expansion case. The occurrence of the secondary vortex on the opposite wall at $\alpha = 0.5 \sim 1.0$ slows down the growth of the primary vortex with Reynolds number (Re_s). The longest recirculation regions are observed in the pipe expansion backstep geometry. For the equivalent Reynolds number (Re_s), the recirculation region (or length of the primary vortex) will be the longest in pipe expansion flow as shown in fig. 4.5.

The predicted size of the secondary vortex is shown in figs. 4.6 and 4.7 for the inner- and outer-radius annular backsteps for different annular radius ratio (α) respectively. The top three curves are for reattachment point x_3 which increases linearly with Reynolds number and bottom three curves are for reattachment point x_2 which also increases linearly with Reynolds number

but the slope of the top three curves becomes more steeper than those of bottom. The secondary vortex on the opposite wall grows bigger in size ($x_3 - x_2$) with annular radius ratio, α at a particular Re_s for both inner and outer radius annular backstep cases.

4.5 EFFECT OF REYNOLDS NUMBERS

The numerical results for the configuration shown in figure-4.1 are presented in this section for a Reynolds number range of 50 ~ 500 and an annular radius ratio range of 0.1 ~ 1.0. The prediction of the recirculation region length were presented by Valentine & Hyde [4]. Their results were produced by solving the Navier-stokes equations for unsteady, incompressible, laminar flow by applying a nearly 2nd-order finite difference method that uses the ADI method coupled with an artificial compressibility scheme to accelerate convergence to steady-state. In addition to verify the previously reported, preliminary results the new solution provide additional information about laminar flow separation over annular backsteps.

Figure 4.8 shows the constant streamline contours for inner- radius annular backstep at $\alpha = 0.1$ [Note that the axial distance has been compressed by 5 times] for several Re_s values. The length of the primary vortex attached to the step increases with Reynolds number. For $Re_s > 100$ the secondary circulation in the recirculation region that occurs in the lower corner of the backstep is significant in size. These secondary circulation increases with Reynolds number. Figure 4.9 shows the constant streamline contours for outer-radius annular backstep at annular radius ratio $\alpha = 0.1$ for several Reynolds number. The length of the primary vortex attached to the step also increases linearly with Reynolds number, but this increment is much higher in the case of outer-radius annular backstep.

Figure 4.10 and 4.11 show constant streamline contours for both inner- and outer-radius annular backsteps at $\alpha = 0.2$ for several Reynolds number respectively. The length of the primary vortex attached to the step increases with Reynolds number in both cases, but this increment is also much higher in the case of outer-radius annular backstep. A secondary vortex is formed at the opposite wall at $Re_s = 500$ for the inner- radius annular backstep. An

additional recirculating flow region (secondary vortex) was observed at the opposite wall downstream of the flow passage (see in fig. 4.10). The presence of secondary vortices are also supported by experimental studies of Armaly et. al. [5]. This separation region develops in the laminar range and remains in existences throughout the transition region [5]. Its appearance is due to the adverse pressure gradient created on the opposite wall owing to the curvature of the streamline for primary vortex. Its existences is largely dependent on the annular radius ratio (α) and Reynolds number for both cases.

Figures 4.12 and 4.13 show constant streamline contours for both inner- and outer-radius annular backsteps at $\alpha = 0.5$ for several Reynolds number respectively. The length of the primary vortex are similar in both the cases. For $Re_S > 300$, the secondary vortex also appears at the opposite wall for inner-radius annular backstep but for $Re_S > 200$, the secondary vortex also appears at the opposite wall for outer- radius annular backstep. The size of the secondary vortex are increases with Reynolds number for both inner- and outer-radius annular backstep and a second secondary vortex also appears at the step side wall for outer radius annular backstep at $Re_S > 400$.

Figures 4.14 and 4.15 show the constant streamline contours for both inner- and outer-radius annular backsteps at $\alpha = 0.75$ for several Reynolds number respectively. The length of the primary vortex are similar of previously discussed above. For inner radius annular backstep, the secondary vortex also appears at the opposite wall beyonds $Re_S = 300$ and for outer-radius annular backstep, the secondary vortex are also appears at the opposite wall beyonds $Re_S = 100$ and a secondary vortex grows bigger in size with Reynolds number and also a second secondary vortex also appears at the step side wall for outer radius annular backstep at $Re_S = 500$ but size of a second secondary vortex is smaller than $\alpha = 0.5$ and $Re_S > 400$. In addition to the secondary vortex on the opposite wall, another secondary vortex appears on the stepside wall downstream of the primary region of the separation. Armaly et al. [5] also reported this separation region for plane sudden expansion geometry. It is very thin. It originates in the reynolds number range corresponding to the early part of the transition region [5] (see fig. 4.33) , where the reattachment length experiences a sharp drop in its magnitude. These strong variations in flow properties to be caused by vortex

shedding from the edge of the step. These vortices were thought to approach the wall, and the secondary recirculating flow might then be due to the sharp change of flow direction which the eddies experience.

Figure 4.16 shows the constant streamline contours for both inner- radius annular backstep for several Reynolds number at $\alpha = 1.0$ (i.e. planar backstep). Predictions of the size of the flow separation region downstream of the planar backstep examined experimentally by Armaly et al. [5] were made to compare with their observation. For the low Re_S planar backstep flows the computed reattachment length increases monotonically with Reynolds number. The increase of reattachment length with Re_S is nonlinear. However, when there is only one vortex in the recirculation region the change in length is linear. The length of primary vortex for both inner and outer backstep increases with Re_S . At this configuration, a secondary vortex appears beyond $Re_S = 200$ for inner radius annular backstep. The secondary vortex grows for both cases bigger with Reynolds number.

Figures 4.17 ~ 4.21 are shown the constant vorticity contours for the inner-radius annular backstep at $\alpha = 0.1, 0.2, 0.5, 0.75, 1.0$ for several Reynolds number respectively. [Note that the axial distance has been compressed by 5 times]. The vorticity lines shown in figures are stretched in the direction of flow as the Reynolds number becomes larger; it is obvious that the peak value of the vorticity cannot coincide with the separation line, because otherwise a contradiction would result at the reattachment point, where the vorticity must be zero. In fact, the vorticity peak first moves into the main flow when separation occurs and then moves back to the wall well downstream from the stream reattachment point. Figures 4.22 ~ 4.25 also shown the constant vorticity contours for the outer-radius annular backstep at $\alpha = 0.1, 0.2, 0.5,$ and 0.75 respectively.

4.6 EFFECT OF ANNULAR RADIUS RATIO

The effect of the annular radius ratio on the flow field are presented in figures 4.26 and 4.27 for inner and outer radius annular backstep at $Re_S = 100$ [Note that the axial distance has been compressed by 5 times] respectively. The length of the primary vortex increases with annular radius ratio for inner

radius annular backstep and decreases monotonically with annular radius ratio for outer radius annular backstep.

Figures 4.28 and 4.29 show the constant stream line contours for inner- and outer- radius annular backsteps at $Re_s = 200$ respectively. The length of the primary vortex attached to the step increases with annular radius ratio for inner radius annular backstep but decreases for outer-radius annular backstep. At these configuration, a secondary vortex appears only outer-radius annular backstep cases at $\alpha = 0.75 \sim 1.0$ and the secondary circulation in the recirculation region that occurs in the lower corner of the backstep is less significant in size at $\alpha = 0.1$ for inner radius annular backstep.

Figure 4.30 and 4.31 also show the constant stream line contours for inner and outer radius annular backstep respectively at $Re_s = 300$. The length of the primary vortex are quantitatively similar in comparison to the case $Re_s = 200$. Secondary vortex appears on the opposite wall for both inner- and outer-radius annular backstep cases beyonds $\alpha = 0.2$.

Figures 4.32 and 4.33 show the constant stream line contours for inner- and outer- radius annular backstep respectively for several annular radius ratio at $Re_s = 500$. The length of the primary vortex attached to the step increases with annular radius ratio (α) for inner- radius annular backstep but decreases for outer- radius annular backstep. The length of the primary vortex much higher at lower Reynolds number for outer- radius annular backstep. For inner- radius annular backstep, the secondary vortex appears at the opposite beyonds $\alpha = 0.1$ and the size of the secondary vortex increases with annular radius ratio (α) also the similar phenomena for outer- radius annular backstep and also the secondary circulation occurs in the lower corner of the backstep at $\alpha = 0.1$ and bottom surface at $\alpha = 0.2$. The second secondary vortex also appears at the stepside wall for outer- radius annular backstep at $\alpha = 0.5 \sim 0.75$.

4.7 VORTICITY DISTRIBUTION ALONG THE WALLS

The shear stress distribution along the walls of the passage are of engineering interest. The local value of the vorticity at the wall (or no-slip boundary) is proportional to the local value of the shear stress. Hence, to examine the

variation in shear stress acting on the walls of the annular passage, we may examine the plots for the vorticity distributions along the step side and the opposite walls for both inner and outer radius annular backstep.

The vorticity at the walls is related to the local skin friction coefficient and is defined as

$$c_f = \frac{2\tau_w}{\rho U^2}$$

where τ_w is the shear stress along the wall, ρ is the mass density of the fluid and U is the characteristic velocity. Newtons Law of viscosity states that

$$\tau_w = \mu \frac{dU}{dr}$$

where μ is the dynamic viscosity of the fluid and r is the direction normal to the wall. For the stepside wall r is R . Hence

$$c_f = \frac{2}{Re_s} \cdot \frac{s}{U} \cdot \frac{dU}{dr}$$

Thus the wall value of the vorticity along the inner wall is related to the local value of the skin friction as follows

$$\Omega_w = -\frac{dU}{dr} = -\frac{c_f \cdot Re_s}{2} \cdot \frac{U}{s}$$

Figures 4.34 (a-f) show the vorticity distribution along the walls for the inner-radius annular backstep for $\alpha = 0.1$. For $Re_s = 50$, the magnitude of the vorticity (on shear stress) along the opposite wall decreases in the direction downstream from the backstep to a minimum at about $x/H = 2.2$ which is a point just downstream of the reattachment point (see fig. 4.34 a). Then it increases to the fully developed flow value. Along the stepside wall the vorticity (or shear stress) increases from zero at the bottom of the backstep to a maximum value at $x/H = 1.0$. The magnitude of the maximum vorticity along

the stepside wall is 1.3. It then decreases to the fully developed value. The reattachment point is at $x/H = 2.0$, which is defined as the point where the vorticity (or shear stress) is zero at the step side wall. For $x/H > 5.5$, the vorticity becomes almost constant. In figures 4.34 (b-f) the vorticity distributions on the both walls are presented for $Re_s = 100, 200, 300, 400$ and 500 respectively. The general trend of the vorticity distribution is similar to that of $Re_s = 50$ except in the cases of $Re_s \geq 200$. In such cases, the vorticity distributions along the stepside wall has a second peak.

In figure 4.35 (a-f) the vorticity distributions along the wall of outer-radius annular backstep is shown.

In the inner radius annular backstep case a "vortex ring" is compressed in the circumferential direction as it moves downstream over the backstep. The compression causes the "ring" to induce higher magnitude of the velocity at points equidistant from the "ring" in any (r, x) plane. At radii less than the radius of the "ring" the relatively larger induced velocity field induced by the compressed "ring vortex" will tend to retard the local velocity and thus the growth of the recirculation region as compared with the equivalent nonstretched "vortex" moving over the 2-D (Planar) backstep (see Mohamed et. al. [15]). Hence the recirculation region in the inner-radius annular backstep problem is indeed expected to be shorter than for the planar backstep problem.

The effects of Reynolds number and annular radius ratio are shown in figures 4.36 ~ 4.37 along the stepside and opposite wall for inner-radius annular backsteps respectively. As we see in the fig. 4.36 , with the increase of Reynolds number the maximum value of the vorticity increases as well as the locations move downstream of the annular flow passage. The value of second peak increases with Reynolds number and locations moves downstream of the passage. For fig. 4.37, with the increase of Reynolds number the negative peak value of the vorticity increases as well as locations moves downstream of the annular flow passage.

The effects of Reynolds number and annular radius ratio are also shown in figures 4.38 ~ 4.39 along the stepside and opposite walls for outer-radius annular backsteps respectively. As we see in the fig. 4.38, with the increase of

Reynolds number both the negative and the positive maximum peak values of the vorticity increase as well as locations moves downstream of the flow passage. For fig. 4.39 with the increase of Reynolds number the maximum value of the vorticity increases.

4.7 CLOSURE

The present computer code is used to simulate the laminar flow separation over annular backsteps. Numerical predictions are compared with the available experimental data and found to have reasonably good matching. The flow was investigated for different Reynolds number, annular radius ratio over annular backsteps. Also the vorticity distribution along the walls was studied for different Reynolds number and annular radius ratio (α). Useful nondimensionalized results are provided with discussions.

CHAPTER - 5

CHAPTER - 5

CONCLUSIONS AND RECOMMENDATIONS

5.1 SCOPE

This chapter summaries the results of the flow fields over the inner- and outer-radius annular backsteps and also suggests the scope of further extension of the present study.

5.2 CONCLUSIONS

The results of this thesis have been presented in the previous chapter. Based on those results the following conclusions can be drawn:

1. The laminar reattachment length is a relatively strong function of Reynolds number (Re_s). The length of the primary vortex attached to the step wall increases with Reynolds number for both the inner- and outer- radius annular backsteps, but this increment is much higher in the case of outer-radius annular backstep. This is a typical characteristics of the separation of laminar flow over backsteps.
2. The length of the primary vortex increases with annular radius ratio (α) in the case of inner- radius annular backstep but decreases in outer- radius annular backstep.
3. For the equivalent Reynolds number the reattachment length for the inner- radius annular backstep is shorter than for the planar backsteps but in case of outer- radius annular backstep reattachment length is larger than the same planar backstep and shorter than for the axisymmetric pipe expansion .
4. Secondary vortex appears on the opposite wall but its occurrence depends on the Reynolds number and annular radius ratio (α)
5. High Reynolds number range with multiple separation bubbles approaching the onset of the transition. In the case of outer-radius annular backstep length of reattachment region linear for low annular radius ratio .

6. The secondary vortex grows bigger in size with annular radius ratio (α) at a particular Reynolds number for both the inner- and outer-radius annular backsteps.

5.3 RECOMMENDATION FOR FUTURE WORK

There are many different ways in which this work can be extended. For future improvement, the following works may be recommended:

1. The effect of an expansion ratio can be studied.
2. Unsteady, compressible laminar flow can also be studied.
3. Heat transfer can be added.
4. The effect of mass transfer can also be added.
5. Turbulent flow can be considered.
6. Concentric annular backsteps with inner pipe rotating can be studied.
7. Annular backstep with outer pipe rotating can also be investigated.
8. The effect of inlet condition on the structure of laminar flow over annular backsteps may be incorporated.

REFERANCES

REFERENCES

1. Moniruzzaman, M., Naser, J.A., and Islam, A.K.M.S., "Prediction Of Secondary Flow Separation In Laminar Backward Facing Step", Int. Cong. on computational Methods in Engineering, Shiraz, Iran, pp.75-82,1993.
2. Macagno, E.O. and Hung, T.K., "Computational And Experimental Study Of A Captive Annular Eddy", J. Fluid Mech. Vol. 28, pp. 43-64, 1967.
3. Iribarne, A., Franlisak, F., Hummel, R.L., and Smith, J.W., " An Experimental Study Of Instabilities And Other Flow Properties Of A Laminar Pipe Jet", A.I.Ch.E. J., Vol. 18, pp. 689, 1972.
4. Valentine, D.T. and Hyde, G.W., " Axisymmetric Laminar Flow Over An Annular Backstep: A Numerical Study", In Proc. 5th Int. Conf. on Numerical Methods in Laminar and Turbulent Flow, Montreal, Canada, pp. 607-618, 1987.
5. Armaly, B.F., Durst, F., Pereira, J.C.F. and Schonung, B., " Experimental And Theoretical Investigation Of Backward Facing Step Flow", J. Fluid Mech., Vol. 127. pp. 473-496, 1983.
6. Durst, F. and Periera, J.C.F., " Time-Dependant Laminar Backward Facing Step Flow In A Two- Dimensional Duct", J. of Fluid Engg., ASME, Vol. 110. pp. 289-296, 1988.
7. Islam, M.Q., Hossain, M., Naser, J.A. and Islam, A.K.M.S., " Effect Of Inlet Condition On The Structure Of Laminar Flow In An Axisymmetric Channel Expansion", 6th Asian Cong. of Fluid Mech., Singapore, pp. 935-938, 22-26 May, 1995.
8. Kwon, O.K., Plectcher, R.H. and Lewis, J.P., " Recirculation Of Sudden Expansion Flows Using The Boundary Layer Equations", J. Fluid Engg., pp. 285, 1984.
9. Cramer, K.R., " On Laminar Separation Bubbles", J. of the Aeronautical Sciences, Vol. 25, pp. 143- 144, 1958.
10. Goldstein, R.J., Eriksen, V.L., Olson, R.M., Eckert, E.R.G., " Laminar Separation, Reattachment, And Transition Of The Flow Over A Downstream- Facing Step", J. Basic Engg., Vol. 92, pp. 732-741, 1970.
11. Sato, H., " Experimental Investigation On The Transition Of Physical Society Of Japan", Vol. 11, No. 06, pp. 702-709, June, 1956.

12. Chapman, D.R., Kuehn, D.M. and Larson, H.K., " Investigation Of Separated Flows In Supersonic And Subsonic Streams With Emphasis On The Effect Of Transition", NACA Report, pp. 1356, 1958.
13. Denham, M.K. and Patrick, M.A., " Laminat Flow Over A Downstream Facing Step In A Two- Dimensional Flow Channel", Trans. Instn. Chem. Engrs., Vol 52, pp. 361, 1974.
14. Atkins, D.J., " Numerical Studies Of Separated Flows ", Ph.D Thesis, University Of Exeter, U.K., 1975.
15. Mohamed, A.G., Valentine, D.T. and Hassel, R.E., " Numerical Study Of Laminar Separation Over An Annular Backstep", Computers and fluids, Vol. 20, No. 02, pp. 121- 143, 1991.
16. Leonard, B.P., " A Stable And Accurate Convective Modeling Procedure Based On Quadratic Upstream Interpolation", Comp. Methods in Appl. Mech. and Engg., Vol. 19, pp. 59-98, 1979.
17. Eaton, J.N. and Johnston, J.P., " Turbulent Flow Reattachment : An Experimental Study Of The Flow And Structure Behind A Backward Facing Step", Report MD- 39, Dept. of Mech. Engg., Stanford University, June, 1980.
18. Ghia, H.N., Oswald, G.A. and Ghia, U., " A Direct Method For The Solution Of Unsteady Two- Dimensional Incompressible Navier-Stokes Equations", 2nd Symp. on Num. Phys. Aspects of Aerodynamics Flows, California State University, January, 1987.
19. Durst, F., Melling, A. and Whitelaw, J.H., " Optical Anemometer Measurements In Recirculating Flows And Flames", Fluid Dynamics Measurements in Industrial and Medical Envirnmnts. Proc. DISA Conf. , Vol. 1, No. II, Leicester University Press.
20. Hung, T., Macagno, E.O., " Laminar Eddies In A Two- Dimensional Conduit Expansion", La Houille Blanche , Vol. 21, pp. 391, 1966.
21. Abbott, D.E. and Kline, S.J., " Experimental Investigation Of Subsonic Turbulent Flow Over Single And Double Backward Facing Steps" J. of Basic Engineering, Trans. ASME D -84, pp. 317, 1962.
22. Acrivos, A. and Leal, L.G., " The Effect Of Base Bleed On The Steady Separated flow Past Bluff Objects", J. Fluid Mech. Vol. 39, pp.111, 1974.
23. Kuman, A. and Yajnik, K.S., " Internal Separated Flows at Large Reynolds Number : J. Fluid Mech., Vol. 97, pp. 77, 1980.

24. Vogel, J.C. and Eaton, J.K., " Combined Heat Transfer And Fluid Dynamics Measurements Downstream Of A Backward Facing Step", J. of Heat Transfer, ASME, Vol. 107, pp. 922-927, Nov. , 1985.
25. Mansour, N.N. and Moin, P. " Computing Of Turbulent Flows Over A Backward Facing Step", 4th Symp. on Turbulent Shear Flow, Karlsruhe, 1983.
26. Aung, W., Baron, A. ,and Tsou, F.K., " Wall Independency And Effect Of Initial Shear Layer Thickness In Separated Flow And Heat Transfer", Int. J. Heat Mass Transfer, Vol. 28, No. 09, pp. 1757- 1771, 1985.
27. Tsou, F.K., Chen, S.J., and Aung, W., " Starting Flow And Heat Transfer Downstream Of A Backward Facing Step", J. of Heat Transfer, ASME, Vol. 113, pp. 583- 589, Aug., 1991.
28. Gosman, A.D. and Pun, W.M., " Lecture Note For Course Entitled Calculation Of Recirculating Flow", HTS/74/2, Imperial College, London, 1974.
29. Reynolds, O., " An Experimental Investigation Of The Circumstances Which Determine Whether The Motion Of Water Will Be Direct Or Sinuous ~~Law~~ Law Of Resistance In Parallel Channels", Phil. Trans. Roy. Soc. Lond., Vol. 174A, pp. 935, 1883.
30. Bird, R.B., Stewart, W.E., and Lightfoot, E.N., " Transport Phenomena", Wiley, New York, 1960.
31. Shaw, C.T., " Using Computational Fluid Dynamics", Prentice Hall International (UK) Ltd., 1992.
32. Lewis, J.P. and Pletcher, R.H., " Limitations Of The Boundary Layer Equations For Predicting Laminar Symmetric Sudden Expansion Flows", J. Fluids Engg., Vol. 108, pp. 208, 1986.
33. Binder, R.C., " Advanced Fluid Mechanics" Vol.II, Prentice- Hall of IndiaLtd., New Dehli, 1964.
34. Patankar, J.D., " Introduction to Fluid Mechanics and Heat Transfer", Addison-Wesley Publishing Company, pp. 77, 1969.
35. Monnet, P., Menard, C., and Sigli, D., " Some New Aspects Of The Slow Flow Of A Viscous Fluid Through An Axisymmetric Duct Expansion Or Contraction. Ii. Experimental Part", Applied Scientific Research, Vol. 39, pp. 233- 248, 1982.

36. Fletcher, D.F., Maskell, S.J. and Patrick, M.A., " Heat And Mass Transfer Computations For Laminar Flow In An Axisymmetric Sudden Expansion", *Computers and Fluids*, Vol. 13, No. 02, pp. 207- 224., 1985.
37. Patankar, S.V., " Numerical Heat Transfer and Fluid flow", Hemisphere Publishing Corporation, McGraw- Hill Book Company, New York, 1980.
38. Badekas, D. and Knight. D.D., " Eddy Correlations For Laminar Axisymmetric Sudden Expansion Flows", *J. of Fluid Engg.*, Vol. 114, pp. 119-121, 1991.
39. Jones, W.P., "Pace: A Computer Program To Solve Three- Dimensional Flow Problems", Rolls Royce Ltd. Report, 1975.
40. Milos, F.S. and Acrivos, A., " Steady Flow Past Sudden Expansion At Large Reynolds Number, Part I: Boundary Solutions", *Phy. Fluids*, ol. 29, pp. 1353- 1359, 1986.
41. Scott, P.C., And Mirza, F.A., " A Finite Element Analysis Of Laminar Flows Through Plane And Axisymmetric Abrupt Expansion", *Computers and Fluids*, Vol. 14, No. 04, pp. 423- 432, 1986.
42. Sinha, S.N., Gupta, A.K. and Oberai, M.M., " Laminar Flow Separation Over Backstep And Cavities Part I: Backsteps", *AIAA J.* , Vol. 19, pp. 1527, 1981.
43. Kovaszny, L.I.G., " Laminar Flow Behind A Two - Dimensional grid", *Proc. Comb. Phil. Soc.*, pp. 58, 1948.
44. Durst, F., Melling, A. And Whitelaw, J.H., " Low Reynolds Number Flow Over A Plane Symmetric Expansion ", *J. Fluid Mechanics*, Vol. 64, pp. 111, 1974.
45. Aung, W., " An Experimental Study Of Laminar Heat Transfer Downstream Of Backstep", *J. Heat Transfer*, Vol. 105, pp. 823, 1983.
46. Valentine, D.T. and Mohamed, A.G., " High- Order Navier-Stokes Solver And A New Test Problems ", *Bull. Am. Phys. Soc.*, Vol. 33, pp. 2265, 1988.
47. Prandtl, L., " The Mechanics of Viscous Fluids, AeroDynamics Theory", Vol. III, Springer BErlin, 1924.
48. Valentine, D.T. and Mohamed, A.G., " Toylor's Vortex Array: A New Test Problem For Navier- Stokes Solution Procedures", *Insuperlarge Problems in Computational Mechanics* (Edited by Kane, J.H. and Carlson, A.D.) Plenum Press, New York, 1989.

49. Meksyn, D., " New Methods in Laminar Boundary Layer Theory", Pergamon Press, New York, pp. 15 and 109, 1961.
50. Chang, P.K., " Separation of Flow", Pergamon Press, New York, 1970.
51. Napolitano, M. and Cinnella, P., " A Numerical Study Of Planar And Axially Symmetric Sudden Expansion Flows", Computers and Fluids, Vol. 17, pp. 185, 1989.
52. Houstic, E. N., Lynch, R.E., Rice, J.R. and Papatheodorou, T.S., " Evaluation Numerical Methods For Elliptic Partial Differential Equations", J. Comp. Phys., Vol. 27, pp. 323, 1978.
53. Dahlquist, G., " Convergence And Stability In The Numerical Intragation Of Ordinary Differential Equations ", Math. Stand., Vol. 04, pp. 33, 1956.
55. Taylor, G.I., " On The Decay Of Vortices In A Viscous Fluid", Phil. Mag. J. Sci. XLVI (Sixth Series), pp. 671, 1923.
56. Leonard, B.P., Leschziner, M.A., and McGuirk, J.J., " Third Order Finite Difference Method For Steady Two- Dimensional Convection", Numerical Methods in Laminar and Turbulent Flows, (Taylor, C., et. al. Ed.) Pentach, London, England, 1978.
57. Leschziner, M.A., " Practical Evaluation Of Three Finite Difference Schemes For The Computation Of Steady State Recirculating Flows", Comp. Methods in Appli. Mech. and Engg., Vol. 23, pp. 293- 312, 1980.
58. Leschziner, M.A. and Rodi, W., " Calculation Of Annular And Twin Parallel Jets Using Various Discretisation Schemes And Turbulence-Model Variations", J. Fluids Engg. ASME, Vol. 103, pp. 352- 360, 1981.
59. Papadimitriou, C., " Prediction Of Turbulent Stably- Stratified Buoyant Flows", Ph. D Thesis, Imperial College, University of London, England, 1985.
60. Patankar, S.V. and Spalding, D.B., " A Calculations Procedure For Heat, Mass And Momentum Transfer In Three- Dimensional Parabolic Flows", Int. J. Heat and Mass Transfer, Vol. 15, pp. 1787-1806, 1972.
61. Back, L.H. and Rösche, E.J., " Shear Layer Flow Regimes And Wave Instabilities And Reattachment Lengths Downstream Of An Abrupt Circular Channel Expansion", Trans. ASME J. Appl. Mech., Vol. 39, pp. 677, 1972.

Figures

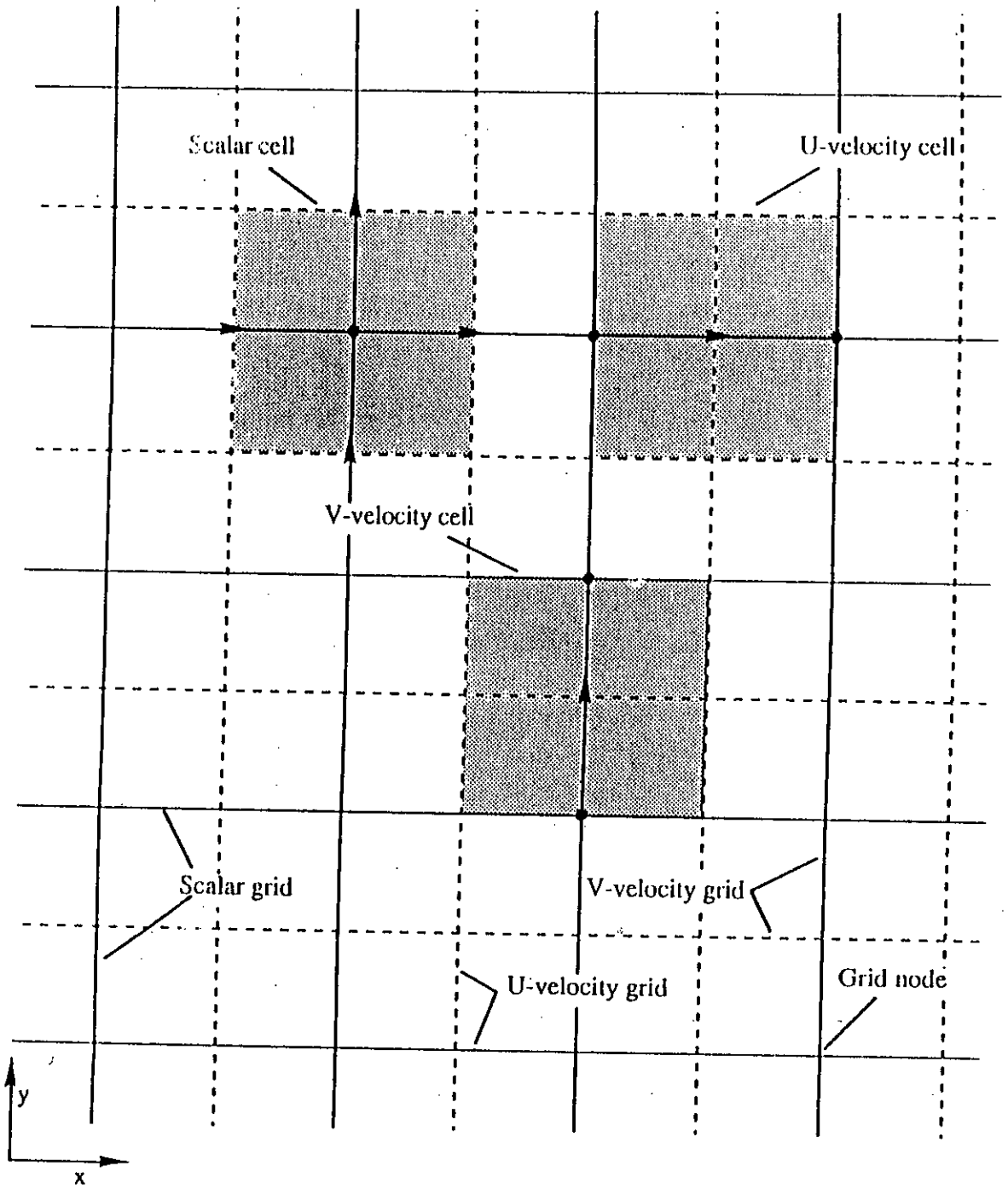
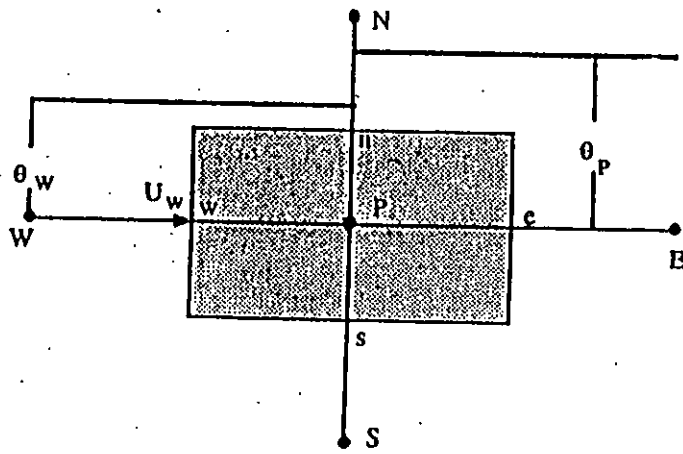


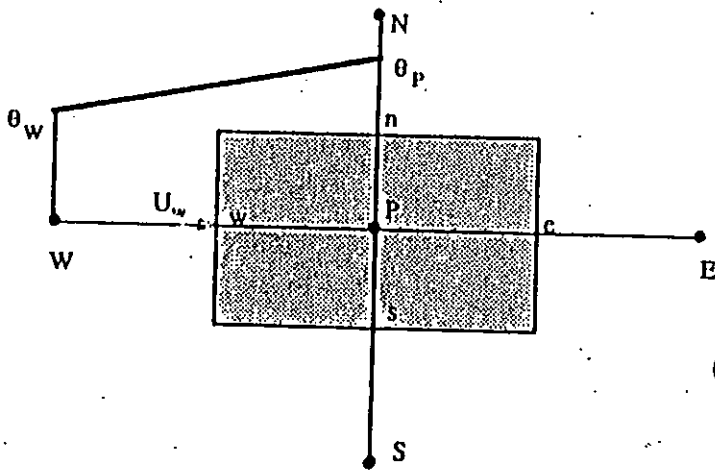
Fig : 3.1 Control volumes for 2-D co-ordinate system



$$\theta_w = \theta_w$$

(for $U_w > 0$)

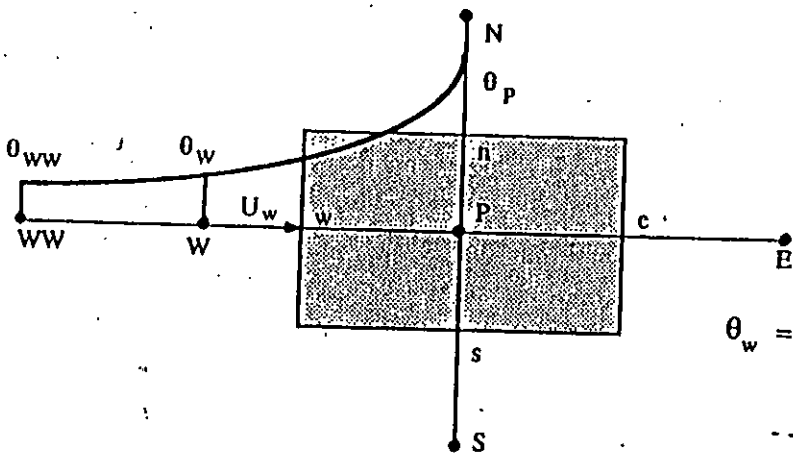
UPWIND SCHEME



$$\theta_w = \frac{\theta_p + \theta_w}{2}$$

(for $U_w > 0$)

CENTRAL DIFFERENCE SCHEME



$$\theta_w = \frac{1}{2} (\theta_p + \theta_w)$$

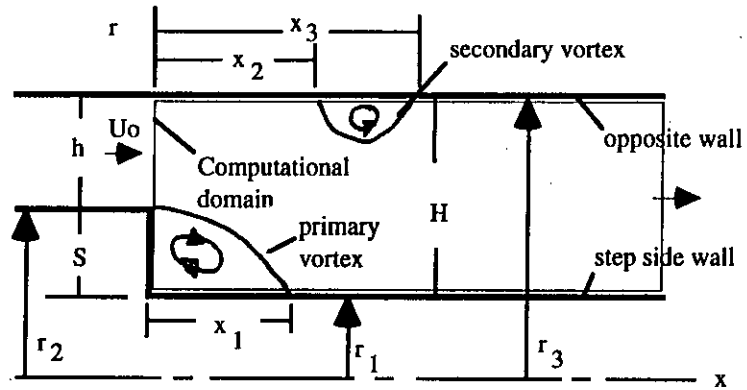
$$- \frac{1}{8} (\theta_p + \theta_{ww} - 2\theta_w)$$

(for $U_w > 0$)

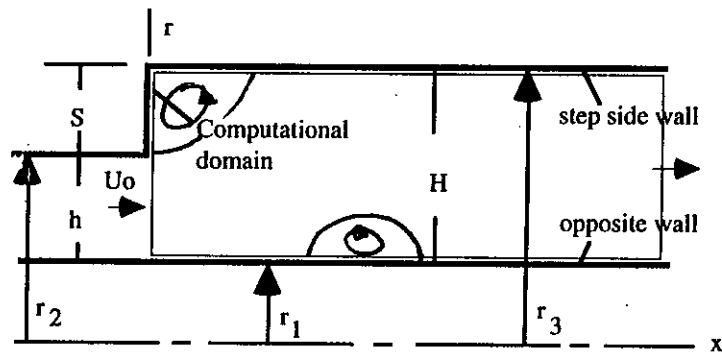
QUICK SCHEME

Fig : 3.2

Cell face value interpolation (for uniform grid spacings) with different discretisation schemes.



(a) Inner-radius annular backstep



(b) Outer-radius annular backstep

Fig : 4.1 Flow configuration and computational domain.

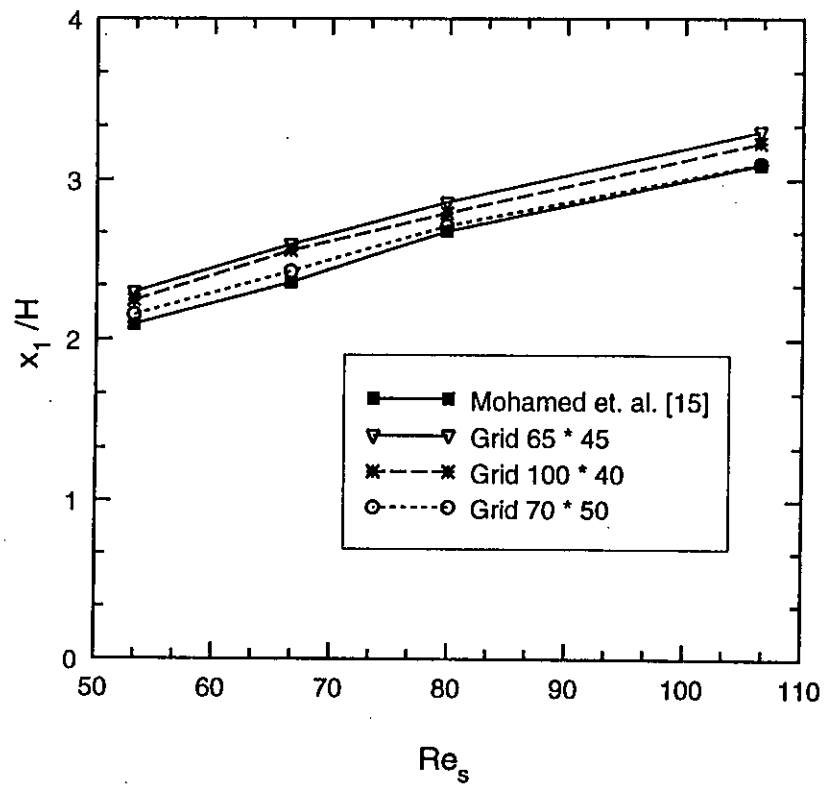


Fig : 4.2 Grid dependency test for $\alpha = 0.2$

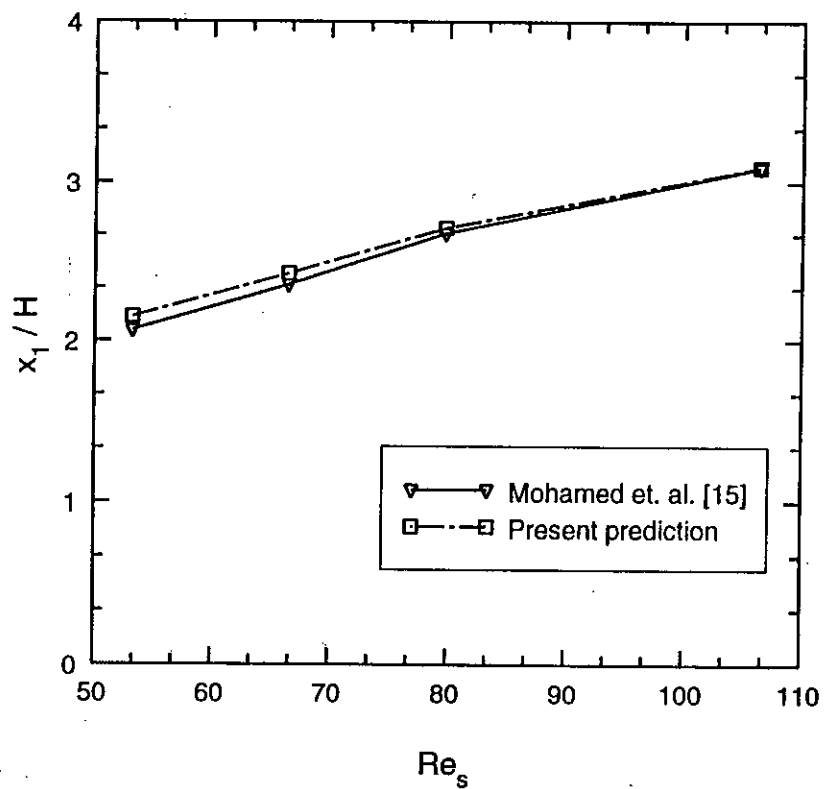


Fig : 4.3 Comparison between Mohamed et. al. [15] and Present prediction.

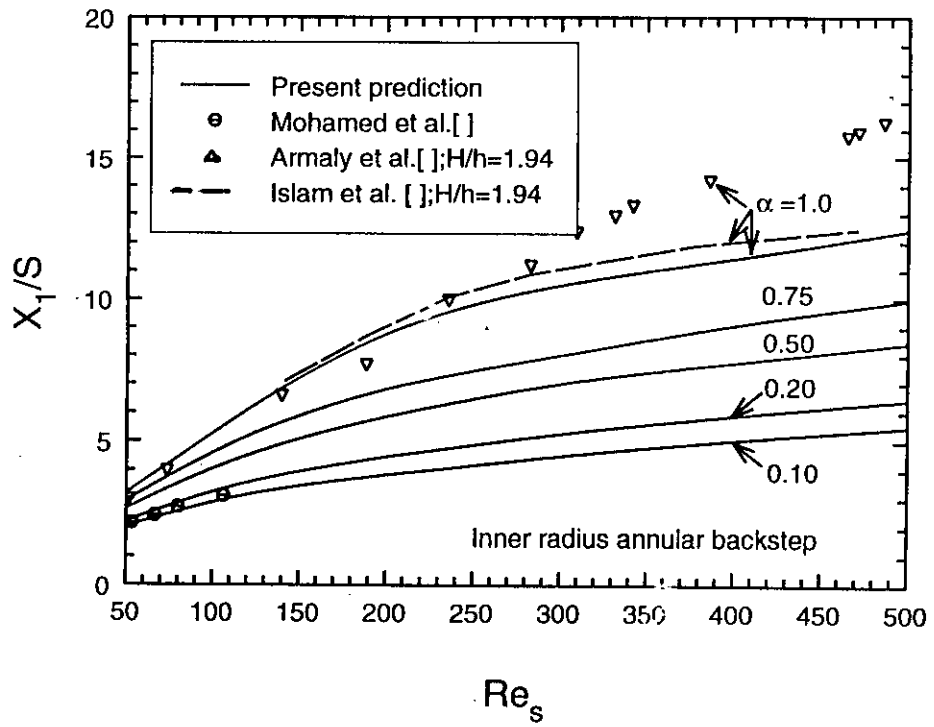


Fig : 4.4 Length of primary vortex for inner-radius annular backstep.

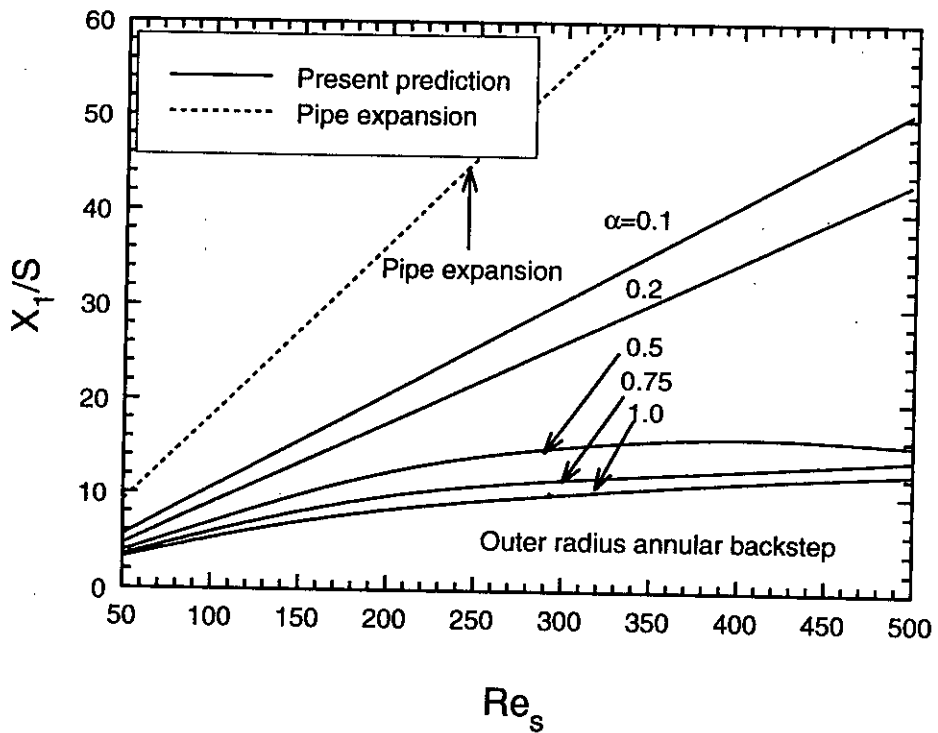


Fig : 4.5 Length of primary vortex for outer-radius annular backstep.

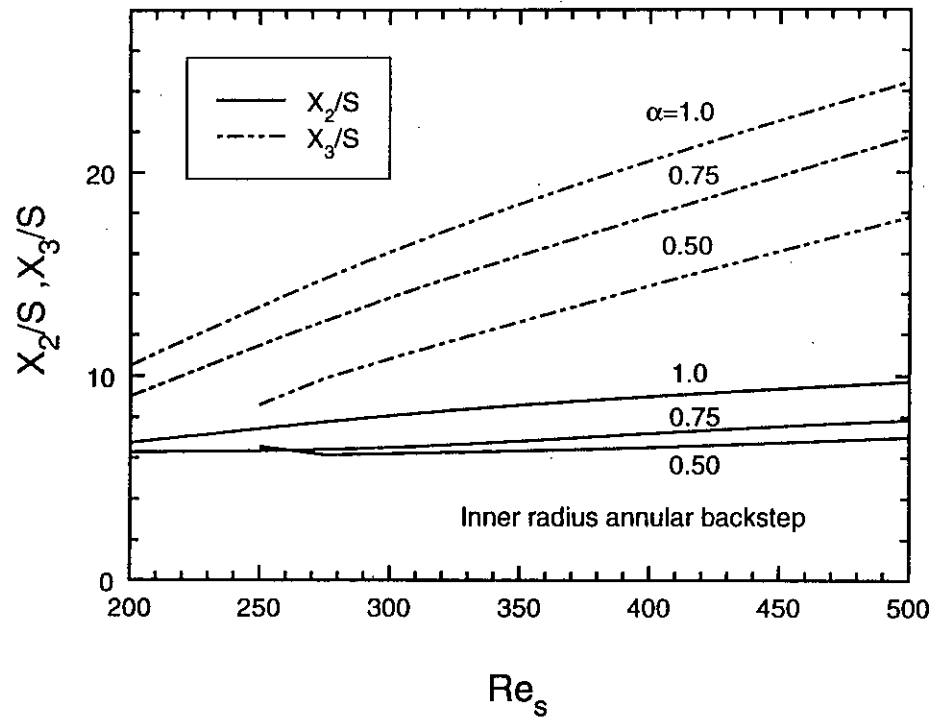


Fig : 4.6 Lengths of secondary vortex for inner-radius annular backstep.

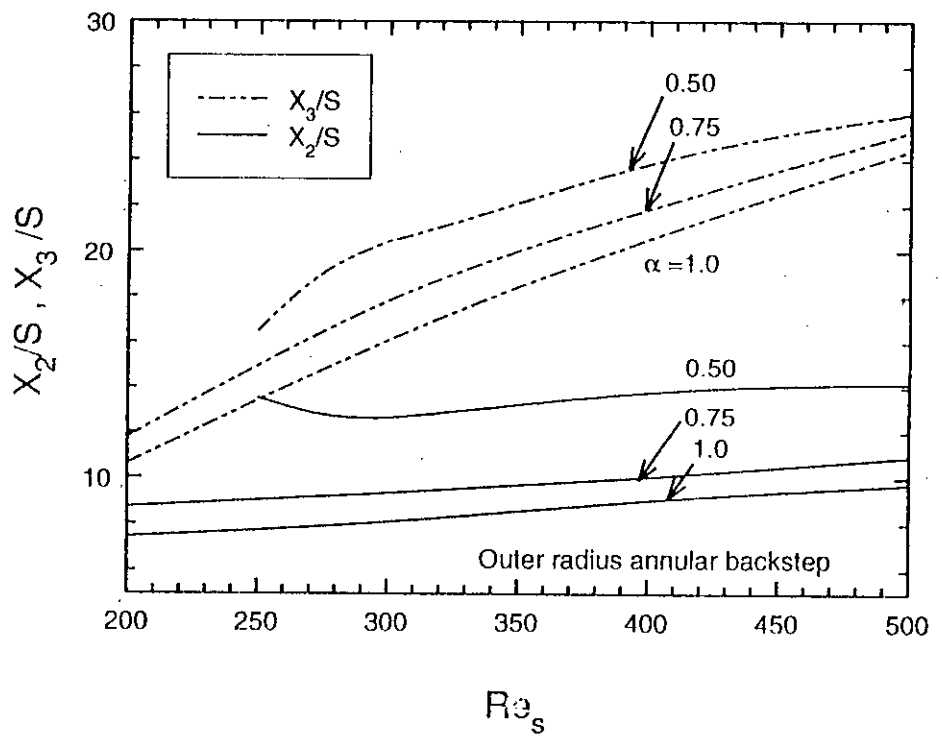


Fig : 4.7 Lengths of secondary vortex for outer-radius annular backstep.

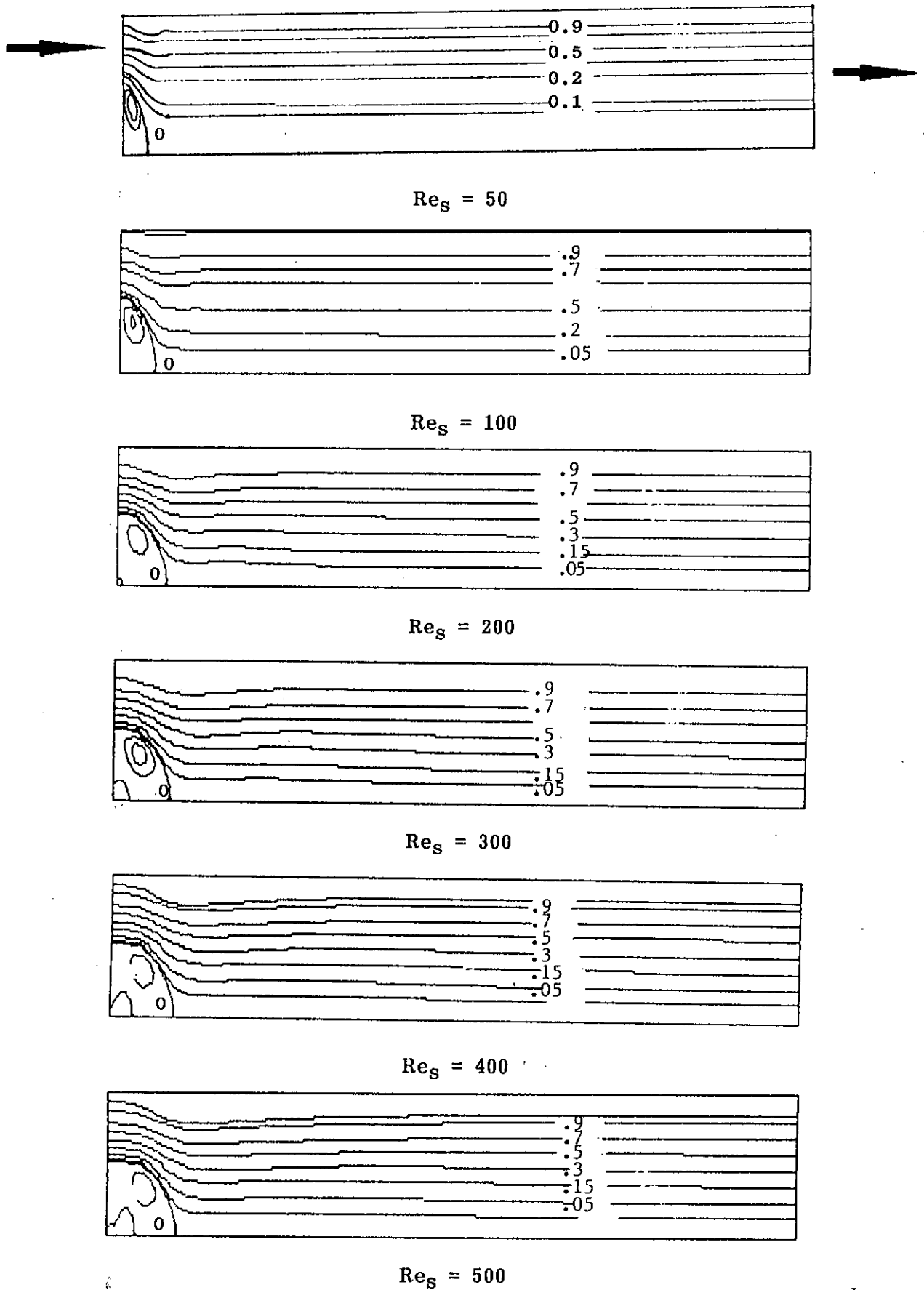


Fig : 4.8 Constant streamline contours for inner-radius annular backstep at $\alpha = 0.1$ [Note that the axial distance compressed by 5 times].

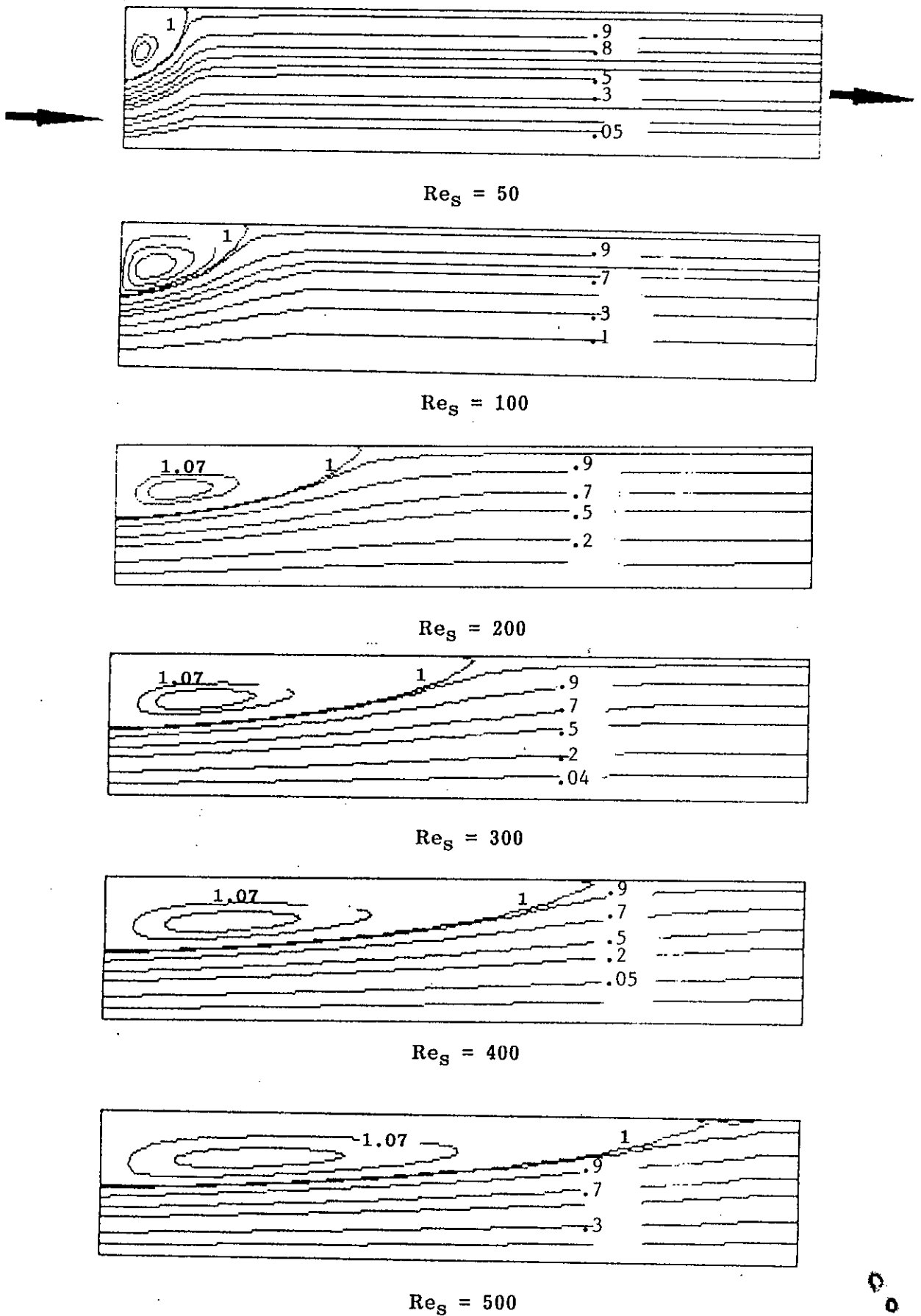


Fig : 4.9 Constant streamline contours for outer-radius annular backstep at $\alpha = 0.1$ [Note that the axial distance compressed by 5 times].

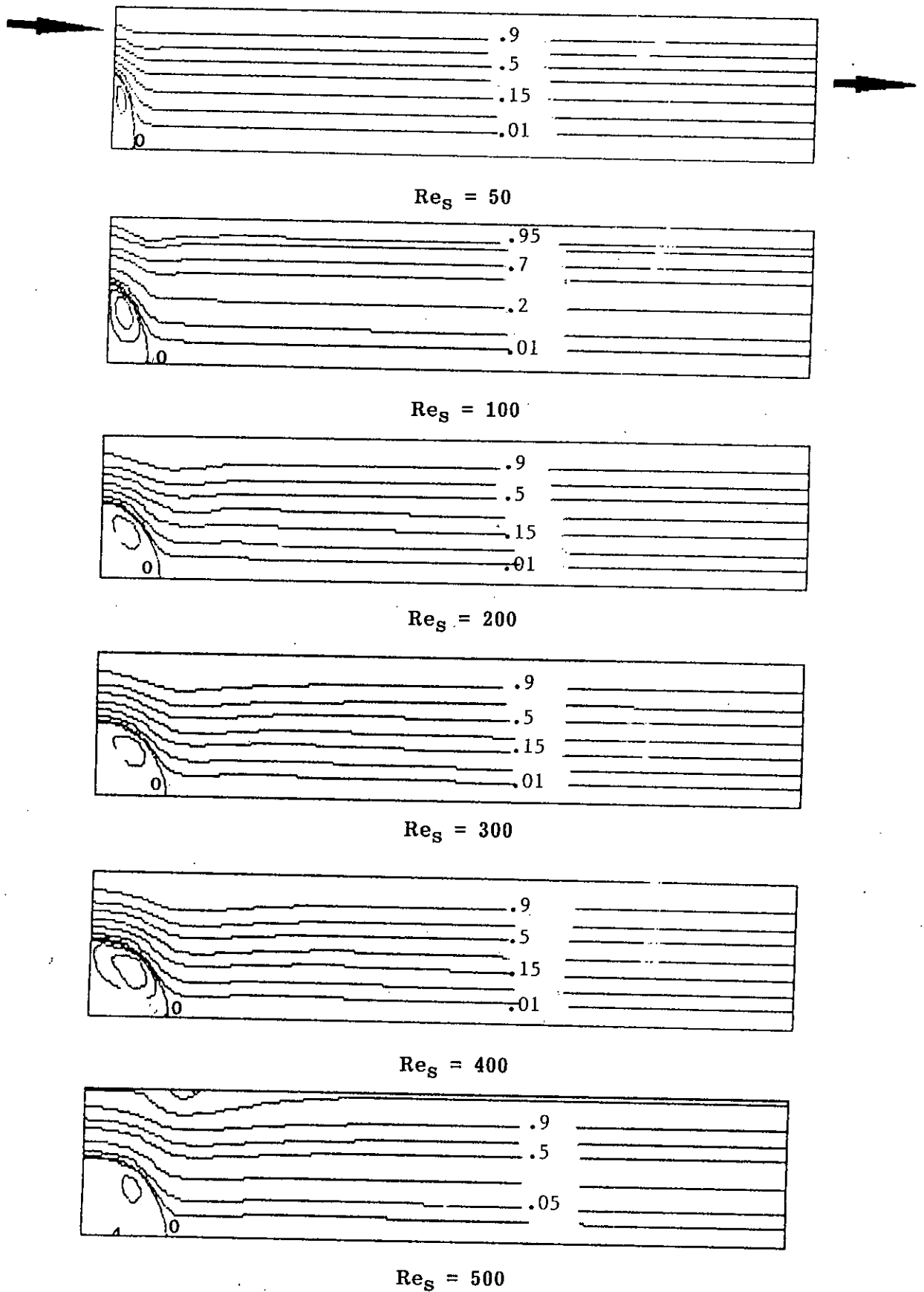


Fig : 4.10 Constant streamline contours for inner-radius annular backstep at $\alpha = 0.2$ [Note that the axial distance compressed by 5 times].

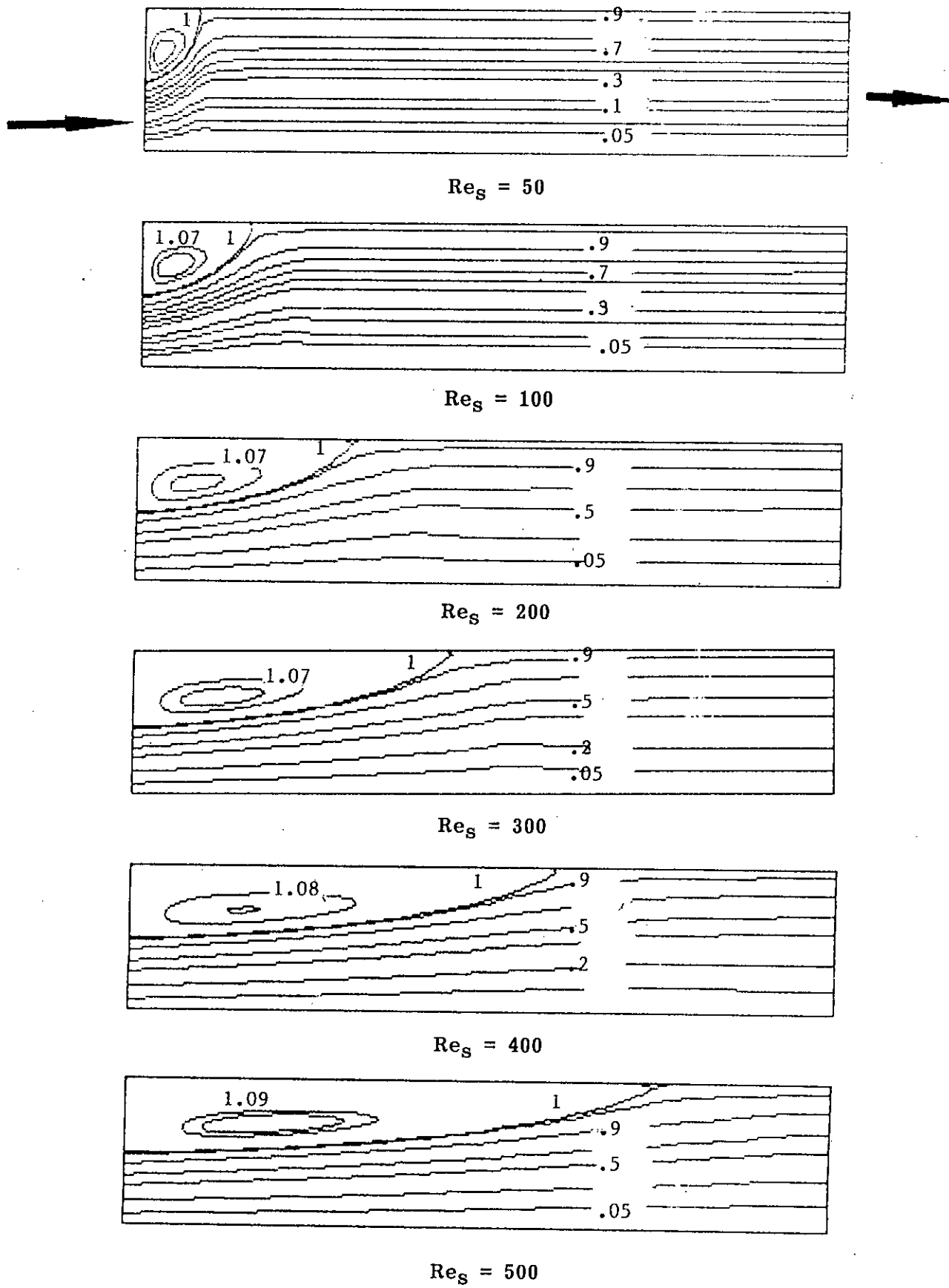


Fig : 4.11 Constant streamline contours for outer-radius annular backstep at $\alpha = 0.2$ [Note that the axial distance compressed by 5 times].

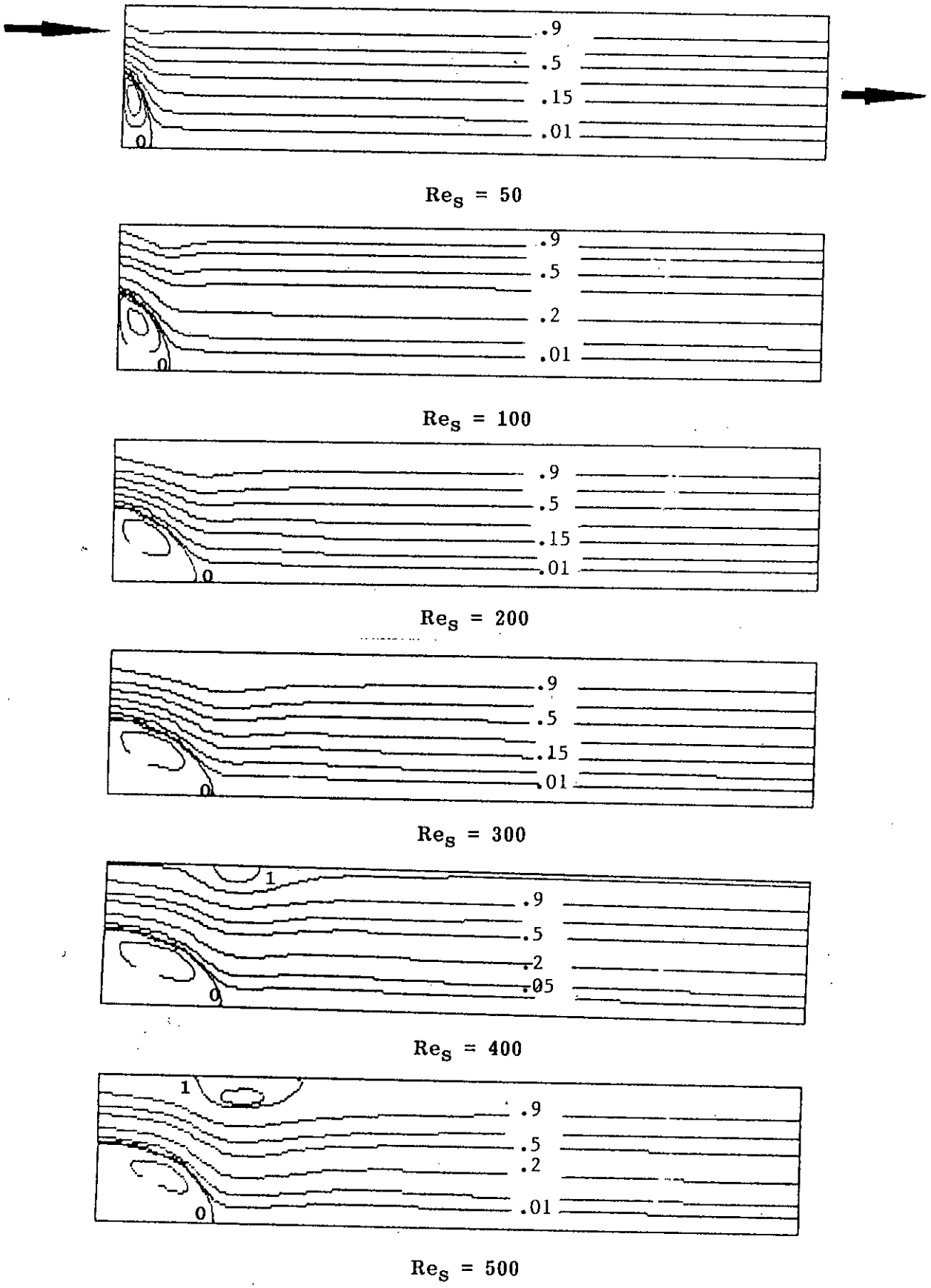
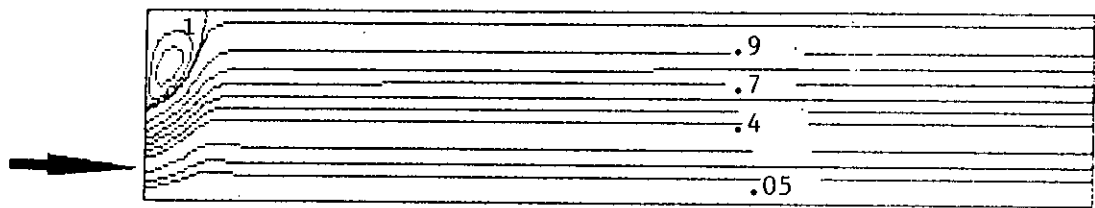
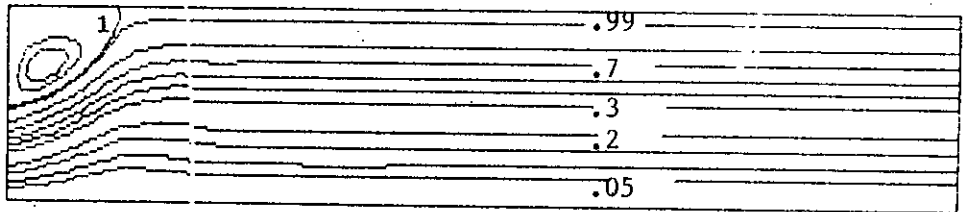


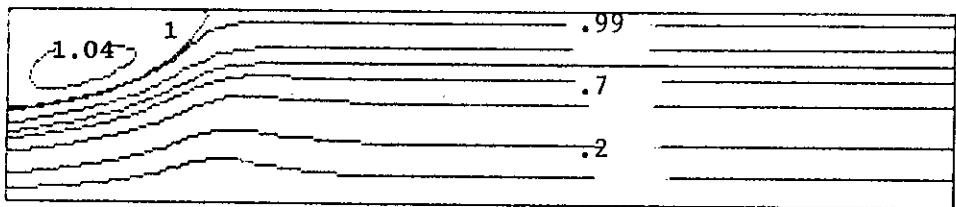
Fig : 4.12 Constant streamline contours for inner-radius annular backstep at $\alpha = 0.5$ [Note that the axial distance compressed by 5 times].



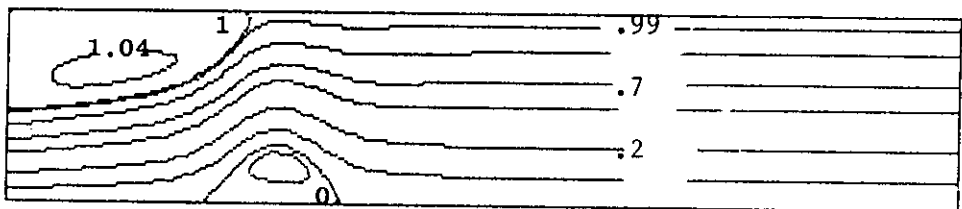
$Re_s = 50$



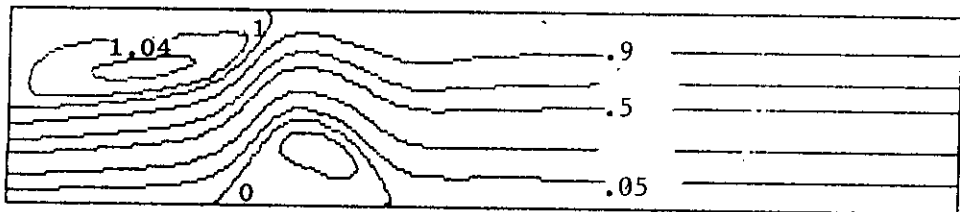
$Re_s = 100$



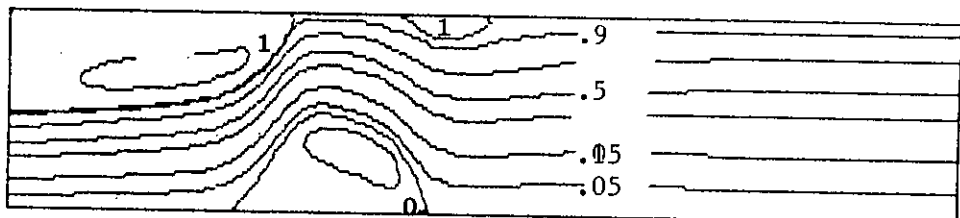
$Re_s = 200$



$Re_s = 300$



$Re_s = 400$



$Re_s = 500$

Fig : 4.13 Constant streamline contours for outer-radius annular backstep at $\alpha = 0.5$ [Note that the axial distance compressed by 5 times].

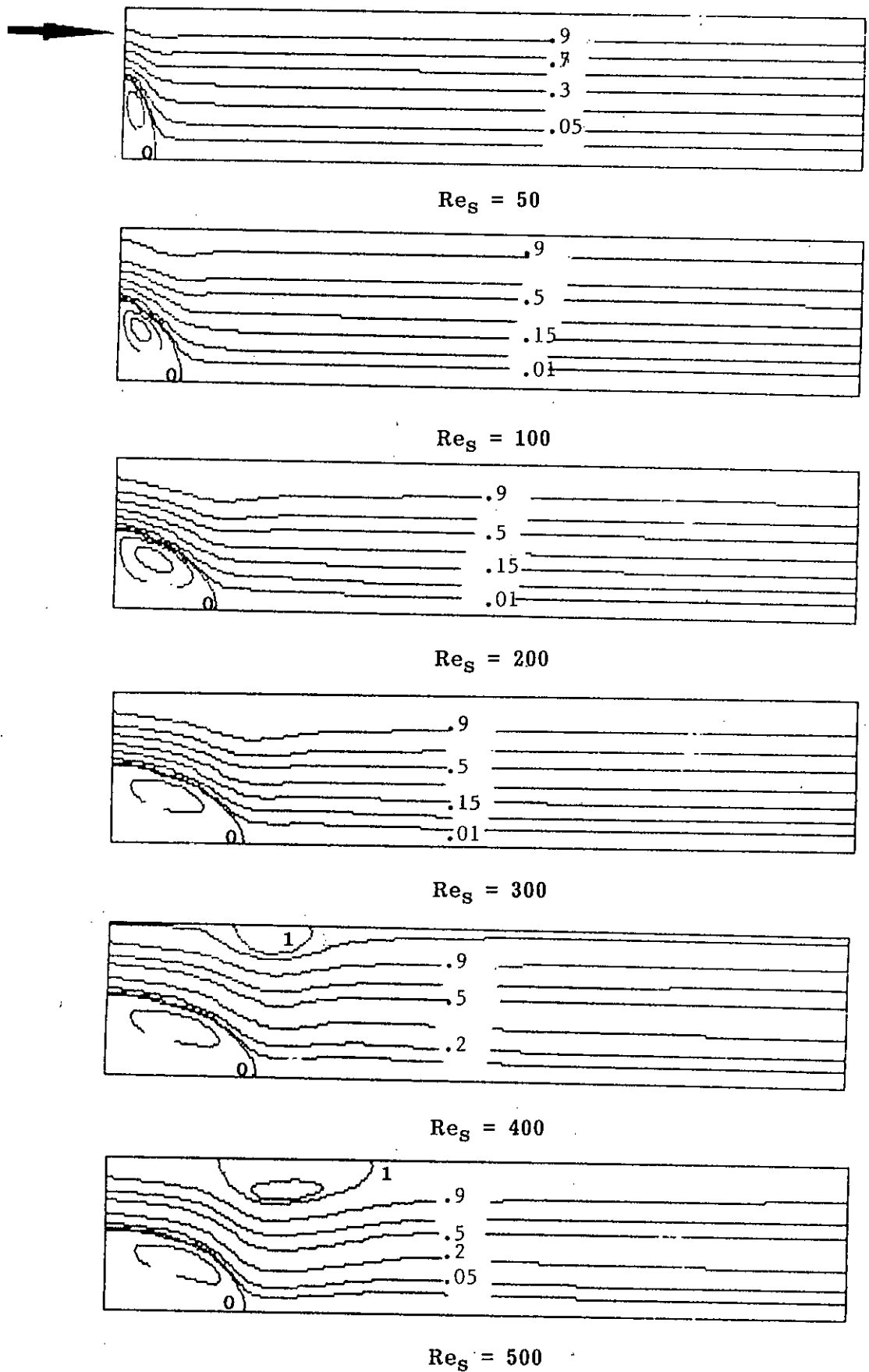


Fig : 4.14 Constant streamline contours for inner-radius annular backstep at $\alpha = 0.75$ [Note that the axial distance compressed by 5 times].

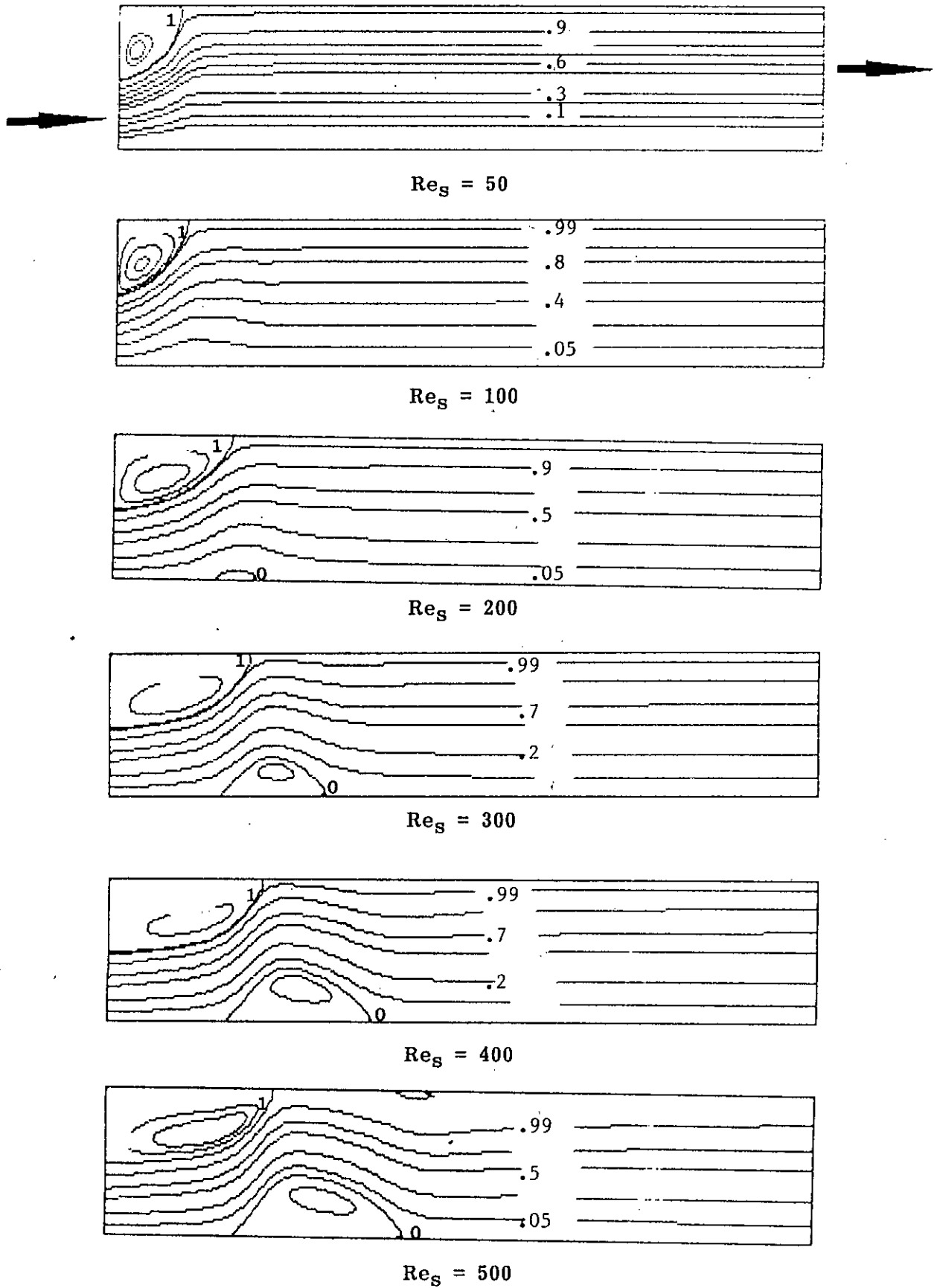


Fig : 4.15 Constant streamline contours for outer-radius annular backstep at $\alpha = 0.75$ [Note that the axial distance compressed by 5 times].

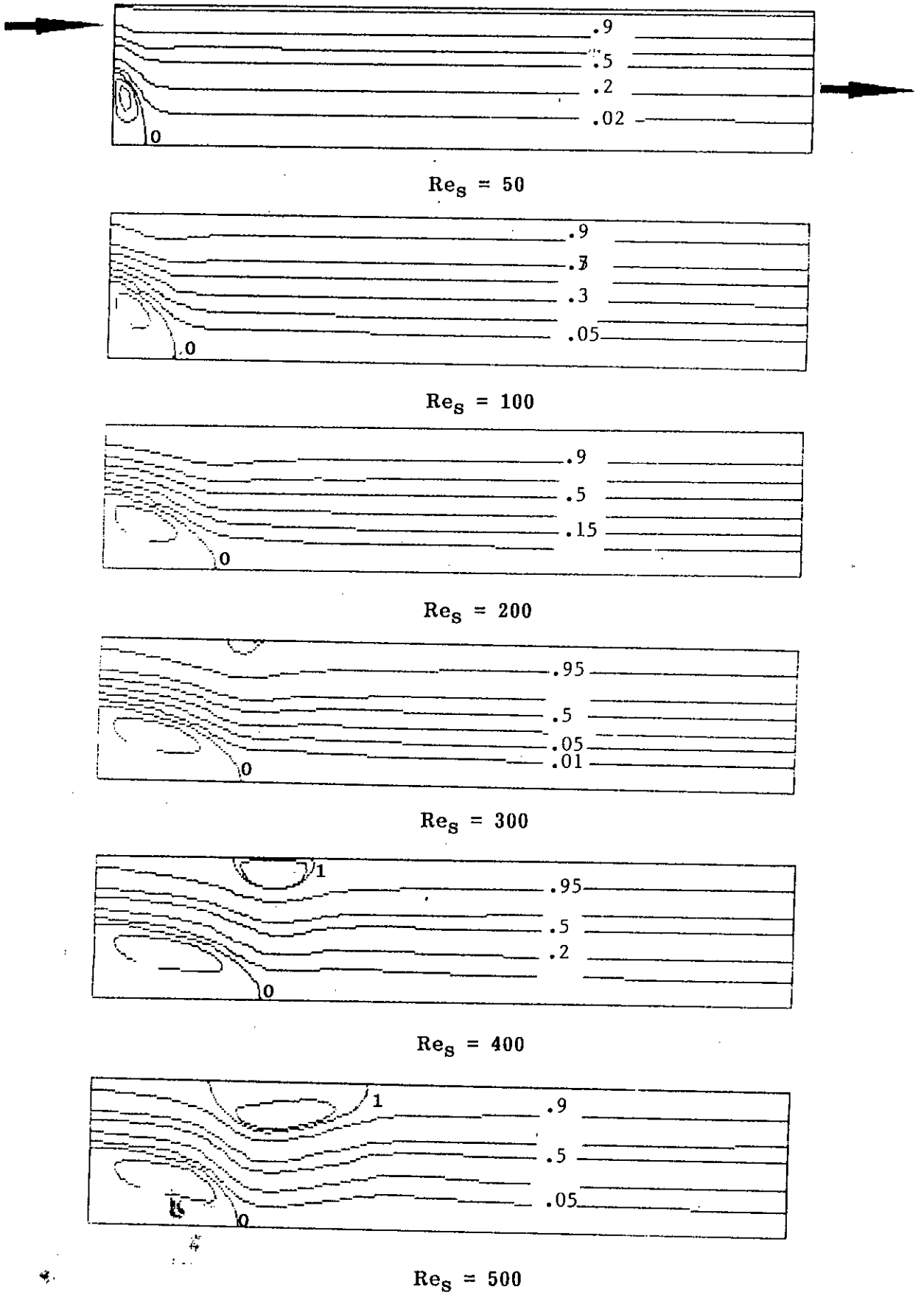


Fig : 4.16 Constant streamline contours for inner-radius annular backstep at $\alpha = 1.0$ [Note that the axial distance compressed by 5 times].

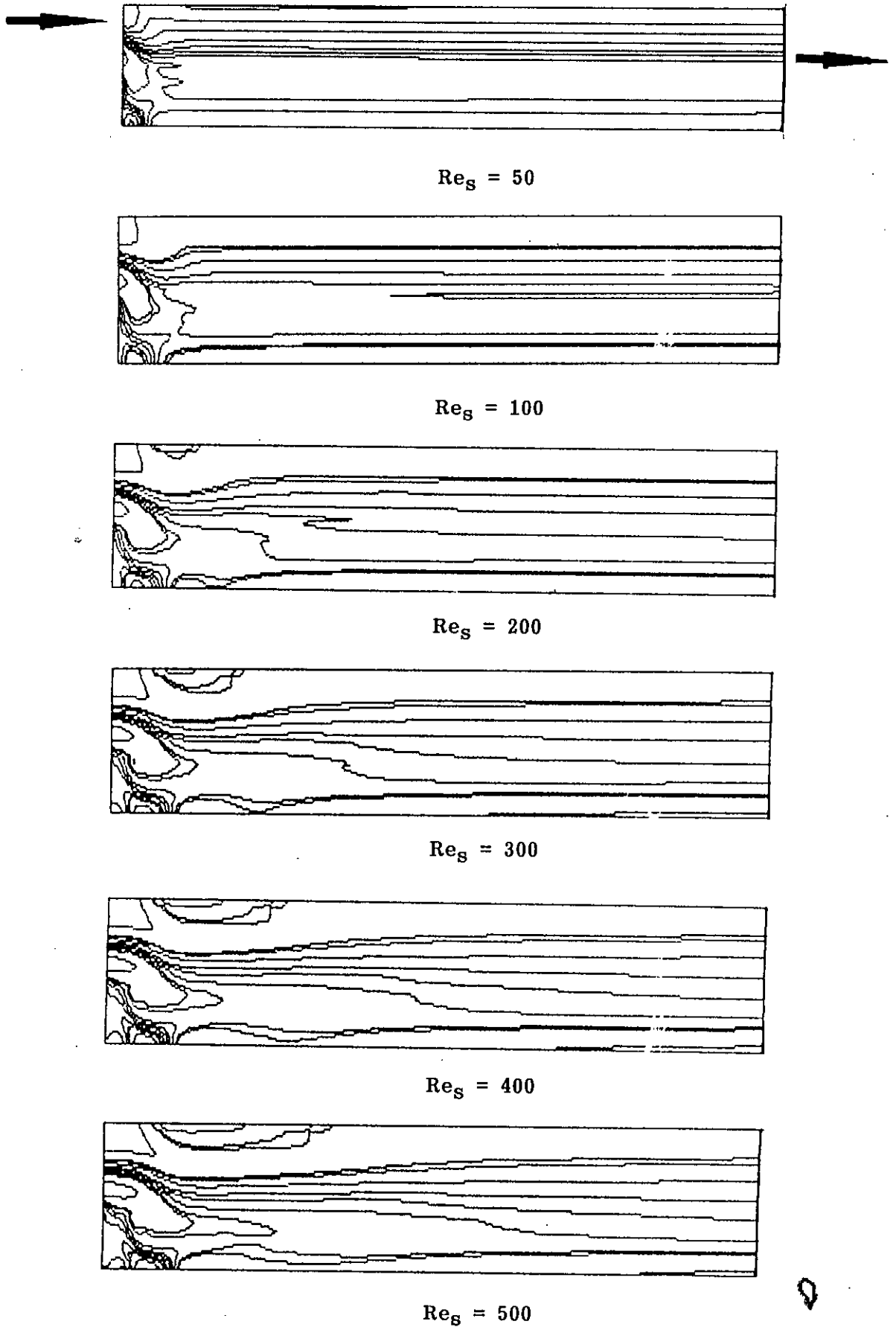


Fig : 4.17 Constant vorticity contours for inner-radius annular backstep at $\alpha = 0.1$ [Note that the axial distance compressed by 5 times].

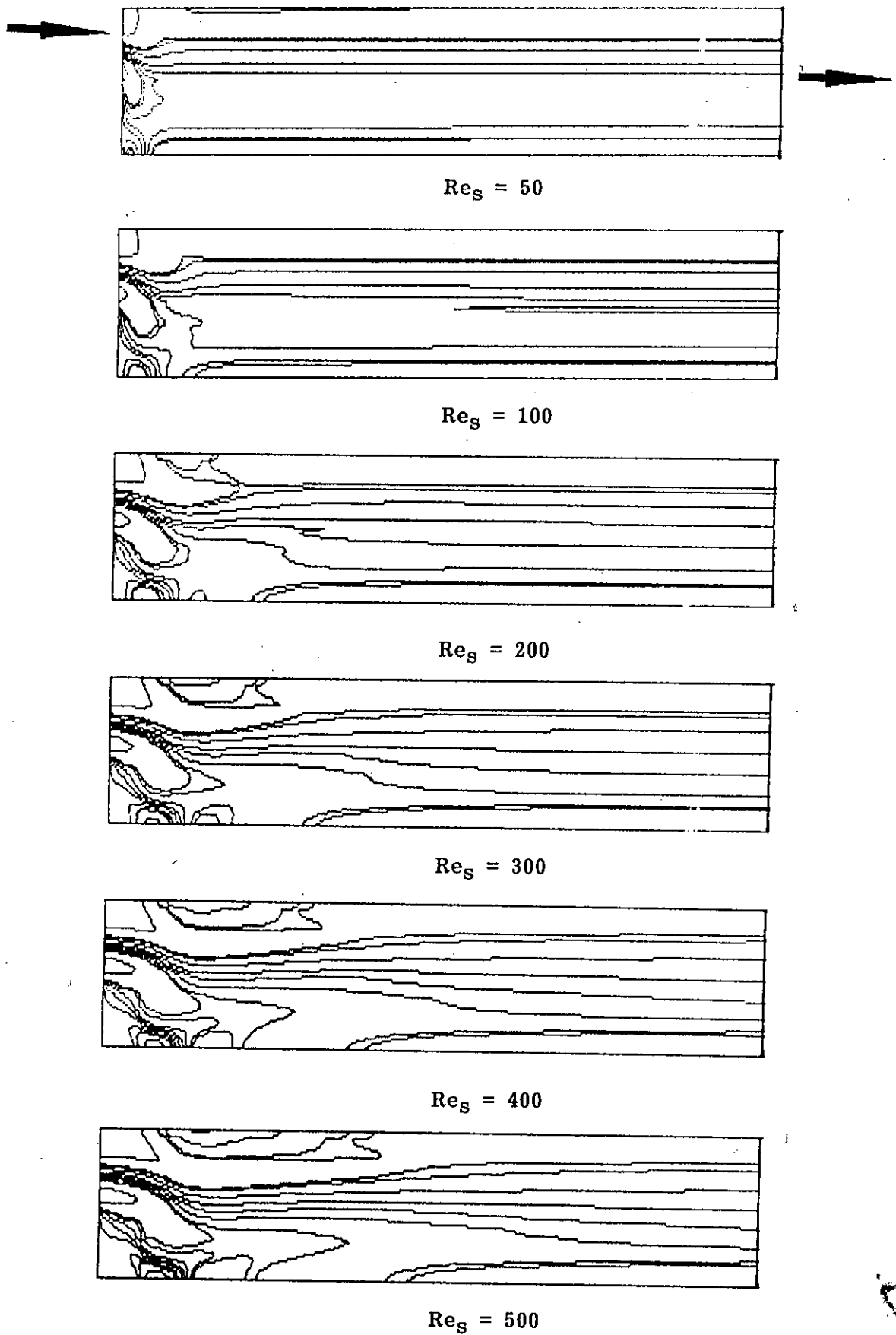


Fig : 4.18 Constant vorticity contours for inner-radius annular backstep at $\alpha = 0.2$ [Note that the axial distance compressed by 5 times].

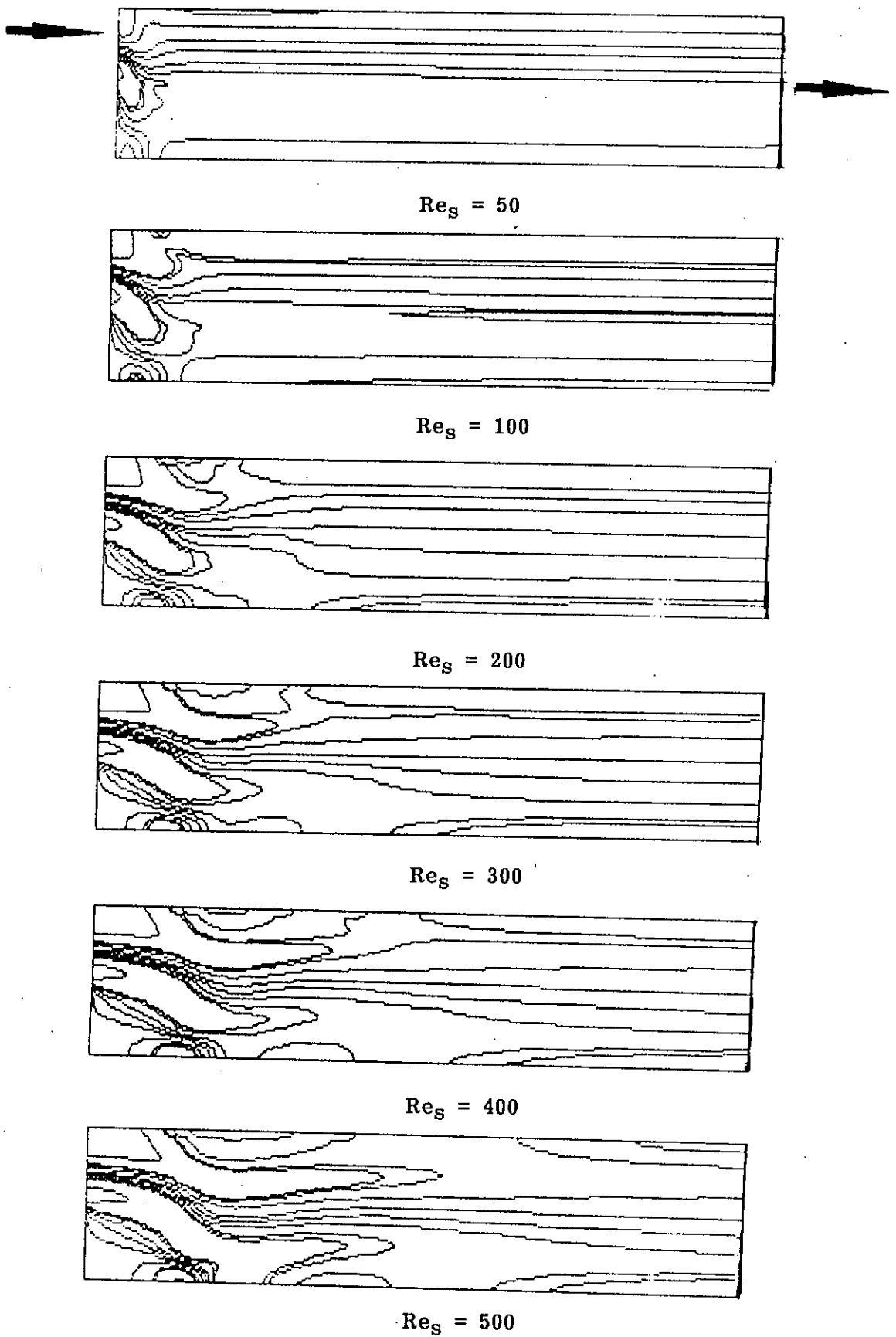


Fig : 4.19 Constant vorticity contours for inner-radius annular backstep at $\alpha = 0.5$ [Note that the axial distance compressed by 5 times].

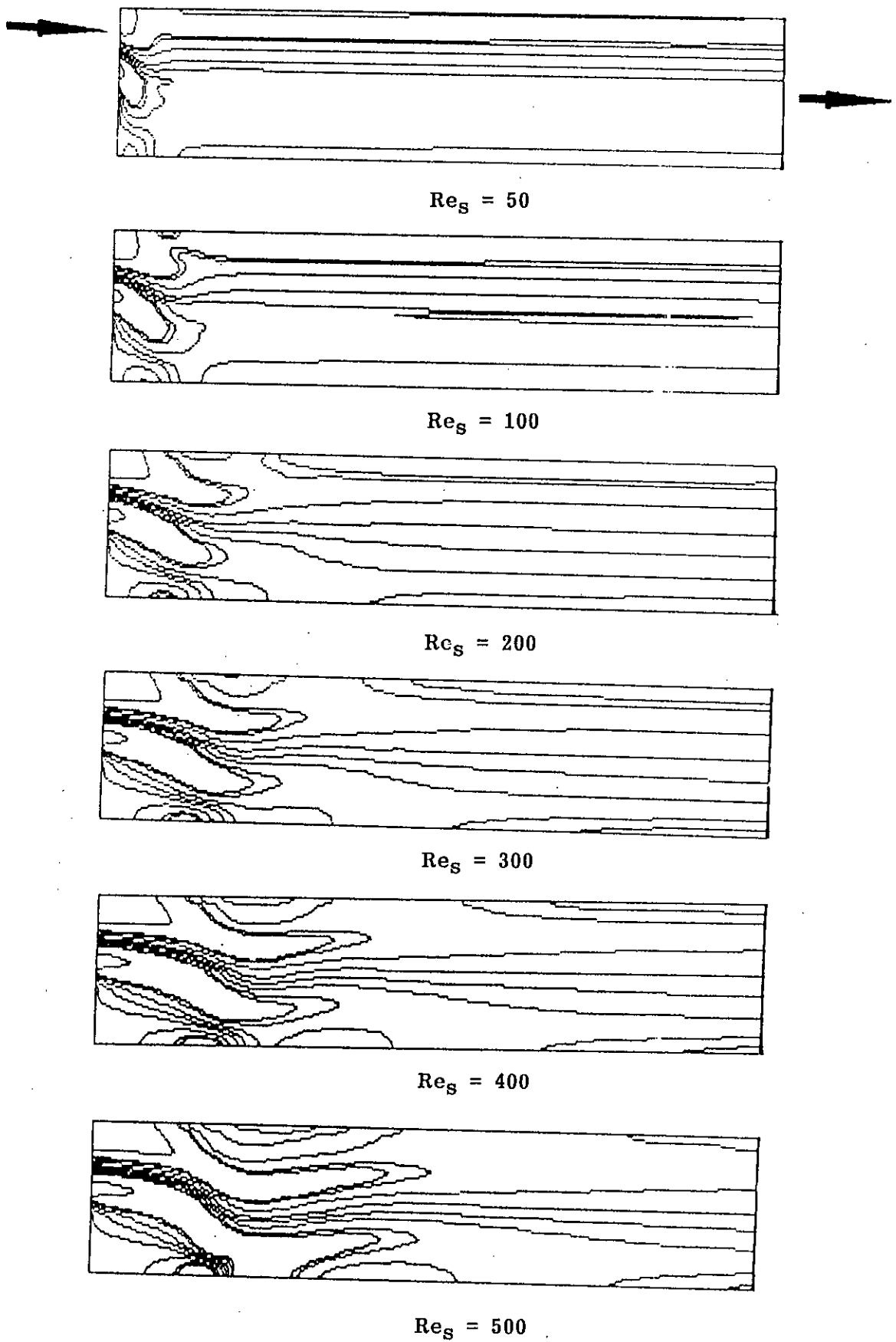


Fig : 4.20 Constant vorticity contours for inner-radius annular backstep at $\alpha = 0.75$ [Note that the axial distance compressed by 5 times].

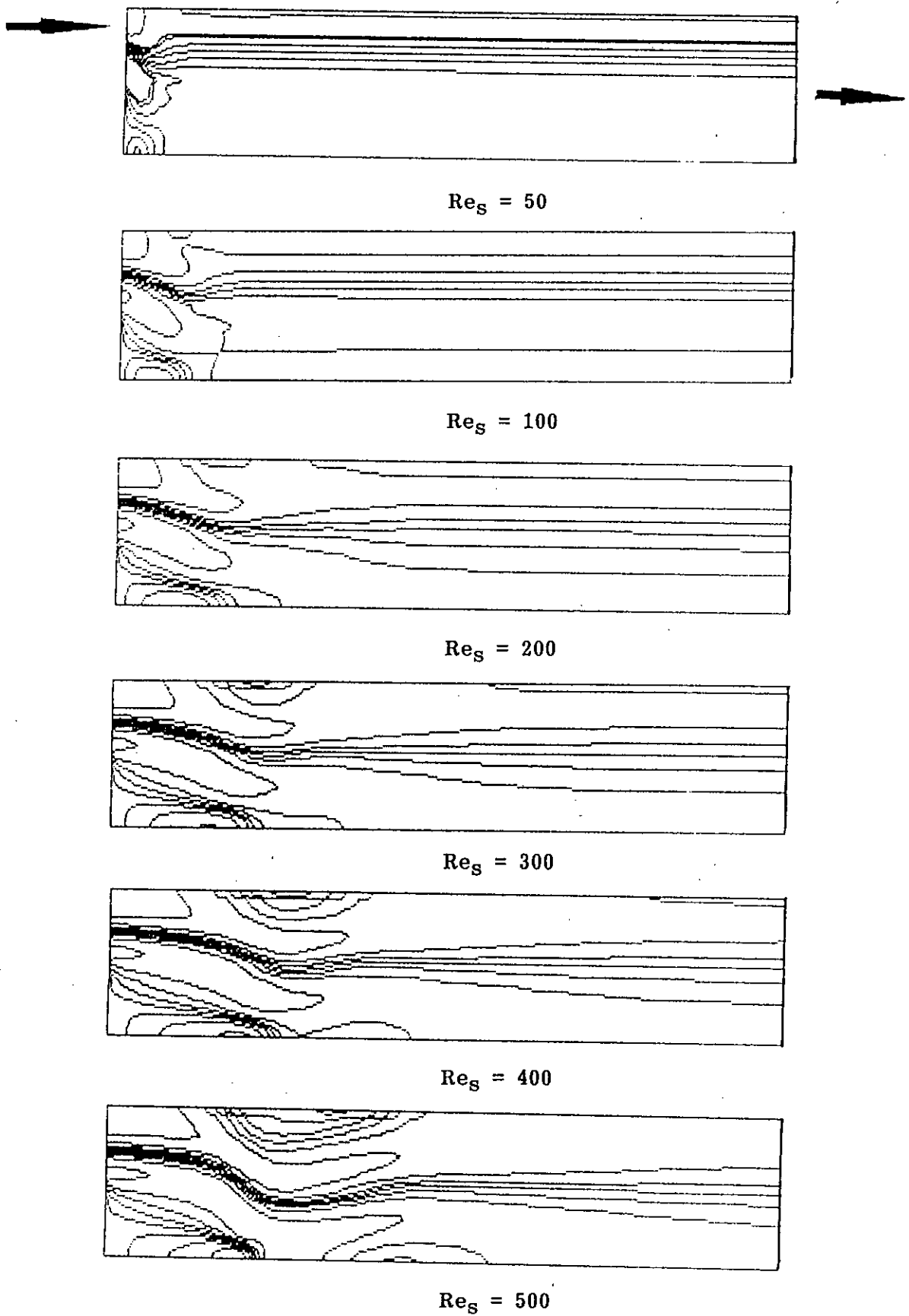


Fig : 4.21 Constant vorticity contours for inner-radius annular backstep at $\alpha = 1.0$ [Note that the axial distance compressed by 5 times].

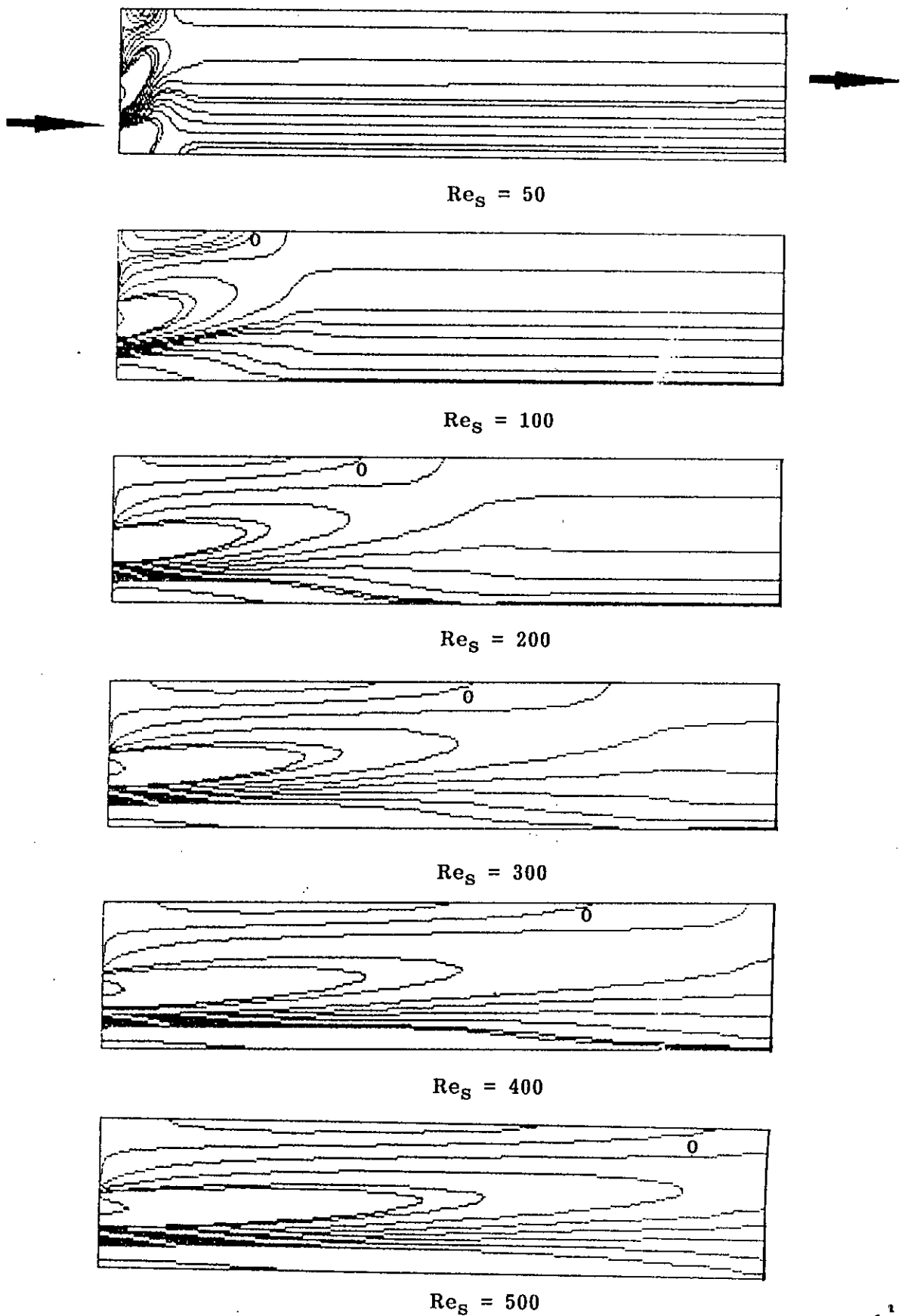


Fig : 4.22 Constant vorticity contours for outer-radius annular backstep at $\alpha = 0.1$ [Note that the axial distance compressed by 5 times].

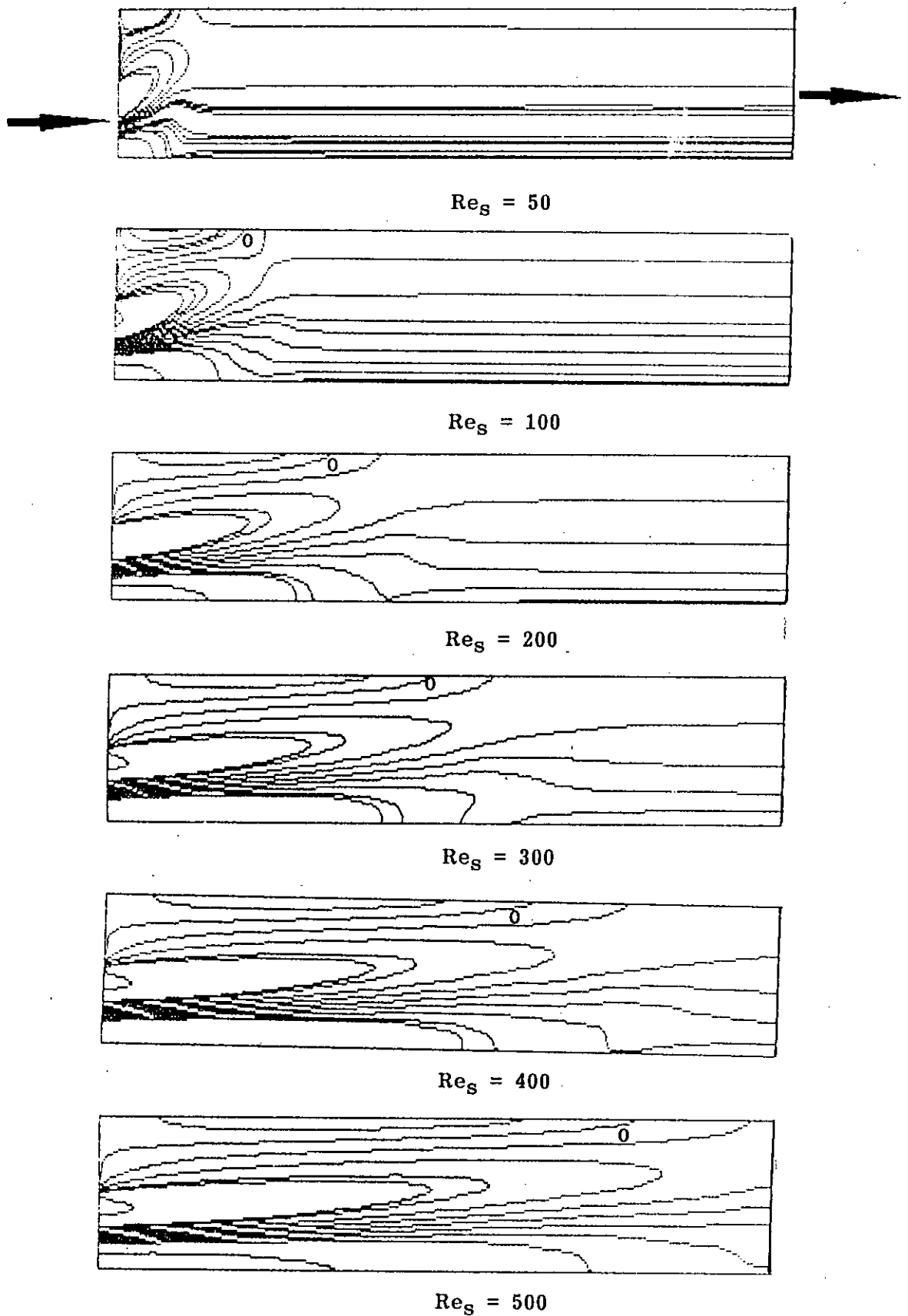


Fig: 4.23 Constant vorticity contours for outer-radius annular backstep at $\alpha = 0.2$ [Note that the axial distance compressed by 5 times].

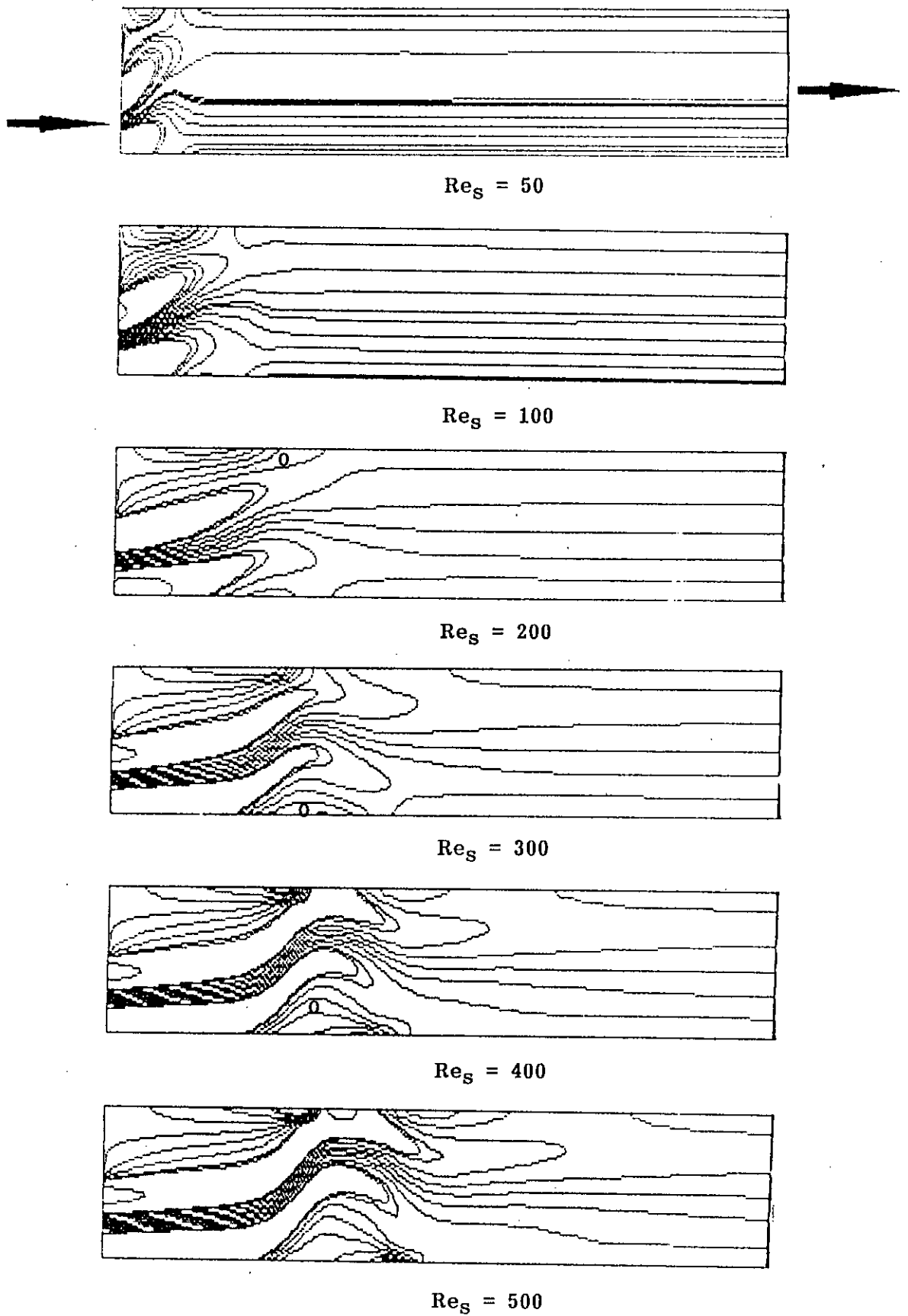


Fig : 4.24 Constant vorticity contours for outer-radius annular backstep at $\alpha = 0.5$ [Note that the axial distance compressed by 5 times].

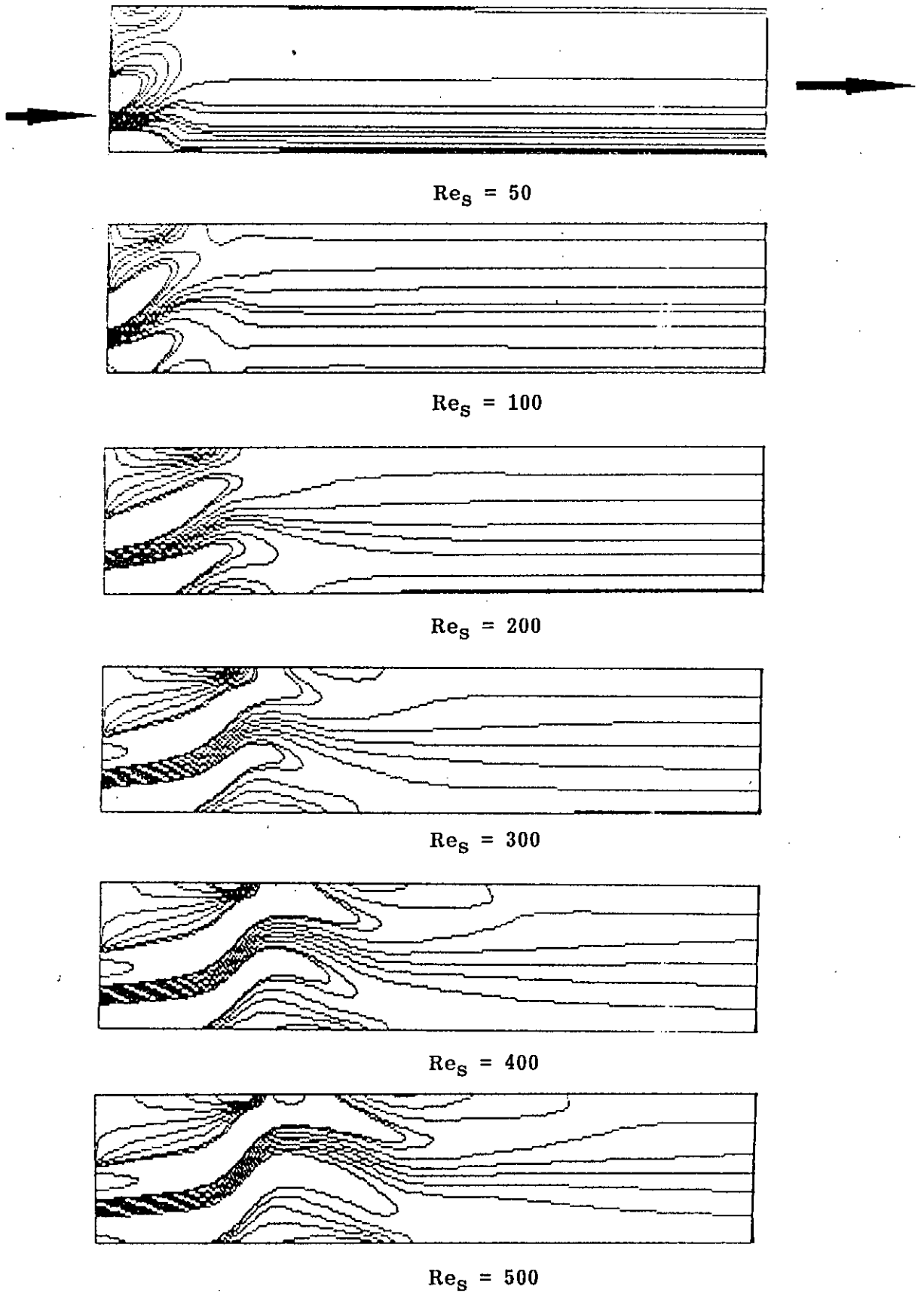


Fig : 4.25 Constant vorticity contours for outer-radius annular backstep at $\alpha = 0.75$ [Note that the axial distance compressed by 5 times]

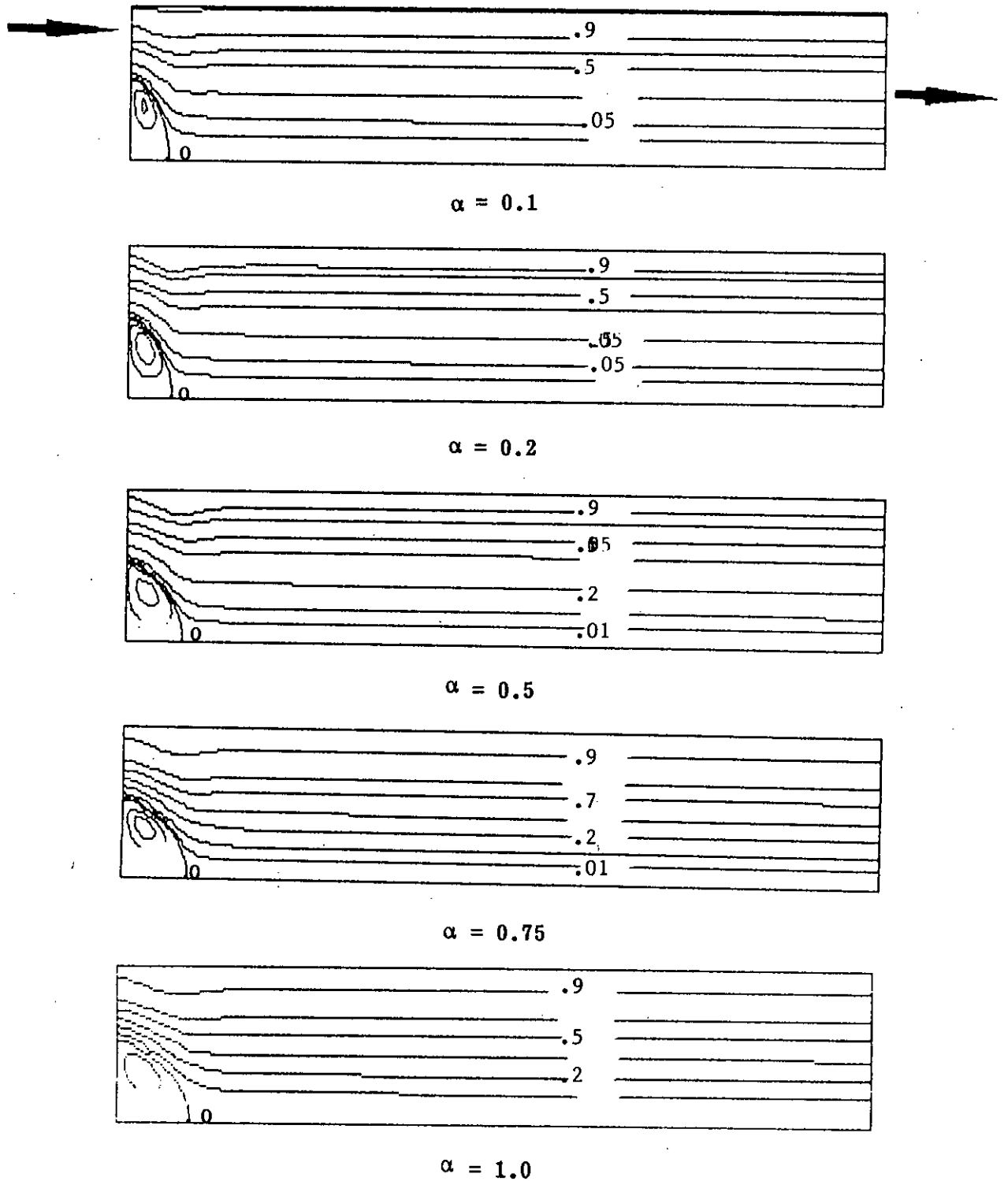


Fig : 4.26 Constant streamline contours for inner-radius annular backstep at $Re_s = 100$ [Note that the axial distance compressed by 5 times].

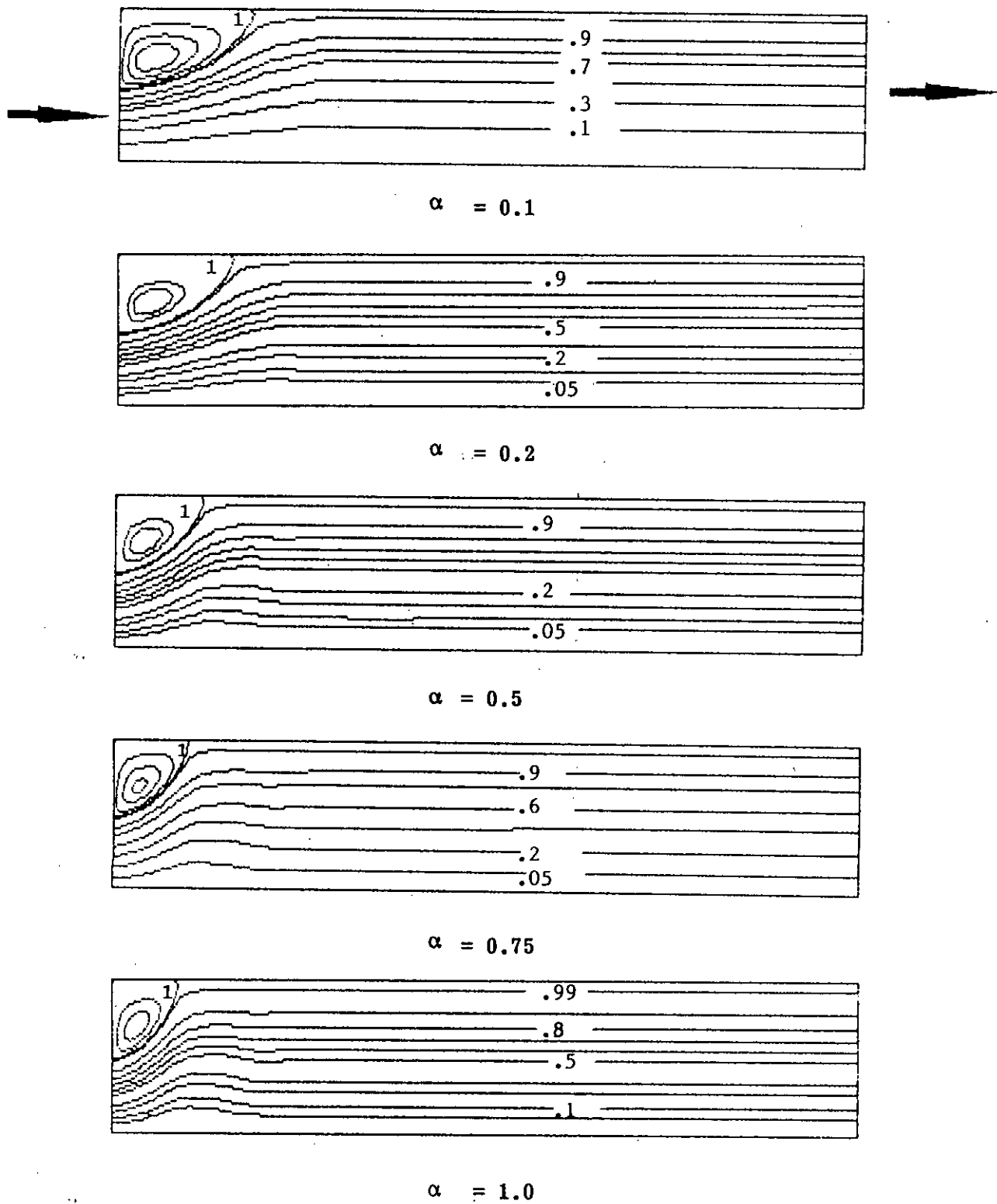


Fig : 4.27 Constant streamline contours for outer-radius annular backstep at $Re_s = 100$ [Note that the axial distance compressed by 5 times].

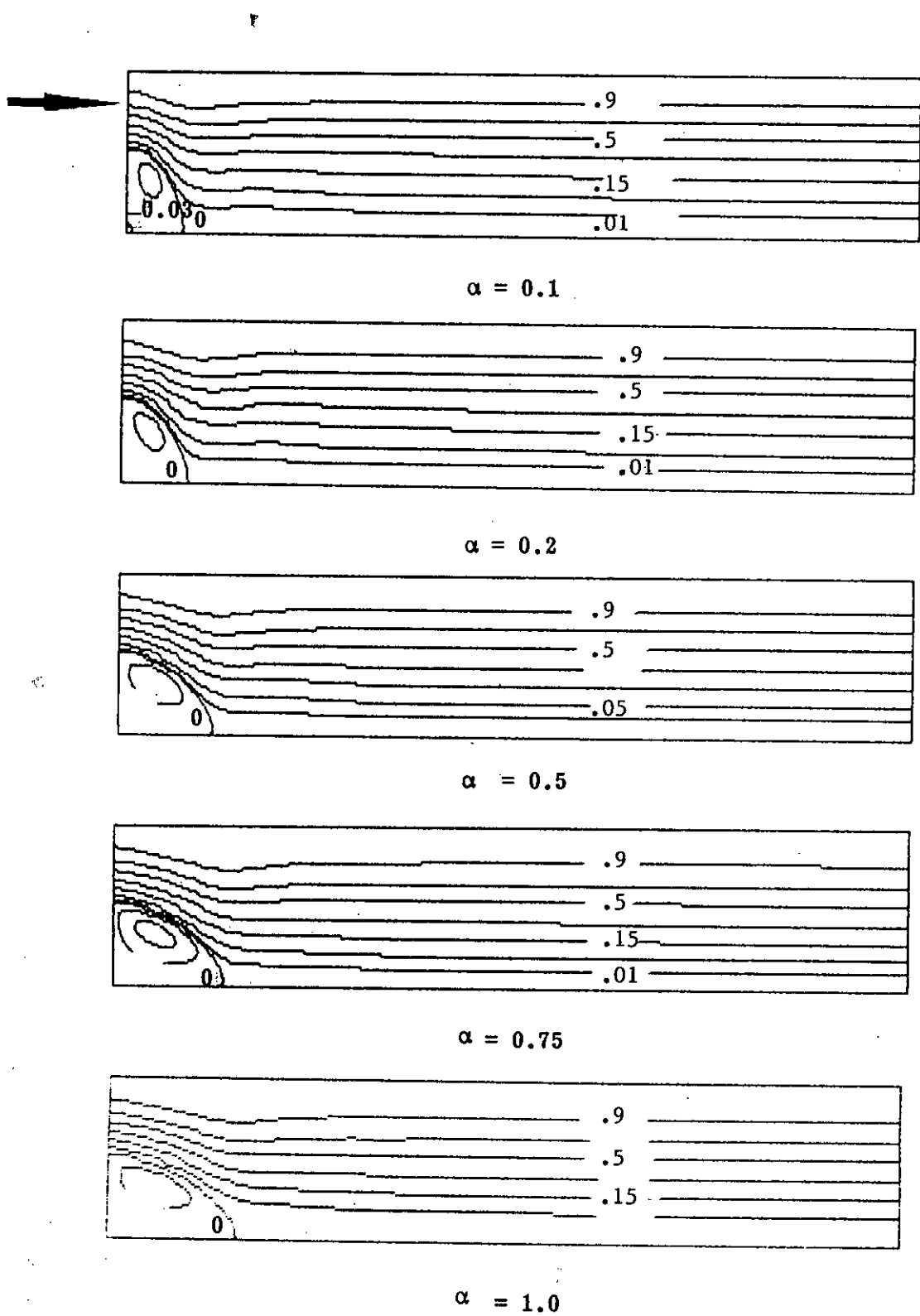


Fig : 4.28 Constant streamline contours for inner-radius annular backstep at $Re_s = 200$ [Note that the axial distance compressed by 5 times].

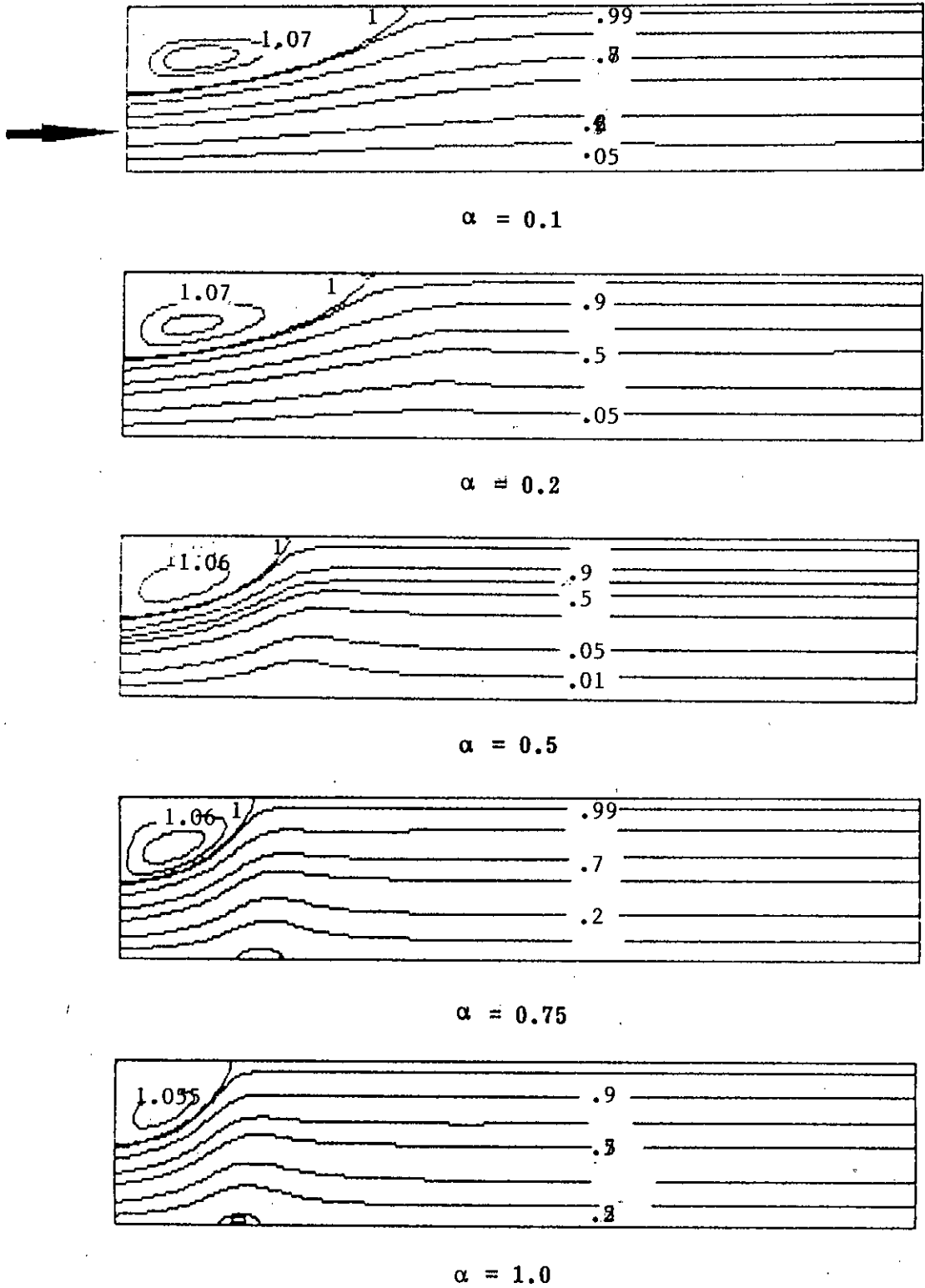


Fig : 4.29 Constant streamline contours for outer-radius annular backstep at $Re_S = 200$ [Note that the axial distance compressed by 5 times].

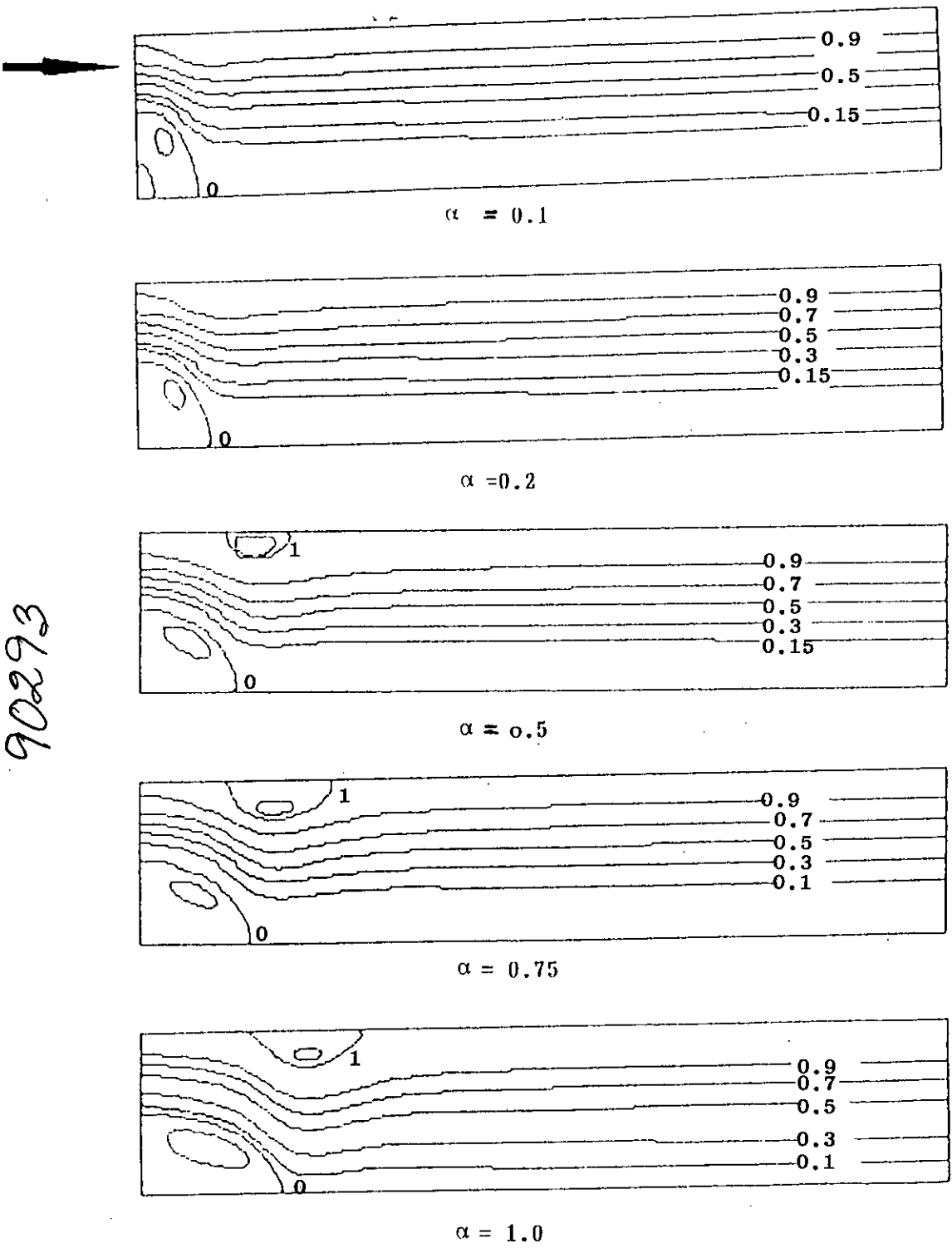


Fig : 4.30 Constant streamline contours for inner-radius annular backstep at $Re_s = 300$ [Note that the axial distance compressed by 5 times].

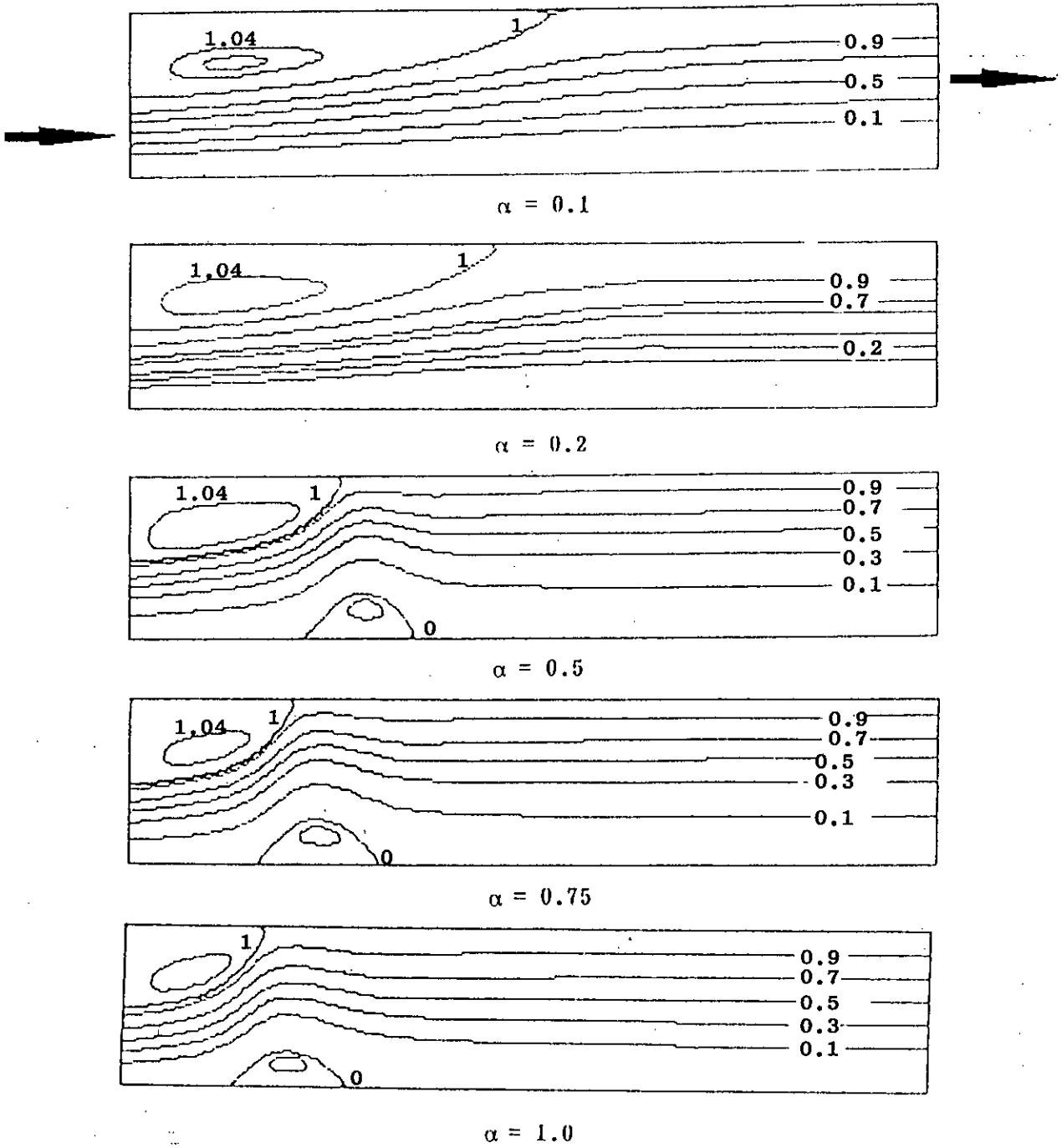


Fig : 4.31 Constant streamline contours for outer-radius annular backstep at $Re_s = 300$ [Note that the axial distance compressed by 5 times].

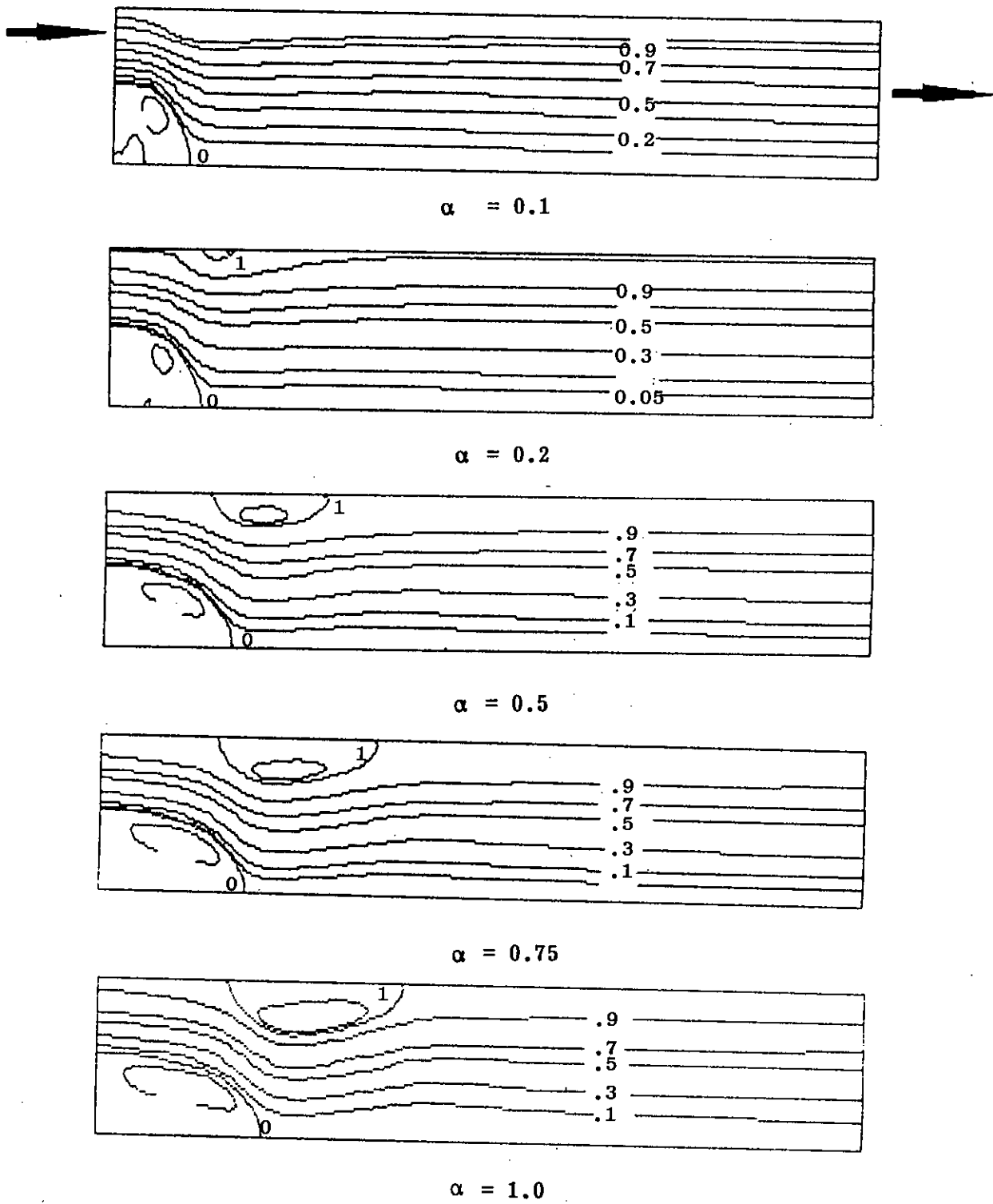


Fig : 4.32 Constant streamline contours for inner-radius annular backstep at $Re_s = 500$ [Note that the axial distance compressed by 5 times].

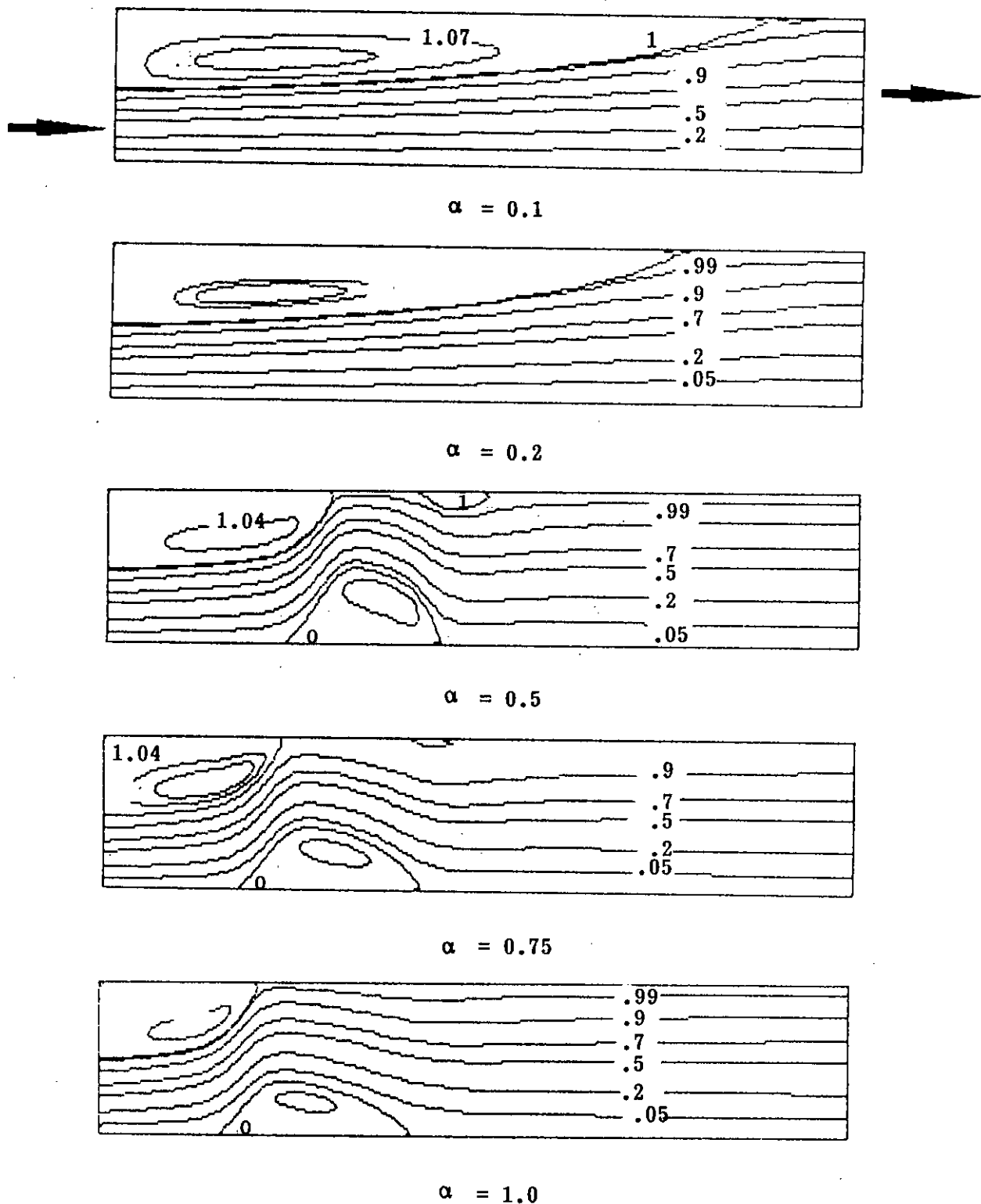


Fig : 4.33 Constant streamline contours for outer-radius annular backstep at $Re_S = 500$ [Note that the axial distance compressed by 5 times].

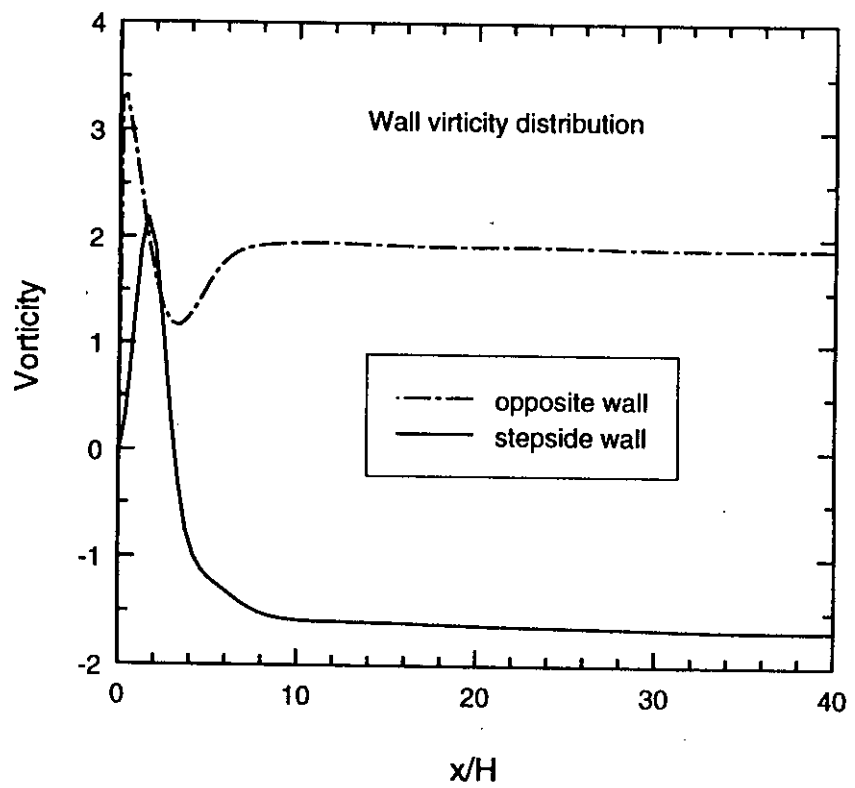
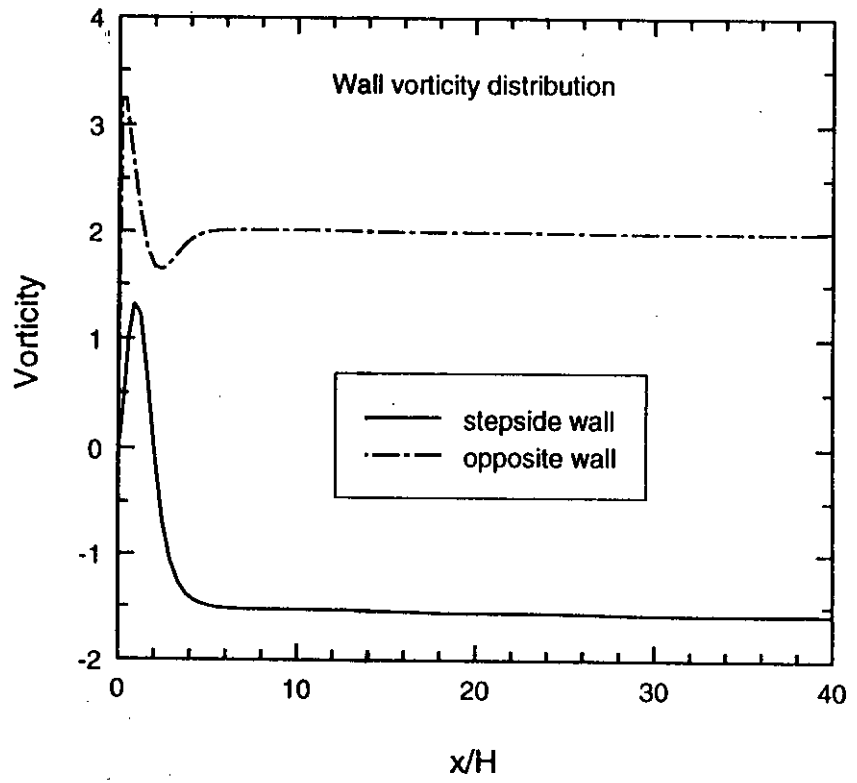
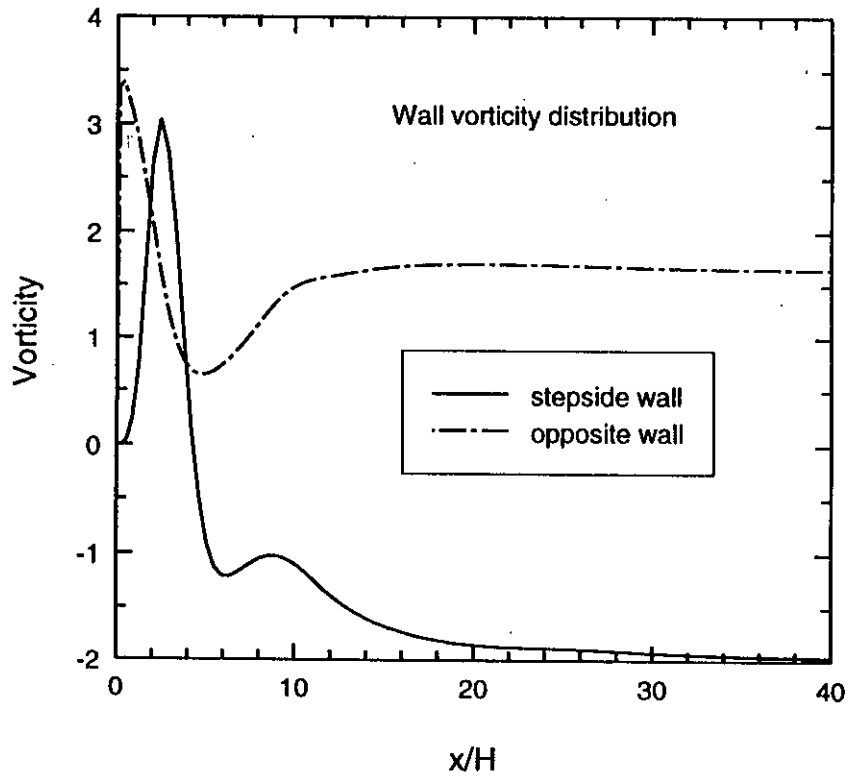
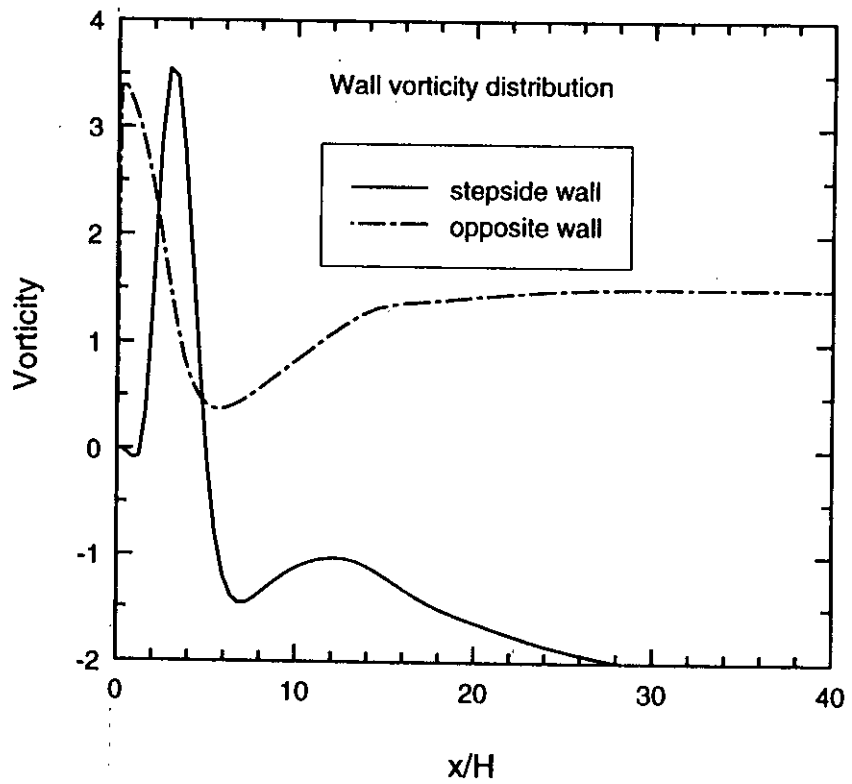


Fig : 4.34 Vorticity distribution along the walls for an inner- radius annular backsteps at an annular radius ratio (α) = 0.1



(c) $Re_s = 200$



(d) $Re_s = 300$

Fig: 4.34 Contd.

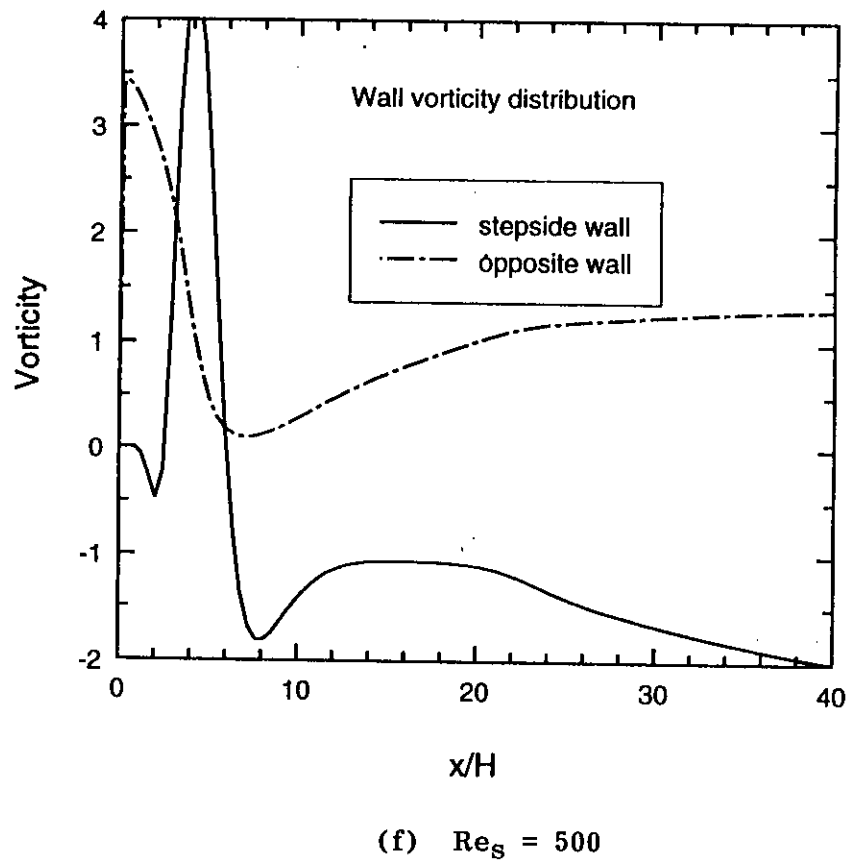
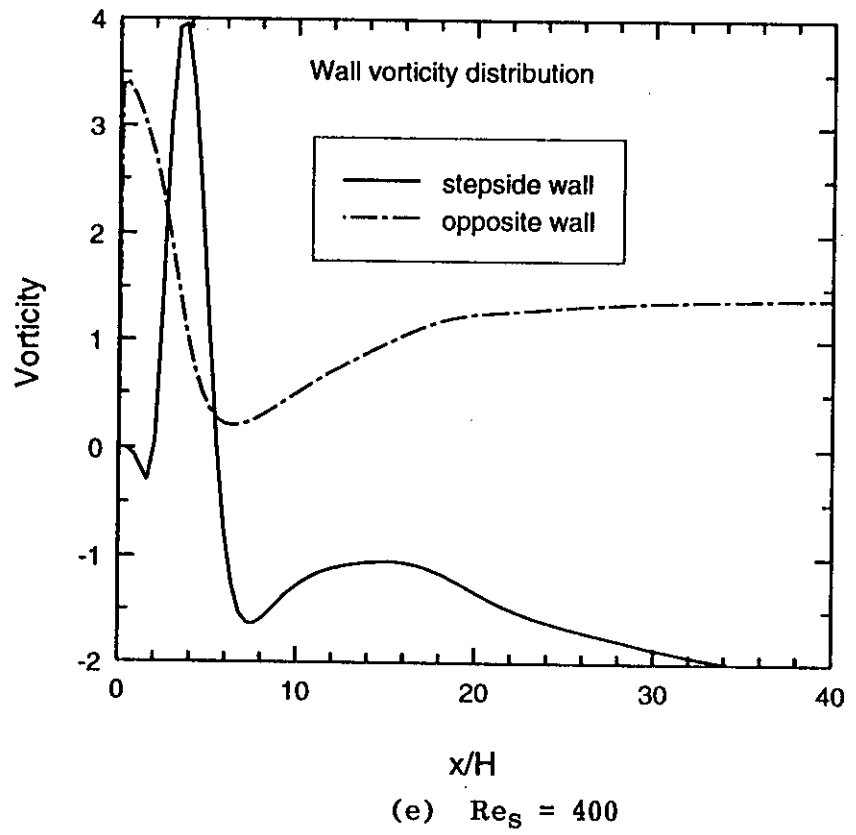
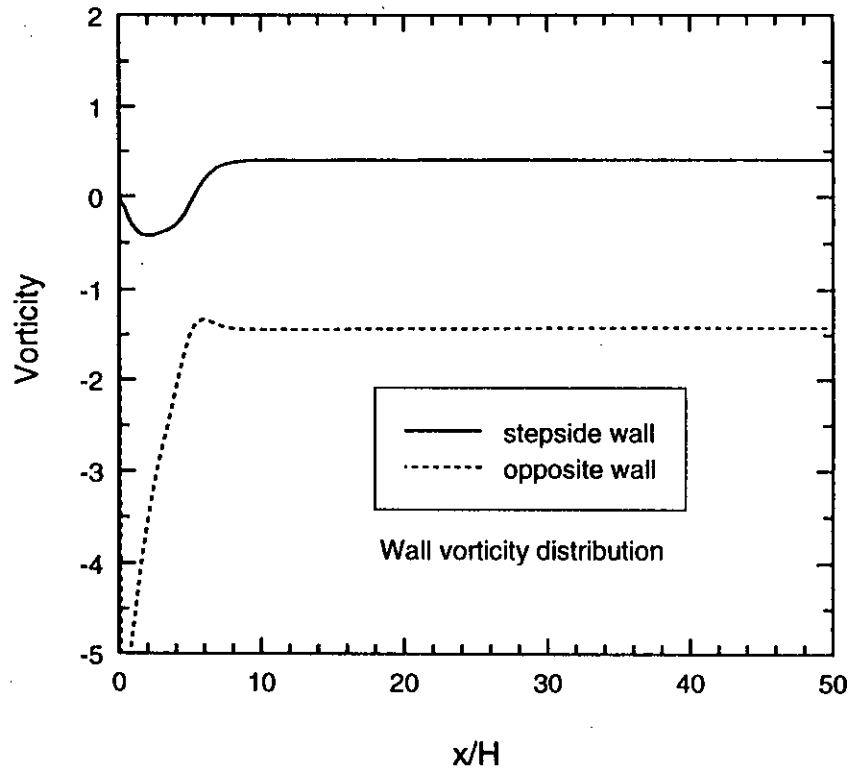
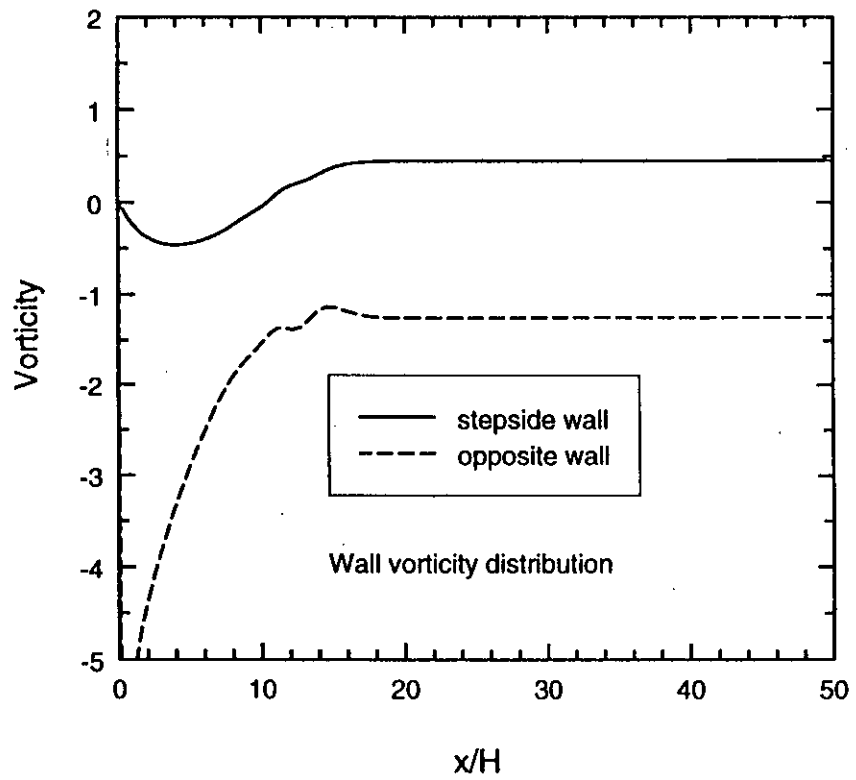


Fig: 4.34 Contd.



(a) $Re_s = 50$



(b) $Re_s = 100$

Fig : 4.35 Vorticity distribution along the walls for an outer-radius annular backsteps at an annular radius ratio (α) = 0.1

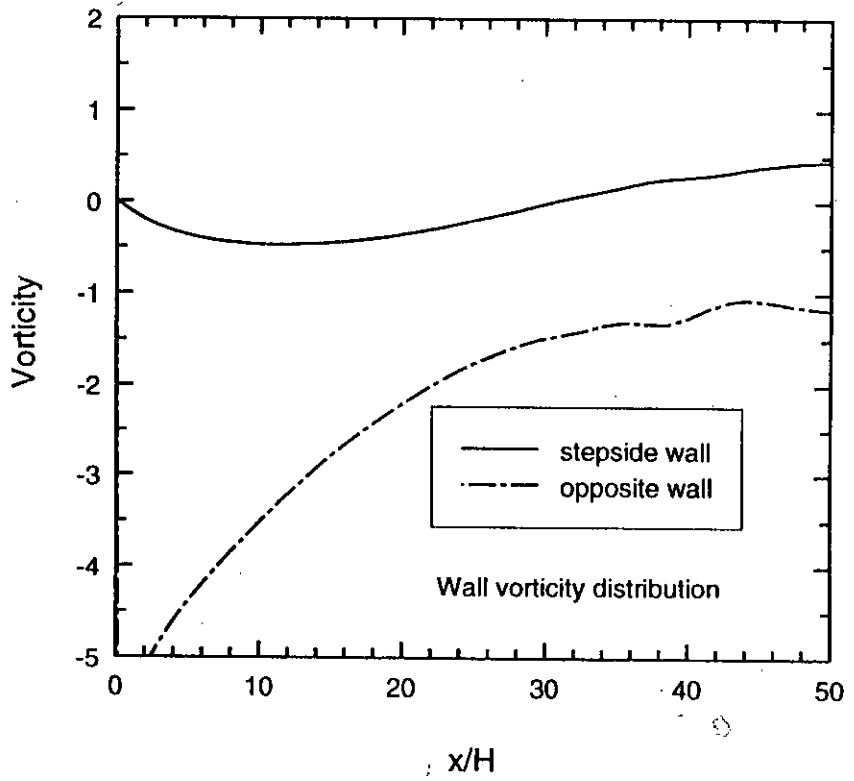
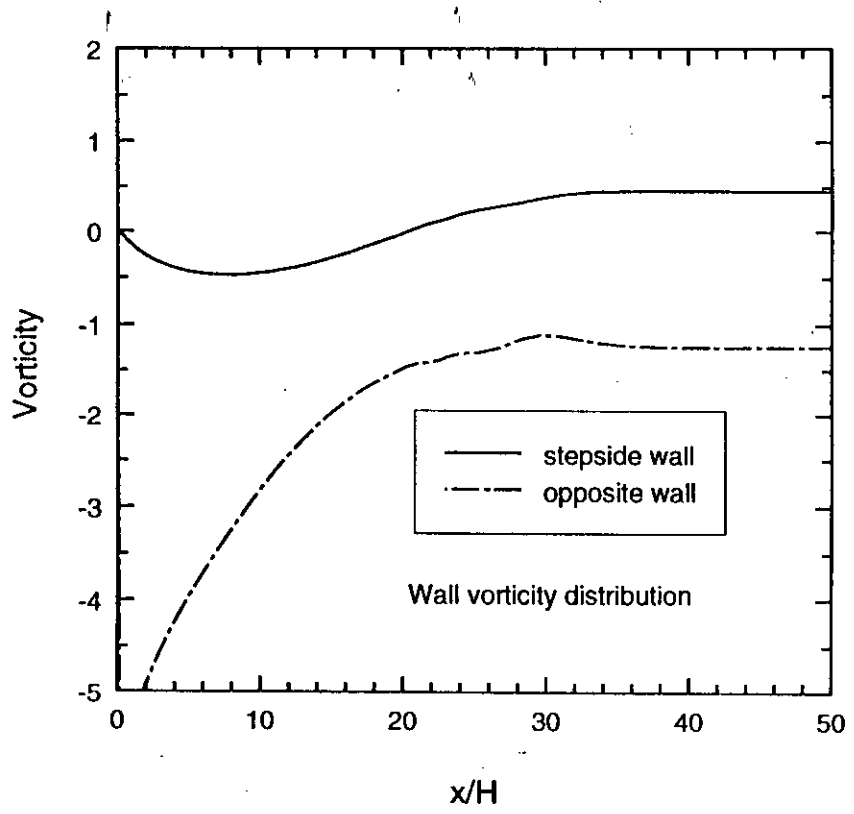
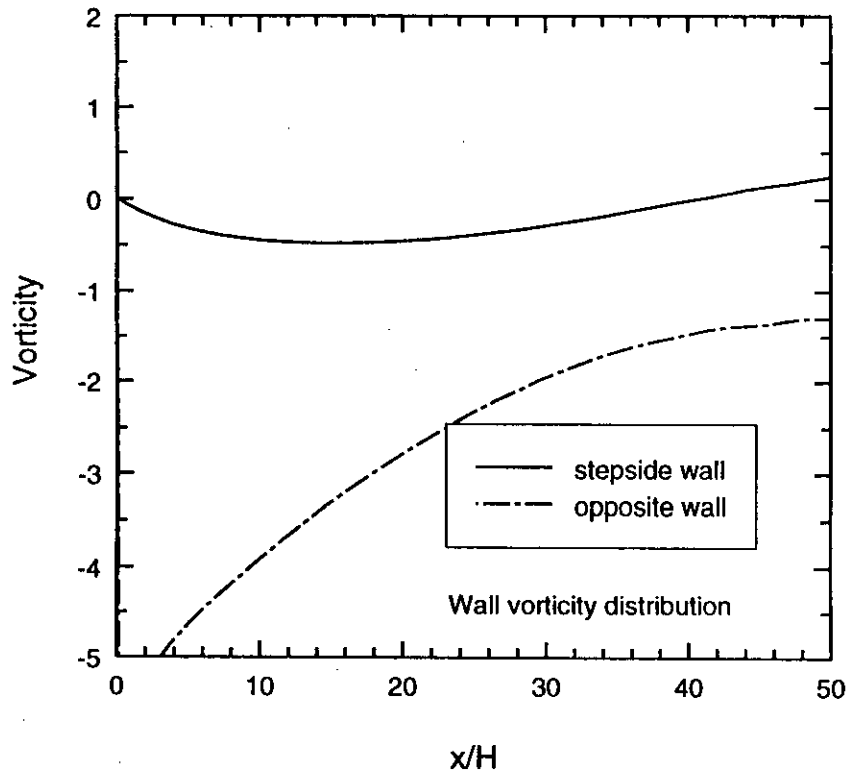
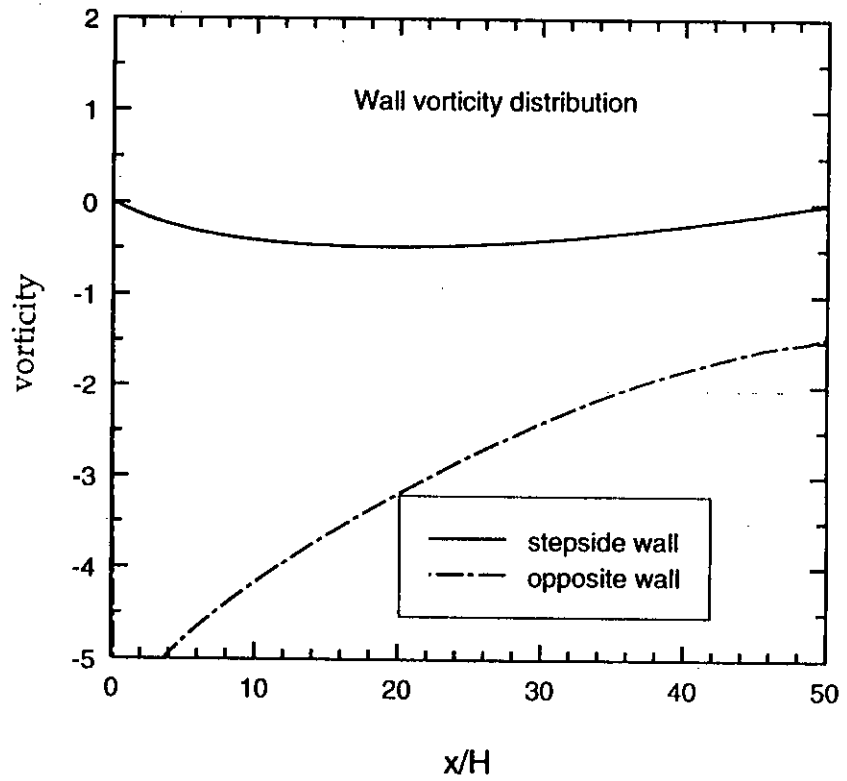


Fig: 4.35 Contd.

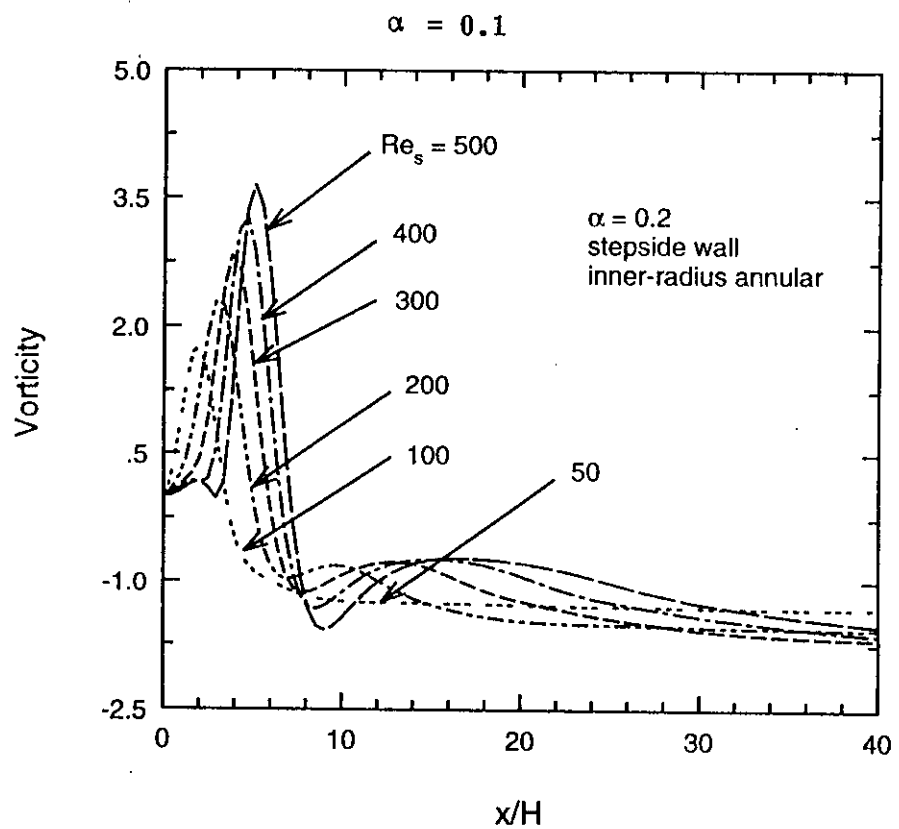
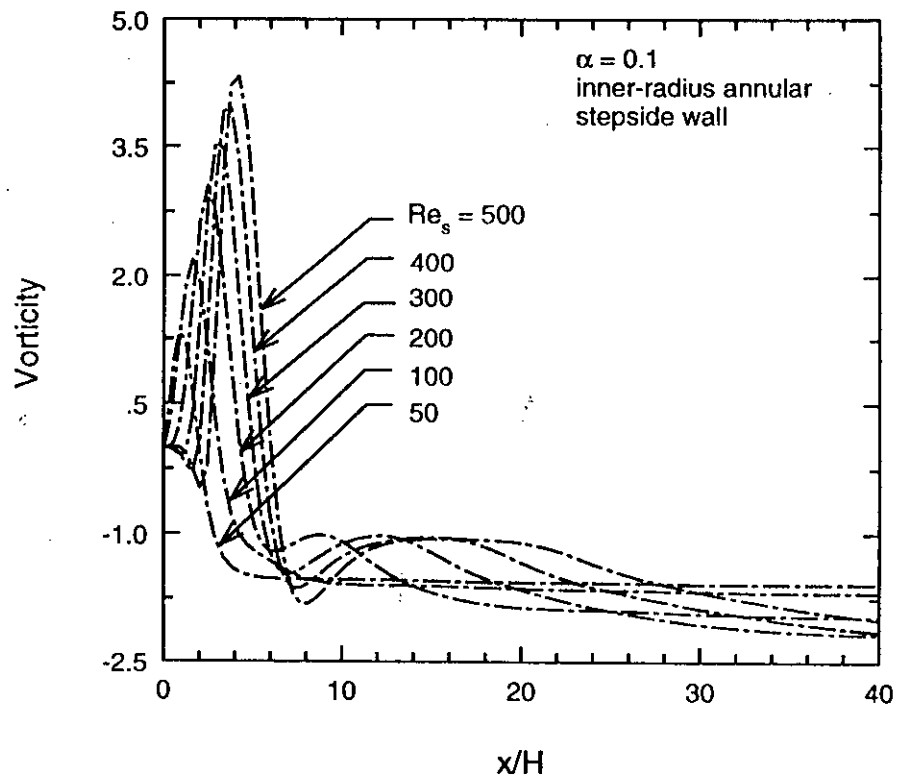


(e) $Re_S = 400$



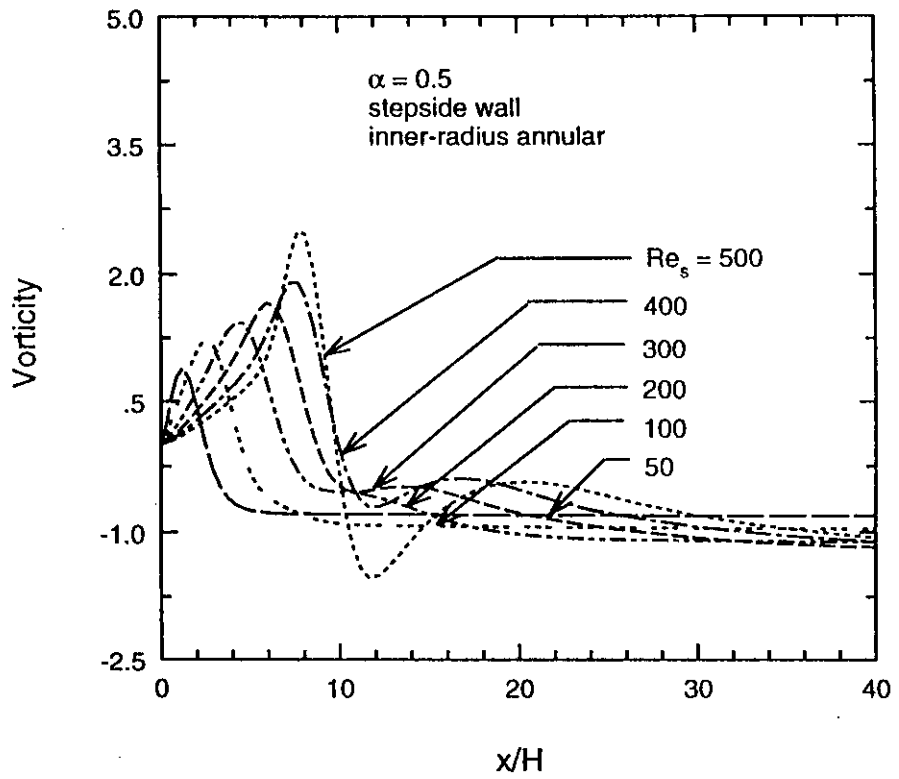
(f) $Re_S = 500$

Fig: 4.35 Contd.

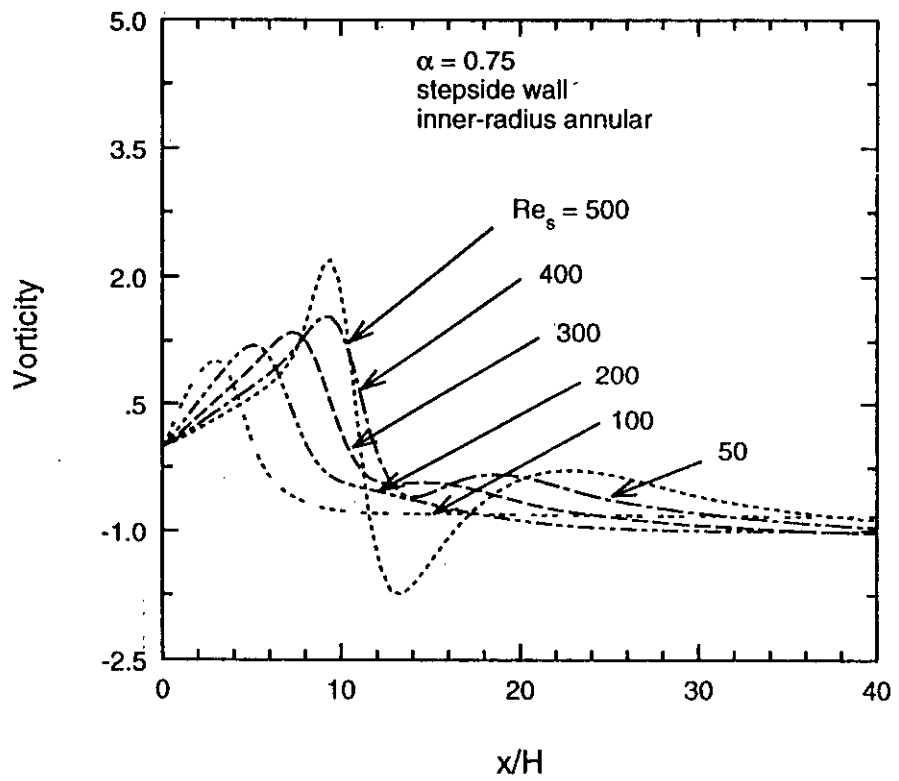


$\alpha = 0.2$

Fig : 4.36 Vorticity distribution along the stepside wall of an inner-radius annular backsteps



$\alpha = 0.5$



$\alpha = 0.75$

Fig: 4.36 Contd.

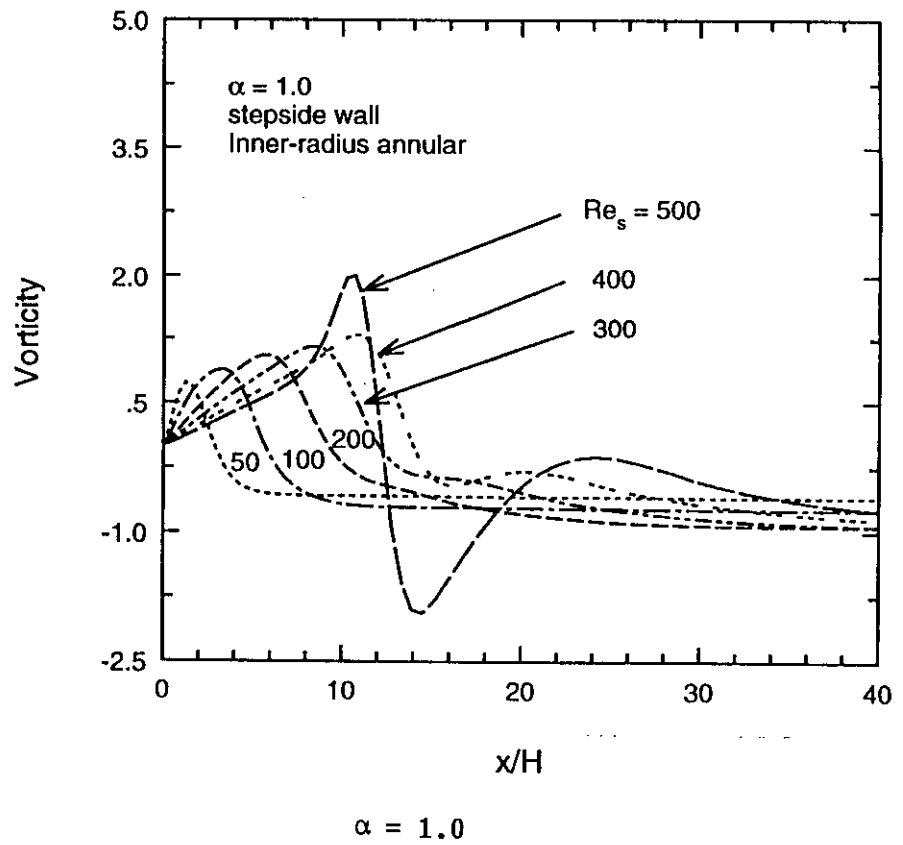


Fig: 4.36 Contd.

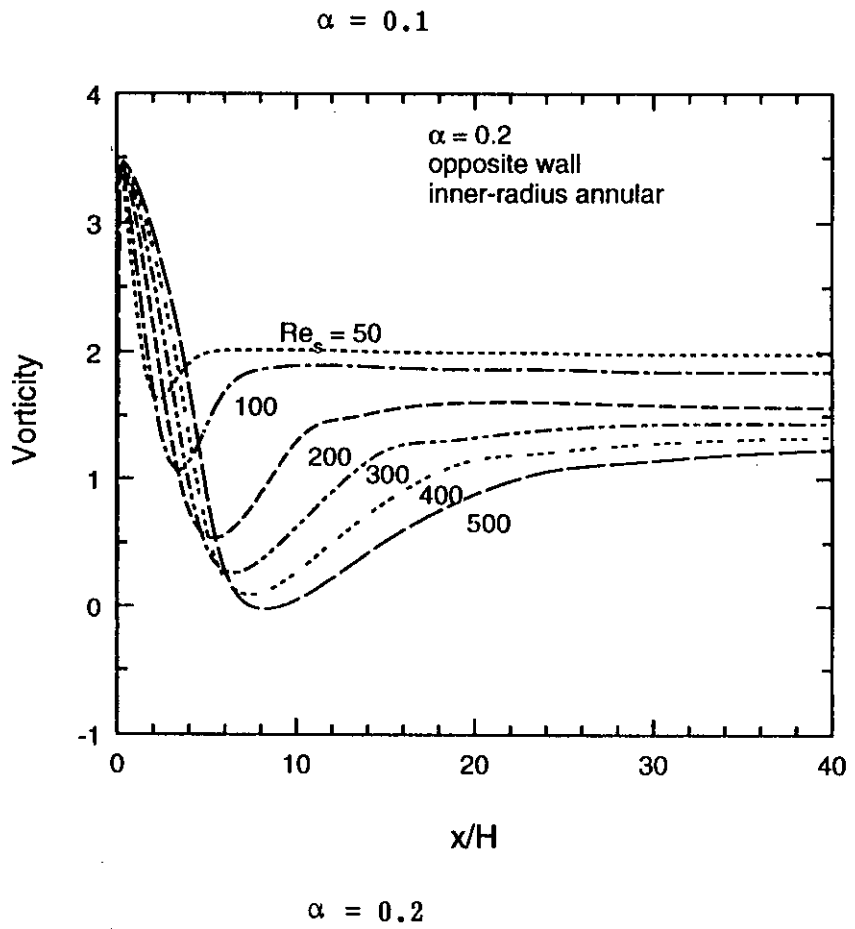
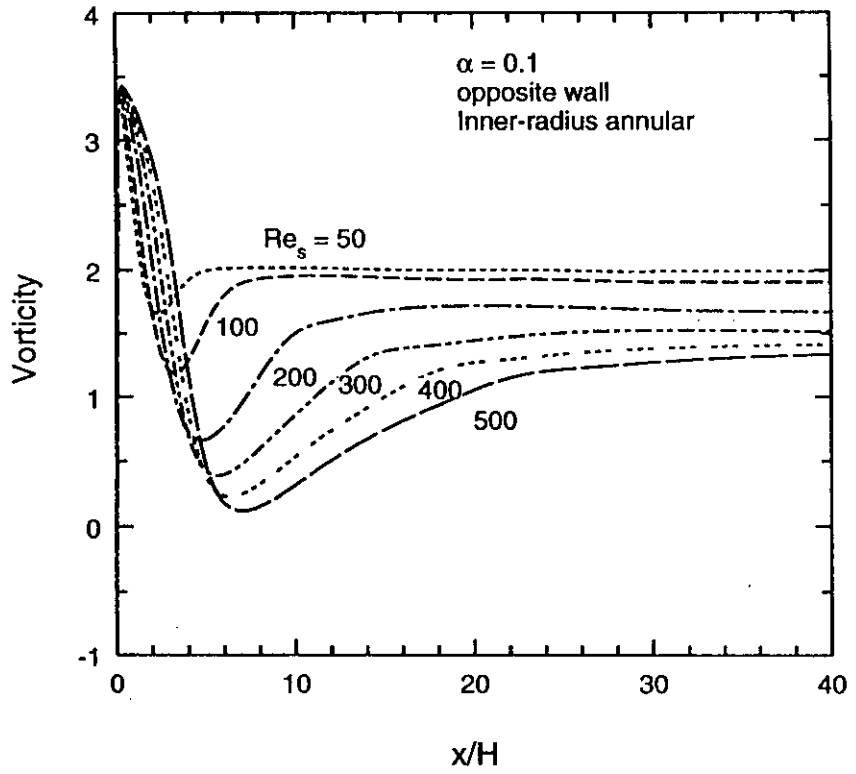


Fig : 4.37 Vorticity distribution along the opposite wall of an inner-radius annular backsteps

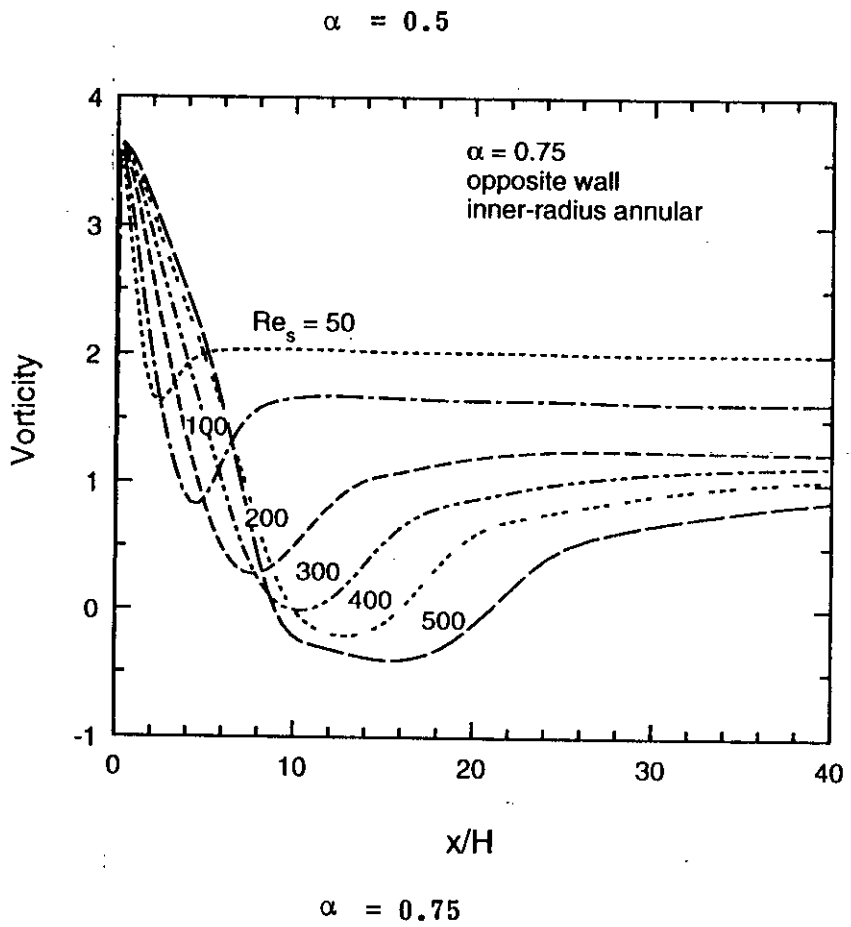
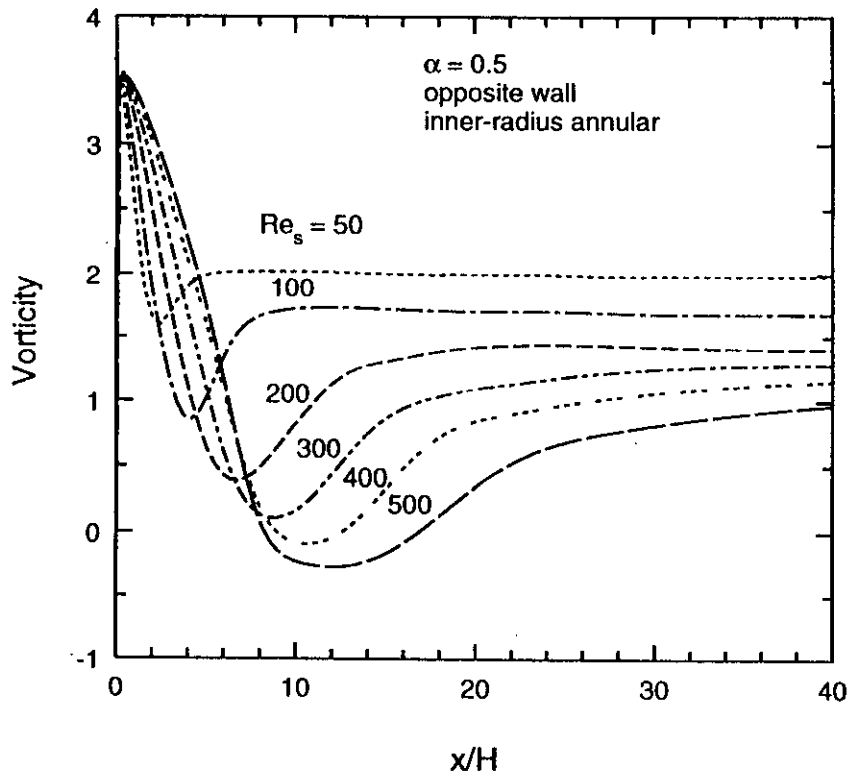


Fig: 4.37 Contd.

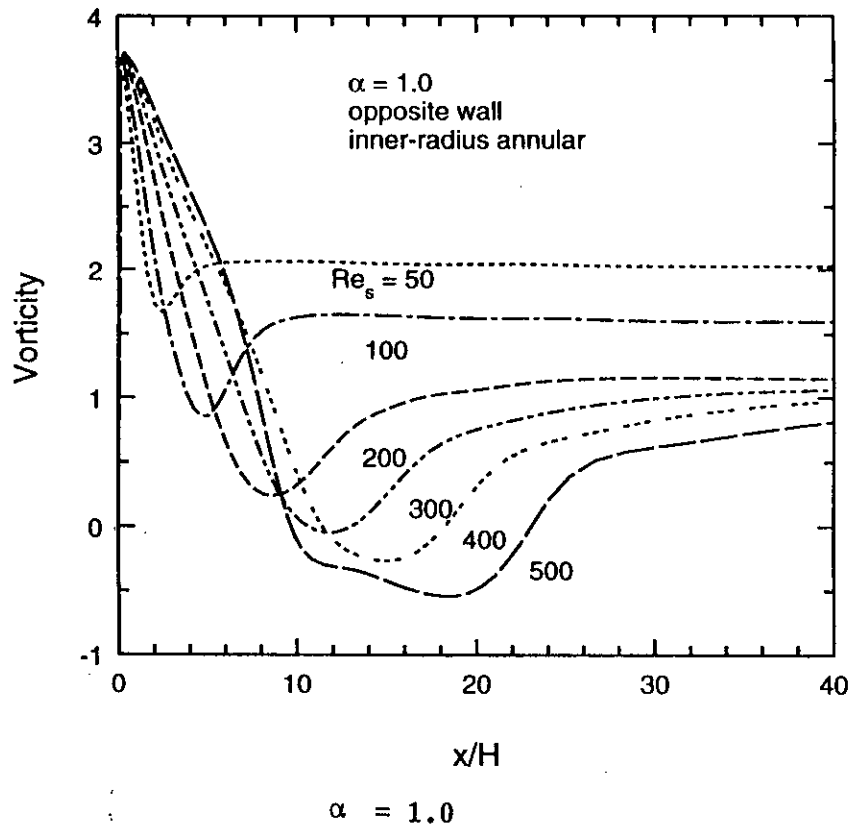
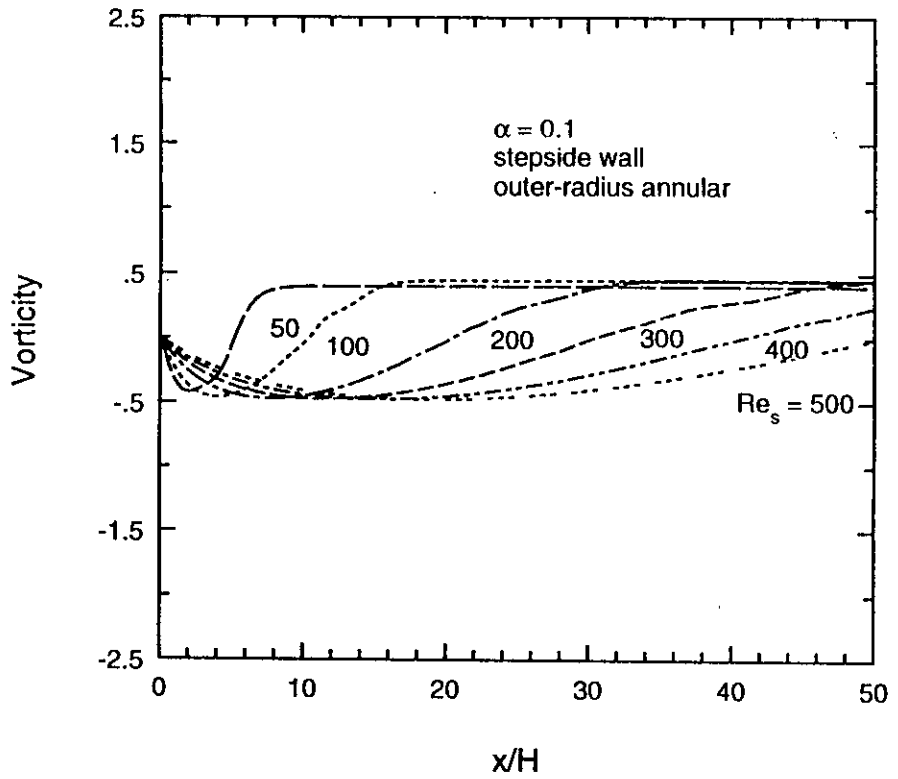
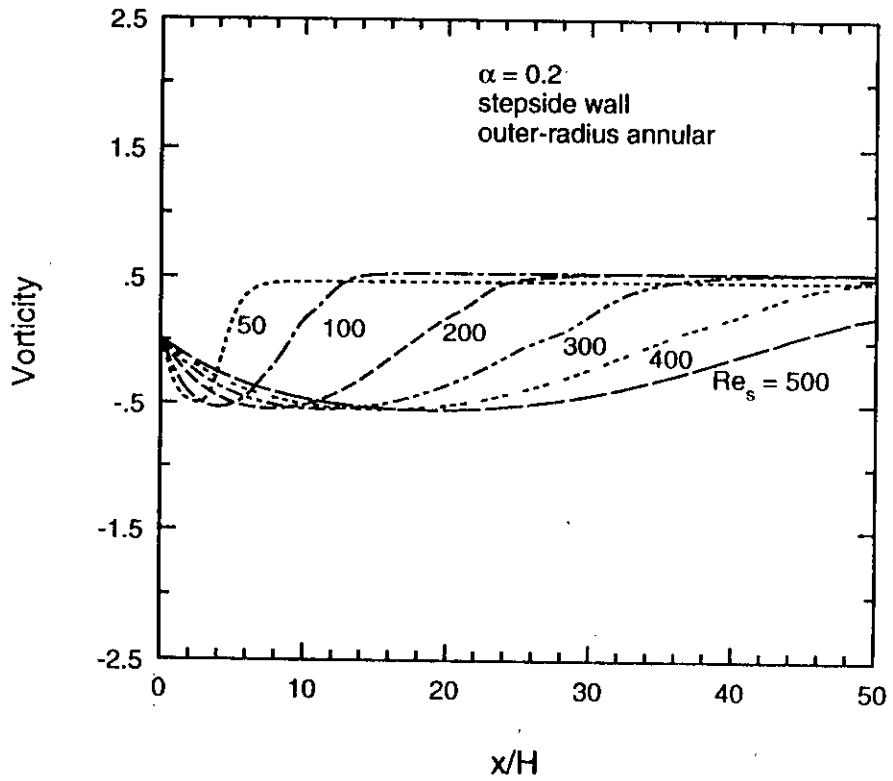


Fig: 4.37 Contd.

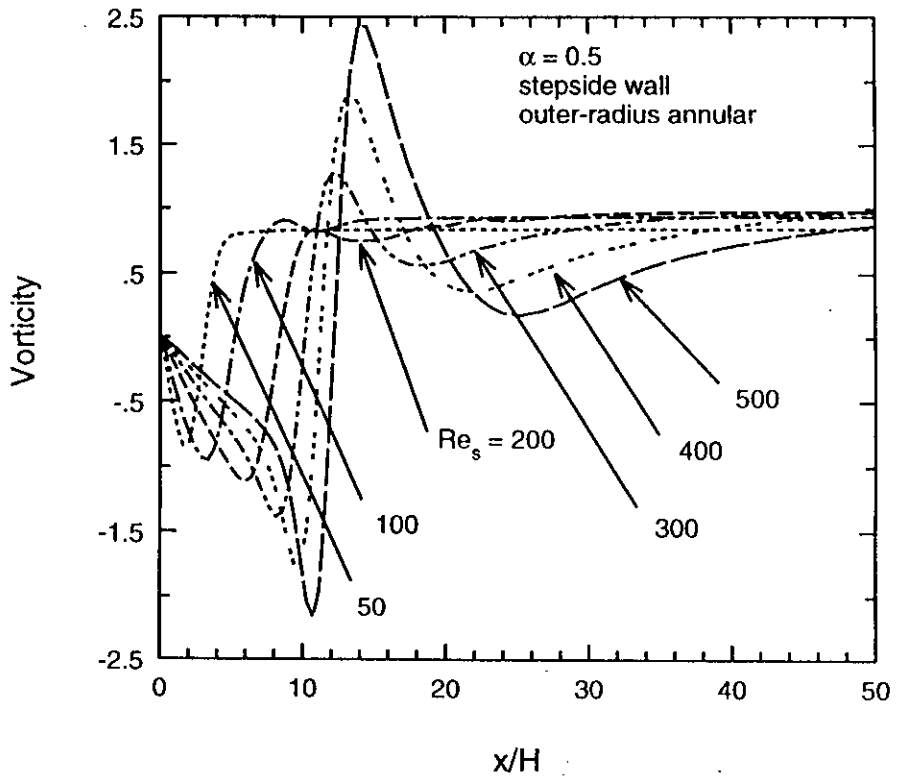


$\alpha = 0.1$

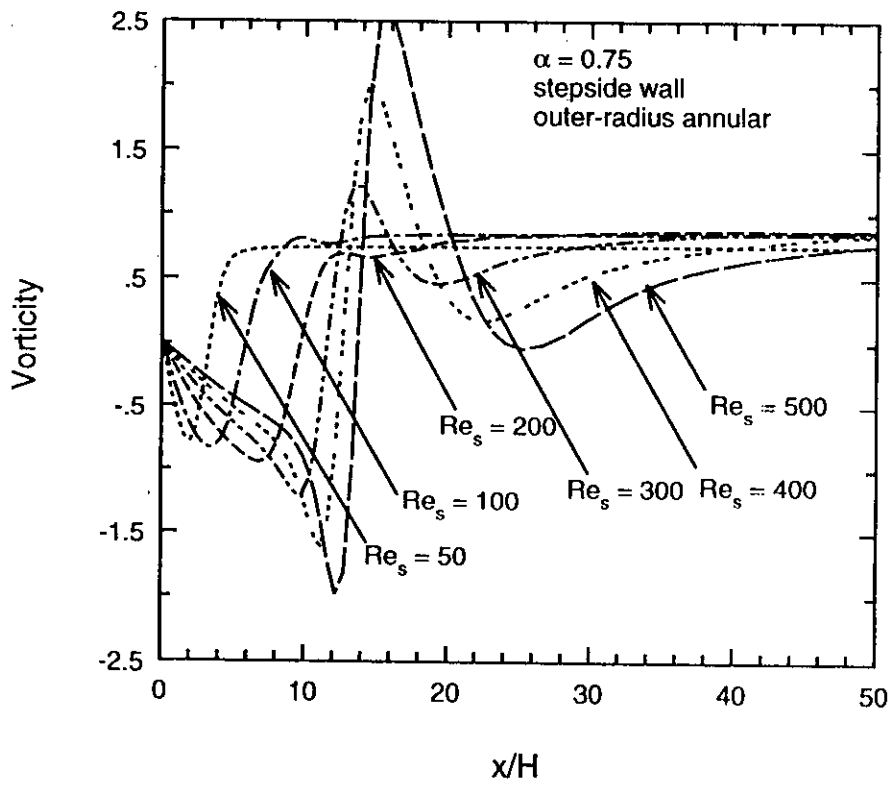


$\alpha = 0.2$

Fig : 4.38 Vorticity distribution along the stepside wall of an outer-radius annular backsteps

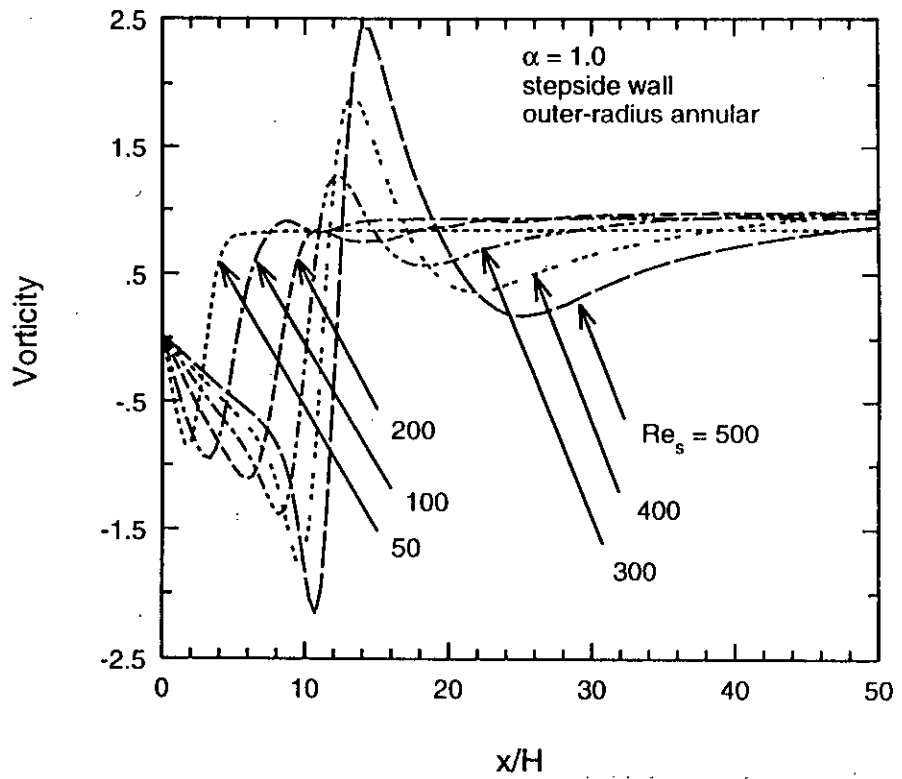


$\alpha = 0.5$



$\alpha = 0.75$

Fig: 4.38 Contd.



$\alpha = 1.0$

Fig: 4.38 Contd.

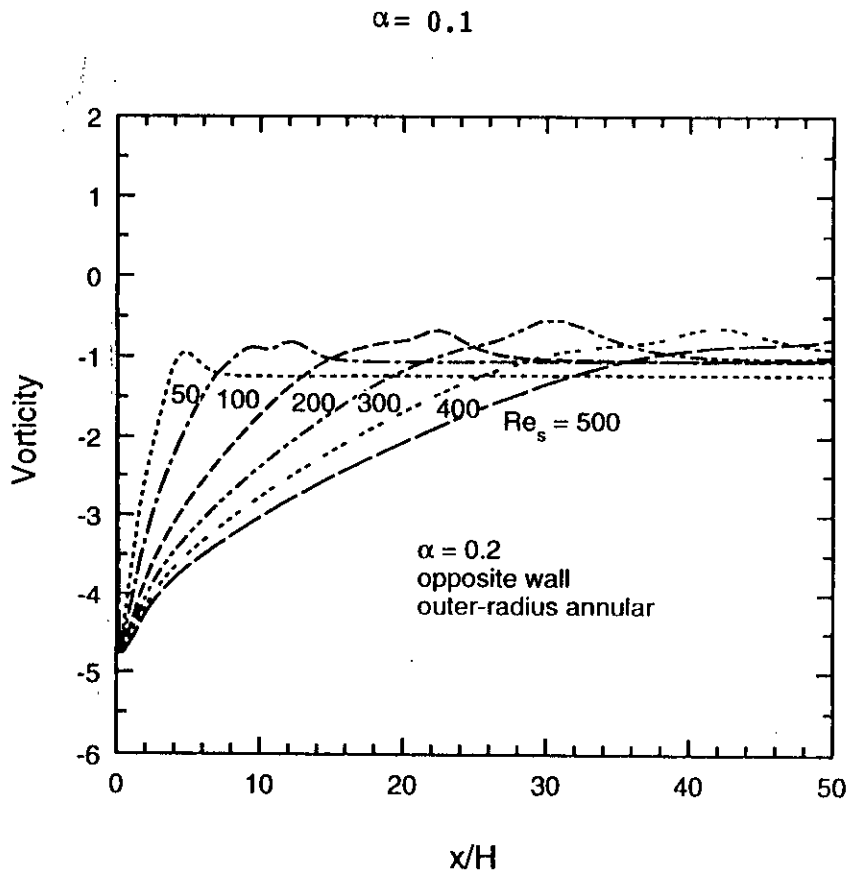
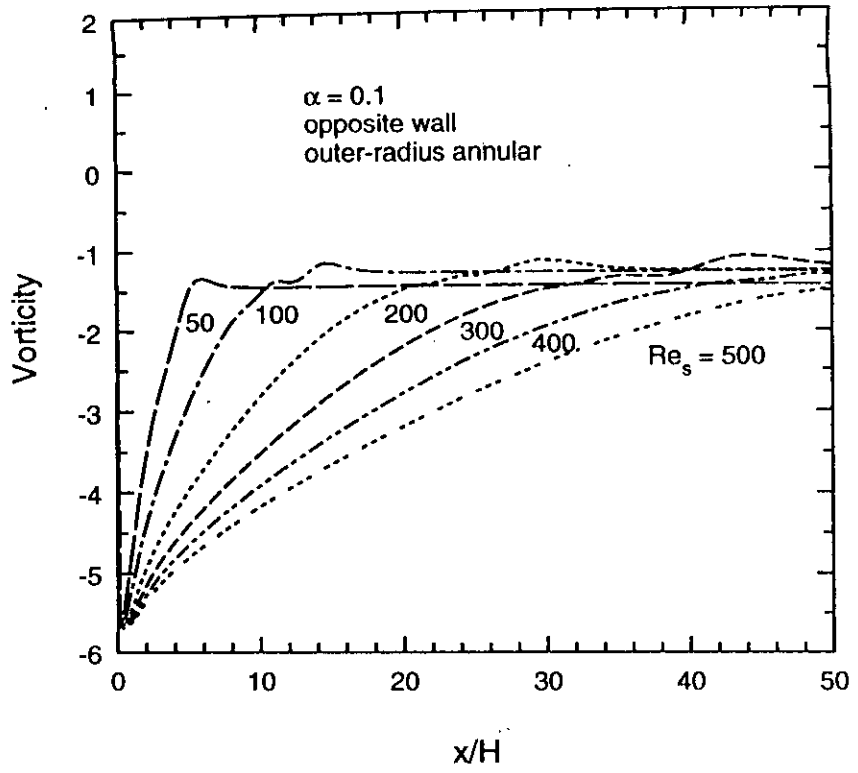
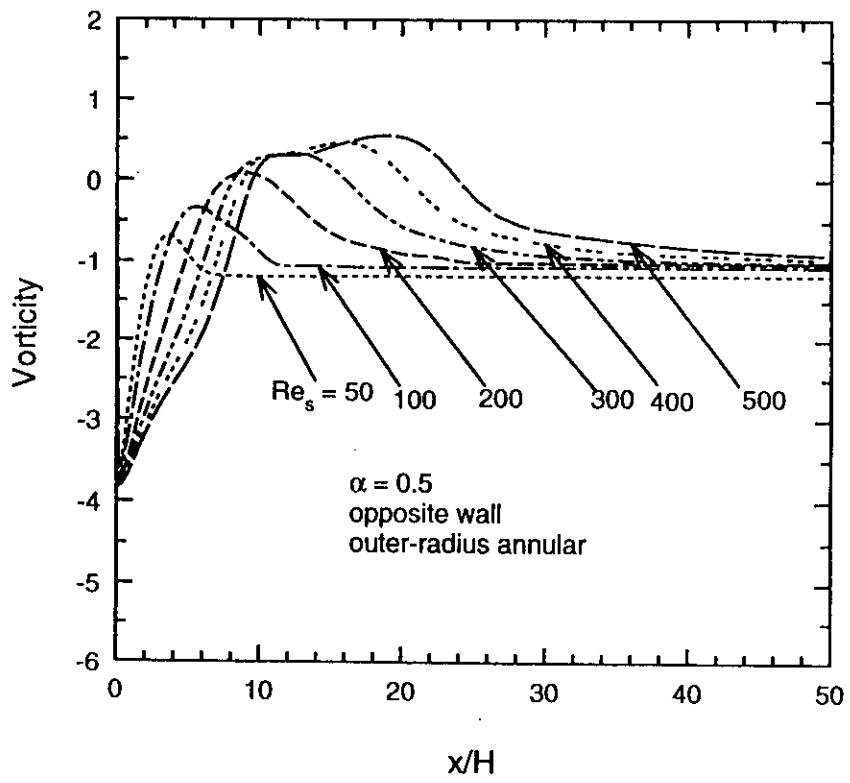
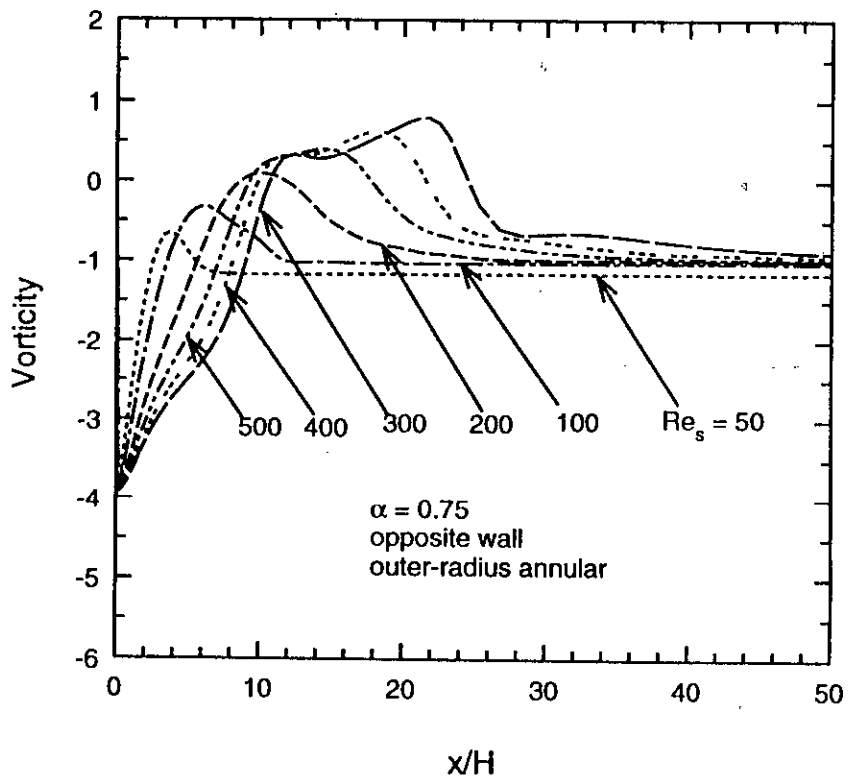


Fig : 4.39 Vorticity distribution along the opposite wall of an outer-radius annular backsteps

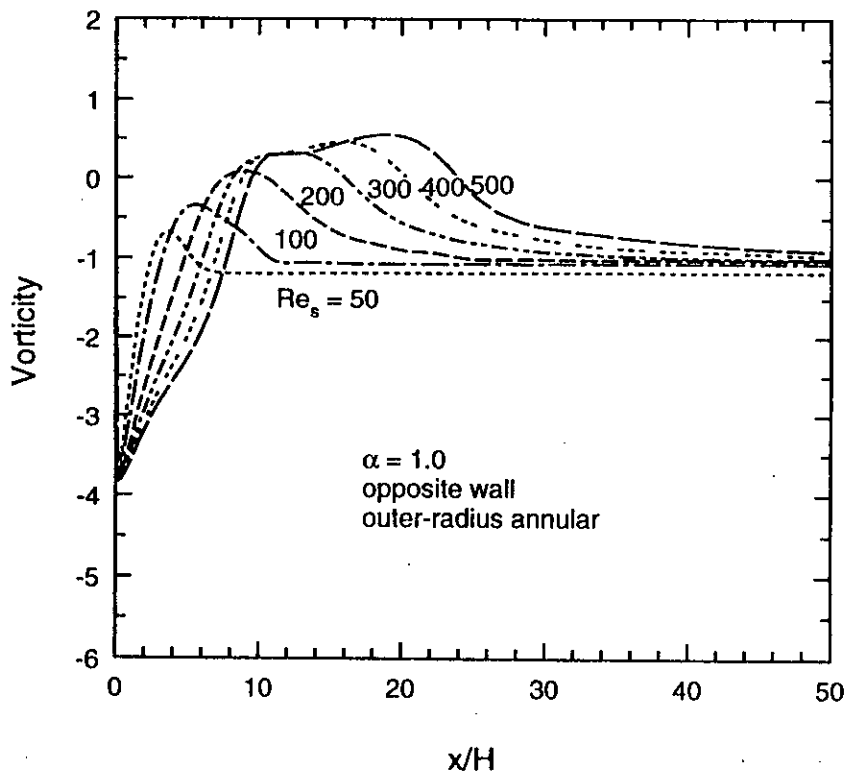


$\alpha = 0.5$



$\alpha = 0.75$

Fig: 4.39 Contd.



$\alpha = 1.0$

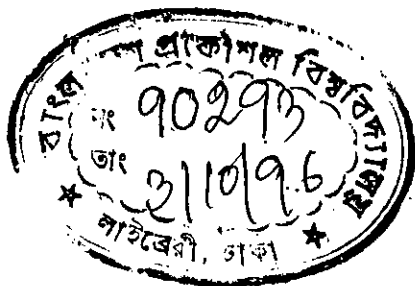


Fig: 4.39 Contd.